# INFORMATION TO USERS

This manuscript has been reproduced from the microfilm master. UMI films the text directly from the original or copy submitted. Thus, some thesis and dissertation copies are in typewriter face, while others may be from any type of computer printer.

**The quality of this reproduction is dependent upon the quality of the copy submitted.** Broken or indistinct print, colored or poor quality illustrations and photographs, print bleedthrough, substandard margins, and improper alignment can adversely affect reproduction.

In the unlikely event that the author did not send UMI a complete manuscript and there are missing pages, these will be noted. Also, if unauthorized copyright material had to be removed, a note will indicate the deletion.

Oversize materials (e.g., maps, drawings, charts) are reproduced by sectioning the original, beginning at the upper left-hand corner and continuing from left to right in equal sections with small overlaps.

Photographs included in the original manuscript have been reproduced xerographically in this copy. Higher quality 6" x 9" black and white photographic prints are available for any photographs or illustrations appearing in this copy for an additional charge. Contact UMI directly to order.

Bell & Howell Information and Learning
300 North Zeeb Road, Ann Arbor, MI 48106-1346 USA

UMI®
800-521-0600

# New Algorithms for Image Analysis, Compression, and 2-D Spectrum Estimation in the Radon Space

Ramesh R. Galigekere

A Thesis

in

The Department

of

Electrical and Computer Engineering

Presented in Partial Fulfillment of the Requirements

for the Degree of Doctor of Philosophy at

Concordia University

Montréal, Québec, Canada

April 1997

# ABSTRACT


**New Algorithms for Image Analysis, Compression, and 2-D Spectrum Estimation in the Radon Space**

Ramesh R. Galigekere, Ph.D.
Concordia University, 1997

New signal/image processing algorithms involving the Radon transform are presented. Algorithms that address computed tomography (CT) are motivated by the desire to process within the Radon space, instead of post-processing a reconstructed image. Algorithms that use the Radon transform as a tool, exploit the properties of the transform to simplify a 2-D processing task.

New image-invariants based on the moments of the projections are developed. The notion of moment-patterns in the Radon space is introduced. A method of rendering the moment-patterns invariant to geometric transformations is presented. An alternative descriptor based on the moment-patterns, invariant to geometric transformations as well as contrast, is proposed.

Selective reconstruction of objects from noisy projections is considered as an application of the 'instantaneous matched-filter'. It involves a combination of the ideas of detection of an object of known shape and location, and an estimation of the associated parameter.

A new approach to binary image compression is proposed, based on a representation of binary objects by a small number of projections. Additional compression is obtained by coding the 1-D non-binary projections. The approach finds applications (i) in CT, involving binary densities, and (ii) as a method of compressing binary

images. A new algorithm developed for reconstructing binary images from their projections, turns out to be a variant of the algebraic reconstruction technique.

Two-dimensional spectral factorization in the Radon space is discussed, and some new applications are indicated. The theory suggests a new approach to 2-D spectrum estimation using the Radon transform, which is considered in the sequel.

Some of the issues associated with the Radon transform of a stationary random field are brought out. A new representation for the Radon transform of a stationary random field (valid upto second-order statistics), is used to study the second-order properties of the transform. Limitations pertaining to the theory and its application to random field data over a finite support, are discussed. A novel approach to spectrum estimation based on the Radon transform of 2-D autocorrelation of the stationary random field data is investigated. Estimation by autoregressive modeling is considered, and an extension to the maximum entropy method is discussed.

**Dedicated to the memory of**

**My Father**

# ACKNOWLEDGEMENTS

I wish to express my deep sense of gratitude to Prof. E.I. Plotkin and Prof. M.N.S. Swamy for their supervision, support, and understanding throughout the course of my Doctoral Program.

I gratefully acknowledge the financial support from Natural Sciences and Engineering Research Council of Canada (NSERC), FCAR, and MICRONET, a National Center of Excellence, through grants awarded to my Supervisors. I thank the University for the support through the Concordia University Graduate Fellowship.

I would like to thank Prof. G.T. Herman, Medical Image Processing Group, University of Pennsylvania, PA, for having provided the Centre for Signal Processing and Communications with SNARK'93. I would also like to acknowledge some early discussion I had with Dr. N. Srinivasa.

I thank the members of the faculty, and my colleagues at the Centre for Signal Processing and Communications, for their cooperation and support.

It is a pleasure to acknowledge the company of Mr. Rajan V.K. Pillai, who has been very helpful to me. I wish to thank Dr. S.K. Krishnan Nayar for his willingness to help at all times.

It is difficult, if not impossible, to list the names of all of my friends and family members, who have been helpful on various occassions. I take this opportunity to thank them all.

Ramesh R. Galigekere

# TABLE OF CONTENTS

# LIST OF FIGURES

# LIST OF ABBREVIATIONS

| | |
|---|---|
| AC | Autocorrelation |
| ACF | Autocorrelation function |
| AR | Autoregressive |
| ARMA | Autoregressive moving-average |
| ART | Algebraic reconstruction technique(s) |
| CAR | Circular autoregressive |
| CR | Compression ratio |
| CAT | Computer assisted tomography |
| CBP | Convolution backprojection |
| CST | Central slice theorem |
| CT | Compute(rize)d tomography |
| DCT | Discrete cosine transform |
| DPCM | Differential pulse code modulation |
| DFT | Discrete Fourier transform |
| DRT | Discrete Radon transform |
| FBP | Filter(ed) backprojection |
| FFT | Fast Fourier transform |
| FT ($\mathcal{F}$) | Fourier transform |
| GIMF | Generalized instantaneous matched filter |
| HT | Hough transform |
| IMF | Instantaneous matched filter |
| IMP | Invariant moment-pattern |
| IIR | Infinite impulse response |
| IRT | Inverse Radon transform |
| LP | Linear prediction/predictive |
| LPC | LP coefficients/coding |

| | |
|---|---|
| m-D | multi-dimensional |
| ME | Maximum entropy |
| MEM | Maximum entropy method |
| MESE | Maximum entropy spectrum estimation/estimate |
| MF | Matched-filter |
| MO | Modified object |
| MP | Moment-pattern |
| NDT | Non-destructive testing |
| *nnd* | Non-negative definite |
| NMSE | Normalized means-square error |
| NSHP | Non-symmetric half-plane |
| PDF | probability density function |
| PHD | Pisarenko harmonic decomposition |
| *pd* | Positive definite |
| *psd* | Positive semi-definite |
| PSD | Power spectrum density |
| QP | Quarter-plane |
| RLC | Run-length coding |
| RLS | Recursive least squares |
| RO | Reference object |
| RT ($\mathcal{R}$) | Radon transform |
| RV | Random variable |
| SAR | Synthetic Aperture Radar |
| SDF | Spectrum density function |
| SE | Spectrum estimation |
| SF | Spectral factorization |
| SNR | Signal-to-noise ratio |

# Chapter 1

# Introduction

## 1.1 Introduction

The central theme of the work presented in this thesis is *multi-dimensional signal processing in the Radon space.* It involves processing the Radon transform, or a set of projections, of a multi-dimensional signal. While the transform arises naturally in many fields of science and engineering, it is also gaining recognition as a tool in multi-dimensional signal processing.

The Radon transform (RT) is a powerful tool that has revolutionized the field of medical imaging involving the reconstruction of an image from its projections [23, 54]. It is also the basis of a wide variety of similar applications such as radio astronomy [11], geophysics [181, 28], electron microscopy [25, 26], non-destructive testing (NDT) [88, 209, 142], underwater acoustic imaging [128], synthetic aperture radar (SAR) [129], and electrical impedance tomography [93]. All the above applications involve the reconstruction of a multidimensional function from the measurements available in the transform domain, the Radon space (RS). These applications are collectively referred to as compute(rize-)d, or computer-assisted, tomography (CT or CAT). For a detailed review of the major fields of applications in which the RT arises in a natural fashion, and the various imaging modalities, see [23, 54, 201].

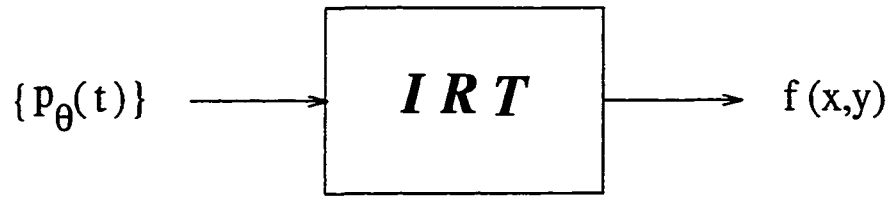


Figure 1.1: Computed tomography

The current trends in medical imaging modalities are reviewed in [51, 202]. Fig. 1.1 depicts the mathematical problem of CT, where the inverse RT (IRT) corresponds to finding the function $f(x, y)$ from the set of its projections, $\{p_\theta(t)\}$. Practically, it represents an algorithm that approximately reconstructs a 2-D function on a finite set of points, from a finite number of discrete projections. Further details regarding the RT, its properties, and inversion are considered in Chapter 2.

Many situations in CT require a processing of the projections in addition to the processing that forms an integral part of the reconstruction algorithm. Typical examples include the suppression of the effects of noise in the projection data [1], image enhancement [203], and the reconstruction from missing, truncated, or hollow projections [98, 203]. Other image processing tasks such as the enhancement of low-contrast objects [176], the enhancement of image features such as edges and lines [57, 130, 161], and the reconstruction of the convex hull of an object [209], also require additional processing in the projection domain.

In certain applications in CT, the ultimate goal is rather to extract certain information about the cross-section (CS) [101, 24, 9, 193, 88, 164, 57]. A straightforward approach to information-extraction consists of applying 2-D image analysis and segmentation techniques on a reconstruction obtained from the projections. However, it is often possible to carry out a part of, or the entire processing in the

[1]The sources of noise in medical CT data are discussed in [110]. In general, CT-noise is signal dependent [55], and uncorrelated noise in projection data results in correlated reconstruction-noise [178]. Further, if the CBP algorithm is used for reconstruction, the $|\omega|$-filter involved, accentuates noise. Hence, it is preferable to suppress the effect of noise in the projections, instead of post-processing a reconstructed image [203].

RS itself, to extract the required information. One can thus avoid a post-processing of the reconstructed image, which can be advantageous in many ways, depending upon the context. For example, filtering is a pre-processing step in many image processing tasks. A linear filtering operation on the image can be merged with the 1-D filtering in the RS that is a part of the reconstruction algorithm [205, 164, 72, 231]. An associated advantage is that the processing-errors in the projections tend to get distributed over the entire image, alleviating the visual effect to some degree. Often, the advantage can be in sheer unnecessity of a reconstruction. For example, the information such as the mass, the centroid and the bounding rectangle of an object, and the presence and location of straight lines in a binary CS, can be inferred easily from the projections themselves. In certain image transmission applications, it may be preferable to code the projections instead of reconstructing the picture followed by coding and transmission [223, 62].

Over the recent years, the RT has been found useful in many applications that do not initially involve a measurement in the transform domain. The basic idea behind the use of the RT as a tool is to exploit some of its properties in an effort to simplify a 2-D processing task that may be otherwise difficult. The theoretical framework of the RT, together with its relationship with the Fourier transform, has provided a new dimension to the utility of the RT as a tool in multidimensional signal processing. The RT of a 2-D function, which is a set of 1-D projections of the function, provides an alternative representation for the function under consideration. The usefulness of such a representation stems from the fact that many of the powerful signal processing techniques that are well understood in 1-D, can be extended to 2-D. The representation can often serve to provide a better understanding of the 2-D problem under consideration. The projections have been used as an aid to character recognition (see [150] and the references cited in [17]), and corner detection [231]. The scope of the RT as a transform has since gradually encompassed various fields of application in 2-D signal and image processing. Such

applications may be referred to as "Radon transform based multi-dimensional signal processing". Examples of projection based image analysis and pattern recognition algorithms include [96, 190, 57, 21, 130, 63, 231, 47]. The use of the RT in data compression has been considered in [147, 163, 16, 35, 223]. Jain and Ansari [76] proposed the use of the RT in 2-D spectrum estimation, which culminated in the work of [204, 206]. The approach of [204] has been applied (with some variation) to polar-raster data [34]. A class of applications of a more recent origin is that of (certain forms of) the discrete Radon transform (DRT) in the development of fast 2-D algorithms [40, 195, 208].

Most of the work involving the RT has been in the deterministic realm. Not much has been reported on the RT of random fields, perhaps because, most of the applications have involved the reconstruction of a deterministic function from (i) its projections (often in the presence of measurement noise) as in X-ray CT (ii) its projections, where the line integral itself is modeled as a random variable, as in emission CT (ECT). Further, the line integral of a random field does not exist [76], making a straight-forward analysis hard. However, the emergence of the RT as a potential tool in m-D signal processing has necessitated a study of the RT associated with a stationary random field (SRF). The RT of 2-D random fields, for example, is encountered in the context of 2-D spectrum estimation.

The large number of physical situations in which the RT arises naturally, and the properties of the RT that render it a potential tool in m-D signal processing, supported by the advent of dedicated hardware and efficient algorithms, provide the motivation for exploring new possibilities. Consequently, this thesis considers new signal/image processing techniques involving the RT. It is convenient to distinguish the applications based on the space in which the data is available: (1) the RS (the projection domain), and (2) the m-D space (spatial domain). The former corresponds to the familiar tomographic scenario, in which two types of applications arise: (a) enhancement, and (b) extraction of information. The second category

corresponds to the use of the RT as a transform/tool in m-D signal/image processing. When the data is available in the Radon space, the motivation is to process the projections, for enhancement and information-extraction *in the Radon space itself, without having to post-process a reconstructed image.* The basic motivation behind the use of the RT as a tool is *to utilize its properties, such as that of reduction of dimensionality*, to simplify a m-D processing task. The techniques that employ the RT as a transform are often naturally applicable to a tomographic scenario. The above applications together constitute 'signal/image processing in the Radon space', depicted in fig. 1.2. Note that the projections $\{p_\theta(t)\}$ in fig. 1.2 represent noiseless, noisy, blurred, or other kind of modified versions of the projections, depending upon the application.

Before presenting an outline of the thesis, a clarification of certain terminologies, is in order. A 2-D function considered in CT is referred variously to as 'density', 'density function', 'reflectivity', 'object', 'function', or 'picture' depending upon the context under consideration. The term density stems from the fact that it is the 2-D distribution of a 'mass', the double integral of the density function. The 'density' could be the coefficient of X-ray absorption in X-ray CT, or the ground reflectivity in spotlight-mode SAR. The 2-D CS that is reconstructed is referred to simply as the 'reconstruction' or the 'reconstructed image'. An object may refer to one or a certain group of density functions in a CS.

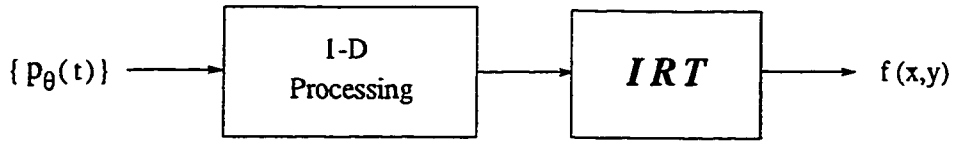


(a) CT Image enhancement by processing in the Radon space

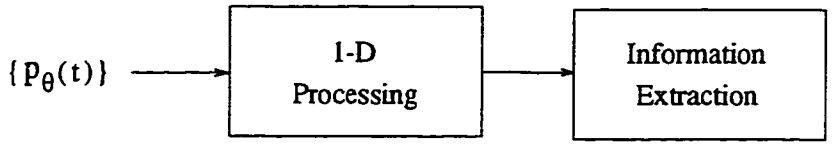


(b) Information-extraction in the Radon space

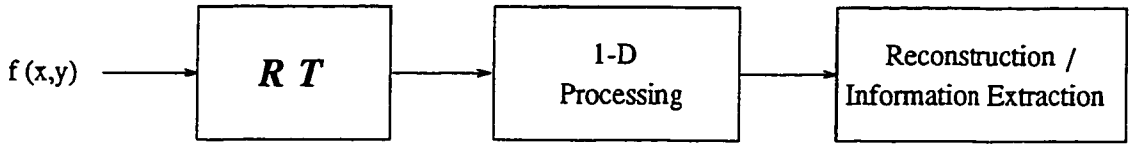


(c) Radon transform-based signal/image processing

Figure 1.2: Signal/image processing in the Radon space

## 1.2 Organization of the thesis

The thesis can be considered to consist of three parts, based on the applications: image analysis, compression, and applications involving 2-D power spectrum. Each of the chapters addresses a new application, the scope and significance of which, will become clear from the context. Review of the literature pertinent to a particular chapter/application is included in the corresponding chapter.

Chapter 2 presents a brief review of the RT, its properties, and image reconstruction from projections.

Description of an object invariant to geometric transformations is very useful in image analysis, object recognition and classification. An important class of invariants is that based on moments. The existing methods that address projection data involve an extraction of the 2-D moments from those of the projections, from which algebraic invariants are constructed. Chapter 3 introduces the notion of moment-patterns (MPs) in the RS, and formulates new moment-based invariants within the Radon space. A technique for rendering the MPs invariant to translation, scaling and rotation, is proposed. Further, an extension of the technique to 3-D is presented. A novel feature-set based on the moment-patterns, that is invariant to geometric transformations as well as contrast, is also developed. The new techniques are applicable to CT as well as spatial data.

Chapter 4 is devoted to an application of the notion of "instantaneous matched filter" (IMF) developed at the Centre [160], and for selective reconstruction of objects from noisy projections. The IMF involves a combination of the ideas of detection of an object of known shape and location, and an estimation of the associated parameter. In this sense, a signal of interest is separated from a noisy linear combination of known shapes in white noise. The IMF is analyzed from a discrete viewpoint, and some new observations are presented. A generalized version that does not require an explicit orthogonalization, is developed. The projections of the object of

interest, separated by the generalized IMF, are used to reconstruct the corresponding object. The method is applied as an alternative to simple subtraction-based methods when the densities of the objects vary by a factor.

The scope of data compression hardly needs an emphasis. Inspite of the tremendous advance in the field and the availability of commercial products, the ever increasing need for efficient representation of data for transmission and storage motivates further application-specific efforts. Chapter 5 represents such an effort, and addresses the compression of binary images in the RS. The application is twofold: (i) in CT, where the object is binary, and (ii) as a method of coding binary images. The basic idea involved is the fact that binary objects are often represented by a small number of projections. Additional compression can be achieved by coding the individual 1-D projections. The approach is extended to compress pictures with closed contours/boundaries. Finally, a new algorithm for reconstructing binary images from their projections collected a general CT scenario, is proposed.

The rest of the work involves topics associated with 2-D power spectrum. 2-D spectral factorization in the RS is considered. Some aspects of the RT associated with the RT of an SRF are studied, and a new approach to 2-D spectrum estimation in the RS is investigated.

The problem of spectral factorization in two-dimensions (2-D) is complicated by the lack of a fundamental theorem of algebra in 2-D. The theoretical aspects of 2-D spectral factorization are considered in Chapter 6. The RT reduces the 2-D problem to a set of independent 1-D problems, which are well understood. Apart from a mathematical point of view of providing a solution to the 2-D spectral factorization problem, the theory can be considered to be the heart of many applications involving signal modeling in the RS. New applications for modeling and processing CT data are indicated. An application involving LPC (linear predictive coefficients)-based invariants is described. The theory suggests a new method of 2-D spectrum

estimation, which forms the topic of Chapter 7.

The problem of estimating the 2-D PSD from SRF data is encountered in many fields of applications such as radar, sonar, geophysics, radio astronomy, and image processing. High resolution spectrum estimation in 2-D, however, has remained a difficult task. A brief survey presented in Chapter 7 is intended to highlight the problems and issues involved in 2-D spectrum estimation, and emphasize the scope of exploring different possibilities. A recent approach that is of particular interest, involves the use of the RT to split the 2-D problem to a set of 1-D problems that are easier to handle [204]. This method is based on the projections of the data modeled as a sample of an SRF. Chapter 7 discusses some of the issues that arise in the context of the RT, where the underlying 2-D signal is modeled as a sample of an SRF. A new mathematical representation for the RT of an SRF, valid upto second-order statistics, is developed. Although it leads to the same final results as those of Jain and Ansari [76], the development helps in highlighting some of the aspects not evident in [76, 204, 34], and their implications on the RT approach to 2-D spectrum estimation. Furthermore, some of the effects of inherent windowing of the 2-D data, ignored in the literature so far, are discussed. The difficulties in characterizing the line integral of an SRF, and the associated issues provide the motivation for investigating alternative approaches. A novel approach to 2-D spectrum estimation based on the RT of 2-D autocorrelation function (ACF) of an SRF, instead of that of the random field itself, is investigated. Estimation by autoregressive modeling is discussed, and an extension to the maximum entropy method is considered.

Simulation results are presented to illustrate the new techniques.

Chapter 8 concludes the thesis. It comprises of a summary of the work carried out and the scope for future work in the realm of signal processing in the Radon space.

# Chapter 2

# The Radon Transform

The purpose of this chapter is to provide a brief introduction to the Radon transform and review some of its properties used in this thesis. In the following section, the Radon transform is defined, and some basic properties are reviewed. The inverse Radon transform and some important algorithms for image reconstruction from projections are briefly discussed. Sampling considerations, the discrete Radon transform, and the computation of the Radon transform of digital data, with an incremental algorithm, are discussed. General references on the topic are the books by Deans [23], Gelfand et al. [39], Herman [54], Rosenfeld and Kak [183], and Jain [72].

## 2.1 The Radon transform

Let $\mathbf{x}$ denote points in the real n-dimensional space. The Radon transform (RT) of an n-dimensional function $f(\mathbf{x})$, is the integral of $f(\mathbf{x})$ over the family of hyperplanes of dimension n-1 defined by:

$$t = \zeta \cdot \mathbf{x} = \zeta_1 x_1 + \zeta_2 x_2 + .... + \zeta_n x_n \tag{2.1}$$

where $\zeta$ denotes a unit vector that defines the orientation of the hyperplane. The RT is given by:

$$\mathcal{R}\{f(\mathbf{x})\} = \int f(\mathbf{x})\delta(t - \zeta \cdot \mathbf{x})d\mathbf{x} = p(t, \zeta) \tag{2.2}$$

where, $\delta$ is the Dirac-delta function. The set of integrals evaluated over a set hyperplanes with the same orientation constitute a *projection* of $f(\mathbf{x})$ at that orientation. Accordingly, the t-$\zeta$ space is referred to synonymously as the *Radon space* (RS) or the *projection space.*

In two-dimensions (2-D), the RT of a function $f(x, y)$ is the integral of $f(x, y)$ over a family of straight lines on the plane containing the function.

$$\mathcal{R}\{f(x, y)\} = \int\int f(x, y)\delta(t - x\cos\theta - y\sin\theta)dxdy = p(t, \theta) \tag{2.3}$$

where,

$$t = x\cos\theta + y\sin\theta \tag{2.4}$$

is the parametric representation of the straight line.[1] The set integrals evaluated over a set of parallel lines constitute a projection $p(t, \theta)$. To emphasize the fact that it is a 1-D function, it will be denoted as $p_\theta(t)$. Fig. 2.1 illustrates the geometry. The space over which the RT is defined, reflecting the periodicity of $p_\theta(t)$ in $\theta$, is illustrated in fig. 2.1(b), and fig. 2.1(c) is the corresponding sketch for functions of finite support (one period is shown). Note that the set $\{p_\theta(t),\ -b \leq t \leq b,\ 0 \leq \theta \leq \pi\}$ (where $b$ denotes the spatial bound) constitute the RT.

It is important to note that the coordinates $\{(t, \theta)\}$ of the RS are *not* polar coordinates of $\mathbf{R}^2$. This is evident by the pictorial description of the space over which the RT is defined. This point is further clarified by noting that $p(0, \theta_1) = p(0, \theta_2) \iff \theta_1 = \theta_2$, in general.

It is easy to observe that not every function $p(t, \theta)$ is a *valid* RT i.e., the RT of some function $f(x, y)$. A function $p(t, \theta)$ is a valid RT provided it is the RT of some

[1] In geophysics, the slope-intercept form of a straight line is employed, and the RT is also referred to as 'slant stack' or the '$\tau - p$' transform.

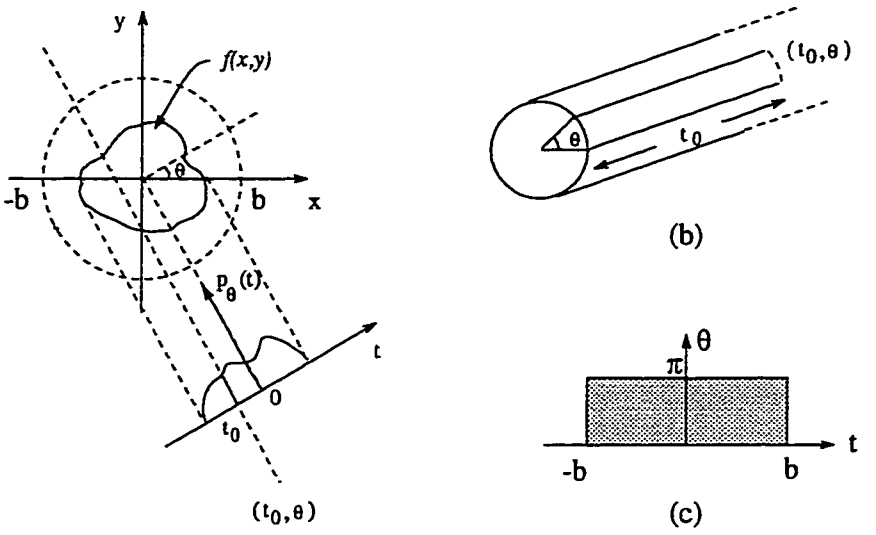


(a) Projection of f(x,y) at an angle θ

Figure 2.1: The Radon transform

function $f(x, y)$. It is easy to generate counter examples. One such is the set of all projections $p(t, \theta)$ of a function $f(x, y)$ in which, only one projection, say $p(t, 0)$ is modified in some way; eg., replaced by $cp(t, 0)$ where $c \neq 1$. Mathematically, a function will have to satisfy a set of consistency conditions to qualify to be a valid RT. These conditions are obviously related to the range of the RT [109].

The RT is essentially a multidimensional transform. In this thesis, the discussion will be restricted to 2-D functions, unless otherwise specified.

## 2.2 Properties of the Radon transform

**Linearity:**

The linearity of a transform is perhaps of foremost significance. The RT of a linear combination of two functions $\phi(x, y)$ and $\psi(x, y)$ is the linear combination of

the respective RTs:

$$p_\theta(t) = a_1\phi_\theta(t) + a_2\psi_\theta(t), \;\; \theta \in [0, \pi) \tag{2.5}$$

where, $\phi_\theta(t)$ and $\psi_\theta(t)$ are the RTs of $\phi(x, y)$ and $\psi(x, y)$ respectively.

**Relation to the Fourier Transform**

A very important and powerful result in the RT theory is its relation with the Fourier transform (FT), known as the central slice theorem (CST) or the projection slice theorem, stated below:

*Central slice theorem*: The (1-D) Fourier transform (FT) of the projection of a function at an angle $\theta$ is a slice of the 2-D FT of the function at the same angle. i.e.,

$$\mathcal{F}\{p_\theta(t)\} = P_\theta(\omega) = F(\omega\cos\theta, \omega\sin\theta) \tag{2.6}$$

A pictorial description of the CST is given in fig. 2.2[2]. Every projection contributes to a radial slice in the (2-D) Fourier space at the corresponding angle. Hence, it is possible to fill the 2-D Fourier space (on a polar grid) by taking the 1-D FT of the projections of $f(x, y)$ at various angles. The CST is the basis of a class of algorithms for image reconstruction from projections, called the direct Fourier method [122]. It also plays a key role in the RT theory and applications.

**Transform of Convolution**

The RT of a convolution of two functions $\phi(x, y)$ and $\psi(x, y)$ is a convolution of the respective RTs:

$$\mathcal{R}\{\phi(x, y) ** \psi(x, y)\} = \{\phi_\theta(t) * \psi_\theta(t)\} \tag{2.7}$$

where, $**$ and $*$ denote 2-D and 1-D (with respect to $t$) convolution operations respectively. Thus, the projection at an angle $\theta$, of the convolution of two functions, is the 1-D convolution of the respective projections of the two functions. This result

[2]Fig. 2.2 is schematic. The Fourier transform is sketched as a real and spatially bouned function, although it is generally neither real nor spatially limited, for illustrative purposes only.

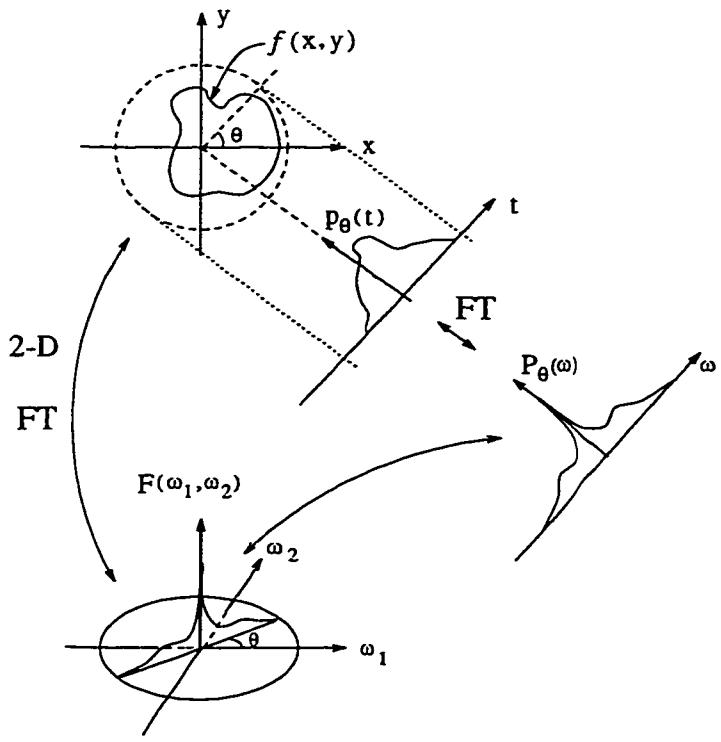


Figure 2.2: The central slice theorem

| | |
|---|---|
| *Mass Conservation* | $\int p(t,\zeta)dt = \int f(\mathbf{x})d\mathbf{x}, \forall \zeta$ |
| *Linearity* | $R\{c_1 f + c_2 g\} = c_1 Rf + c_2 Rg$ |
| *Homogeneity* | $p(\alpha t, \alpha\zeta) = \lvert\alpha\rvert^{-1} p(t,\zeta)$ |
| *Shift* | $R\{f(\mathbf{x}+\mathbf{b})\} = p(t+\zeta\cdot\mathbf{b},\zeta)$ |
| *Convolution* | $R\{f * *g\} = \{Rf * Rg\}$ |

Table 2.1: Some properties of the RT

is a direct consequence of the linearity of the RT and the CST. An implication of the above properties is the fact that a 2-D filtering operation can be achieved in the RS, by convolving each of the projections, with the corresponding projections of the 2-D filter (impulse response or the point-spread function [162, 72].

Some of the fundamental properties of the RT are listed in table 2.1. Its property with respect to rotation is of special use in this thesis, and is discussed in Chapter 3. Other properties and proofs are available in [23], and in [72], especially for the 2-D case.

## 2.3 The inverse Radon transform, and image reconstruction from projections

It is the invertibility of the RT that has made it extremely useful in CT, involving image reconstruction from projections. The inverse Radon transform (IRT) mathematically corresponds to solving the integral equation (2.2). A solution was published by J. Radon in 1917 [158], expressing $f(x,y)$ in terms of $p_\theta(t)$ [3] The general formula in n-dimensions depends upon whether $\mathbf{R}^n$ is of even or odd dimension [23]. It is desirable to have a single inverse formula regardless of dimension. The possibility of the existence of a unified formula can be appreciated by the fact that the CST is valid regardless of dimension. For a discussion on a unification of

[3]The line integral of a function has come to be referred to as the 'Radon transform' due to the inverse formula given by Radon.

the Radon inverse formula, see Deans [23] and the references therein. Recently, it has been observed that the results become zero when the dimension requirement is violated, resulting in a unified formula for the inverse RT of arbitrary dimensions [102].

Major image reconstruction algorithms fall into three broad categories: (1) the convolution or filter backprojection technique, based directly on the Radon inverse formula, (2) those based on the Fourier slice theorem, called direct Fourier inversion (DFI), and (3) the algebraic reconstruction techniques, based on an algebraic formulation of the forward and inverse problems. The first two of the reconstruction techniques mentioned above, are briefly discussed. A glimpse of ART is contained in Chapter 5.

In 2-D, the Radon inverse formula is given by:

$$f(x,y) = \int_0^\pi \tilde{p}_\theta(x\cos\theta + y\sin\theta)d\theta \tag{2.8}$$

where, $\tilde{p}_\theta$ is given by:

$$\tilde{p}_\theta(t) = p_\theta(t) * \phi(t), \qquad 0 \le \theta < \pi \tag{2.9}$$

where, $\phi(t) = \mathcal{F}^{-1}(|\omega|)$, and '$*$' denotes convolution. The variable $\omega$ has the dimensions of spatial frequency, and is referred to as the radial frequency variable. The operation in (2.8) is termed *backprojection*. The IRT is therefore the backprojection of convolved projections, and hence the name *convolution backprojection* (CBP) for reconstruction methods based on the above formula. Since convolution is equivalent to filtering, the CBP method is also referred to as the *filtered-backprojection* (FBP) method, especially when the filtering is performed in the frequency-domain. The following succinct notation for the inverse formula summarizes the CBP/FBP algorithm itself:

$$f(x,y) = \mathcal{B}\mathcal{C}\{\mathcal{R}f(x,y)\} = \mathcal{R}^{-1}\{\mathcal{R}f\} \tag{2.10}$$

where, $\mathcal{B}$ represents backprojection, and $\mathcal{C}$ denotes the operation of convolution (2.9) in the Radon space. $\mathcal{B}$ is the *adjoint* of $\mathcal{R}$, and is equivalent to a blurring by the

point-spread function $\frac{1}{\sqrt{x^2+y^2}}$, which is the Fourier inverse of $\frac{1}{\sqrt{\omega_1{}^2+\omega_2{}^2}}$. One can thus appreciate the role of the filtering function $|\omega| = \sqrt{\omega_1{}^2 + \omega_2{}^2}$ in the inverse formula, which can be conveniently implemented in its 1-D form in the projection domain, thanks to the CST.

The function $\phi(t)$ is not well-behaved, and is a singular distribution, making the problem ill-posed. One way to overcome this problem is to define a filter function $C(\omega) = |\omega|W(\omega)$, where, $W(\omega)$ is the FT of a smoothening window, $w(t)$. Several windows suggested have been named after the inventors [54]. However, the CBP algorithm has been the most popular one due to its accuracy. Further, the computation of the image intensities in the CBP method is cumulative, unlike that in the DFI techniques. The implications of this 'image evolution' process can be important in practice, as partial images could be produced with the collection of every projection [27]. Angular spacing of the projections need not be uniform. Further, point-by-point and 'region-of-interest' reconstruction are possible with the CBP.

Another class of reconstruction algorithms, based on the CST, is called Fourier inversion or direct Fourier technique [122]. The reconstruction procedure consists of three steps. The first step involves the computation of the FT of each of the projections, thus filling the 2-D Fourier space on a uniform polar grid. The values of the 2-D FT on the polar grid are then mapped onto a rectangular grid by interpolation. Finally, the 2-D function is reconstructed by a 2-D inverse DFT. An advantage of DFI is the speed it can afford.

Algebraic reconstruction techniques (ART), introduced by Gordon et al. [46], involve formulation of the projection-process as a multiplication of the image vector by a matrix of weights [45]. The IRT, or the process of reconstruction consists of an inverse of the matrix operating on the vector consisting of values of the RT. The method is generally iterative in nature, alternating between the projection and image domains, involving the re-projection of an estimated image. Although this method is computationally intensive and often involves huge matrices, there are

many situations in CT, such as those involving limited angle data and/or noise, in which it is superior to the conventional methods such as the CBP or Fourier methods. ART methods also allow the incorporation of prior knowledge and the use of estimation theory in image reconstruction.

A vast literature exists on the basic image reconstruction algorithms and their variants. A detailed description of computer implementation of image reconstruction formulas given by Rowland [54] is a useful reference. The simulation involving the projection and reconstruction of gray-level images, reported in this thesis, has utilized the software package SNARK'93[4]

## 2.4 Sampling considerations

In the previous section, the RT and the IRT of continuous functions were discussed. In general, an infinite number of continuous projections are required to represent a continuous 2-D function exactly. In practice, however, it is possible to work with a finite number of discrete projections. The number of projections required to represent a function depends upon the nature of the function. For example, a single projection is sufficient to represent a circularly symmetric function completely; $N$ projections of $N$ uniformly spaced points are sufficient to represent a bandlimited function of order N $\times$ N [122]. Thus, the number of projections, and the number of samples per projection, that adequately represent the function under consideration, is an important issue. This is the classical problem of sampling the RT, for which results already exist. If the RT is adequately sampled, the continuous RT can (in principle) be determined and the IRT found.

Traditionally, the sampling requirement on the RT has been considered as two independent problems: of finding the number of projections, and the number

[4]J.A. Browne, G.T. Herman, and D. Odhner, *A programming system for Image Reconstruction from Projections*, TR No. MIPG 198, Aug. 93, Medical Image Processing Group, University of Pennsylvania, Philadelphia, PA

of samples per projection. Each of these is solved by using the 1-D Shannon's sampling theorem, in conjunction with the CST. Several papers address the sampling requirement on the RT, and the results of Rattey and Lindgren [174] are given below. Let $f(x,y)$ be a function with finite space-bandwidth product, i.e., $f(x,y) \approx 0$, $x^2+y^2 \geq \rho^2$ and $F(\omega_1,\omega_2) \approx 0$, $\omega_1^2+\omega_2^2 \geq {\omega_m}^2$, $\omega_m$ being the bandlimit. Then, the minimum number of samples per projection is approximately,

$$N_m = (2/\pi)\omega_m \rho \tag{2.11}$$

The sampling requirement in the angular direction is obtained by assuming that the projection for each $\theta$ is known continuously in $t$ (by virtue of having imposed a sampling rate for each projection), and then invoking the CST. The minimum number of equispaced angles over $[0,\pi)$ at which the RT must be sampled is:

$$M_\theta = [\rho\omega_m] + 2 \tag{2.12}$$

where, $[\cdot]$ indicates a rounding off to the nearest integer.

By treating the problem as one in 2-D sampling theory, hexagonal sampling of the RT results in a requirement that is half of that corresponding to rectangular sampling, which is about as efficient as a rectangular sampling of the 2-D function itself [174].

The above specifications were based on the sampling theory. One can in general specify the number of projections representing an image ensemble, in terms of parameters representing the ensemble, in some optimal way. Such specifications would also be useful in being able to adapt projection acquisition to the associated parameters. For example, Ibikunle [61] has discussed an allocation of the number of projections for reconstructing an image ensemble represented by separable 2-D Gauss-Markov statistics, in terms of image smoothness and area, such that the average reconstruction distortion is minimized over an ensemble. In general, the sampling of the RT is based on available prior knowledge regarding the 2-D object and experience.

## 2.5 The discrete Radon transform

The discrete Radon transform (DRT) is defined in various ways in the literature. The phrase is often used to refer to a discretization of the RT. The DRT of a continuous function $f(x,y)$ therefore refers to the set of integrals along lines whose parameters are discretized. When the data is available on a discrete support, the DRT corresponds to the integrals of the discrete data along various straight lines on the plane containing the data grid. This invariably involves an interpolation of the available data values to a denser grid. Interpolation can be avoided by using the 'pixel' assumption to define the continuous image (which is often physically justified). When the DRT is computed using the pixel assumption or interpolation (as described in the next section), then the above two descriptions of the DRT become identical. In some situations, on the other hand, the DRT has been defined as the sum of values of the discrete data along straight lines passing through the lattice points. Thus, depending upon the application and computational convenience, the DRT has been defined in various ways. Scheibner [191] was the first to coin the word and give a systematic formulation of the DRT. The idea of DRT, however, began in the context of its application to seismic signal processing, where the slope-intercept form of the straight line is employed. In this thesis, the term DRT is understood to refer either to a discretization of the RT, or the RT of discrete data as defined in (2.13) or (2.14).

## 2.6 Computation of the Radon transform

In CT applications, the data is available in the form of a discrete set of projections of a continuous function. When the RT is to be used as a tool, the available 2-D data is generally discrete. Further, computer simulation involves digital data. Thus, it is necessary to approximate the RT of discrete data. The usual approach involves the 'pixel' assumption that is fundamental in digital image processing. This consists

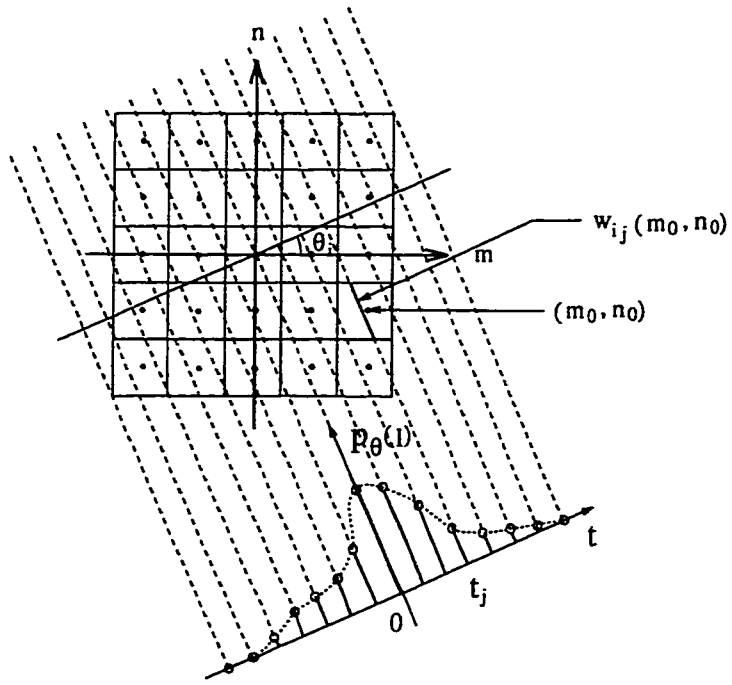


Figure 2.3: The Radon transform of digital data

of assuming a unit pixel with a constant value equal to the value of the data at that point, around each discrete point on the rectangular grid on which the data is available. The projection $p_{\theta_i}(t_j)$, along a line parameterized by the discrete variables $\theta_i$ and $t_j$, is approximated by a weighted sum of pixels along the linear path, as follows:

$$p_{\theta_i}(t_j) = \sum_m \sum_n w_{ij}(m,n) f(m,n) \tag{2.13}$$

where, $w_{ij}(m,n)$ are the weights, given by the length of intersection of the line with the corresponding pixels [54, 23]. The above approximation corresponds to the Riemann-sum approximation to the line integral. See Fig. 2.3.

Another approach to computing the RT involves obtaining an analytical expression for the same, by interpolating the discrete 2-D data into a continuous version and then applying the convolution theorem in the RS [140]. The RT can be computed for any $\theta_i$ and $t_j$ as a function of the values of $f(m,n)$ on a discrete grid,

as follows:

$$p_{\theta_i}(t_j) = \sum_m \sum_n h^{(I)}_{\theta_i}(t_j - m\cos\theta_i - n\sin\theta_i) f(m,n) \tag{2.14}$$

where, $h^{(I)}_\theta(t)$ is the RT of the interpolating function, $h^{(I)}(x,y)$. The RT computed as above is referred to as 'DRT in a continuous space'. The method is flexible as the interpolation function can be chosen depending upon the type of data under consideration. The pixel-assumption may be treated as a special case, but does not possess a simple analytical expression.

### An Incremental Algorithm

The linearity of the RT facilitates its computation in an incremental fashion, as the data arrives by rows/columns. The analytical formulation given by (2.14) is particularly amenable to such an incremental computation. The basic idea is to consider the image itself to be incremented (updated) with the rows being added one-by-one. To begin with, the DRT of the image, in which all the rows except the first are zero, is computed. As the second row arrives, the new image consists of the two rows. The DRT of the new image, is the sum of the DRT of the first image, and that of the second image in which all the rows except the second are zeros. Thus, the updated DRT is obtained by adding the 'incremental' DRT associated with the second row to that which has been computed. The rest of the computation proceeds in the same fashion, and by the time all the rows have arrived, the DRT of the complete image would have got fully updated.

The computation above may be made much faster by restricting the range of summation in (2.14) to within a small strip ($\pm\Delta t$) along the given line. Such a restriction also improves the accuracy of the line integral estimates. *The above algorithm can be used for the detection of straight lines in images*, similar to the Hough transform (HT), in an efficient way for data that comes in a row-row fashion. In this sense, it would serve as an *incremental HT*.

The ever increasing demand for fast computing and efficient implementation of

sophisticated algorithms in CT, and the growing number of applications of the RT, have resulted in a number of fast algorithms and dedicated hardware for computing the forward and inverse RT [57, 196].

# Chapter 3

# Moment-based Invariants

New image-invariants based on the moments of the projections of an image are developed. The notion of moment-patterns (MPs) in the RS is introduced. Properties of the MPs are studied. A method of rendering the MPs invariant to translation, scaling, and rotation, is presented. An extension of the technique to 3-D is presented. A means of retrieving the parameters of the geometric transformations is given. An alternative method of obtaining circular-shift and contrast invariant features from each of the translation and scale invariant MPs, resulting in a descriptor that is invariant to geometric transformations as well as changes in gray-scale, is proposed. The new descriptor is relatively smaller in size. The invariant descriptions are useful for analysis, recognition and classification of CT data, in the RS itself. The proposed approach can also be used for spatial data analysis. Illustrative simulation results are presented.

The moment-based invariants developed in this chapter are patterns in the Radon space. This is unlike the previous approaches involving algebraic combinations of 2-D moments.

## 3.1 Introduction

Description of objects invariant to geometric transformations such as translation, scaling, rotation, and contrast (intensity scaling) is useful in image analysis, and object recognition and classification. Such an invariant description is usually in terms of a set of numbers, referred to as invariants or features. The feature-set computed from a given image may be compared with that of a reference object for recognition and classification.

There are many approaches to obtaining invariant descriptions based on different types of feature-sets, such as cross-correlation, Fourier descriptors, moment-based invariants, and autoregressive models. The choice of a certain approach and the associated feature-set depends upon the particular application under consideration. For example, Fourier descriptors and autoregressive models are used to describe closed boundaries extracted by suitable pre-processing. Moment-based invariants, introduced by Hu [58], are applicable to a general class of images, and have been a subject of extensive research in image processing [211, 111, 175, 1, 213, 177, 151, 43, 222, 52, 10, 123].

The classical Hu-invariants involving a combination of moments, are based on algebraic theory of invariants. Modification of the Hu invariants to handle changes in contrast was suggested by Maitra [111]. Orthogonal moments based on Zernike polynomials were studied by Teague [211] from the point of view of constructing invariants, as well as of reconstruction. Radial and angular moments [175] and complex moments [1] have been proposed as alternative and simpler means of deriving invariants. Analysis with respect to image representation ability, sensitivity to noise and discretization, and information redundancy have been considered by [1, 212, 213, 151].

In many applications in CT, the ultimate objective is rather a recognition and classification of an object, and not its reconstruction. It is useful to develop invariant descriptions of an object directly from its projections i.e., data in the RS,

than from a reconstructed image. Further, it is desirable to construct the invariants within the RS. Past efforts on the construction of invariants from the projections include the use of moments [190, 57, 43, 222, 52], and the use of transforms [153]. Extraction of some basic details of the image from certain low-order moments of the projections has been considered in [57, 190]. The construction of algebraic invariants in the image space by solving for the (2-D) moments of the object from those of the projection data had been proposed in optics [43, 222][1]. A generalization of the approach, with applications to CT, has been described by [52]. It involves the inversion of a matrix, the size of which grows with the number of moments (a considerable number would be required since segmentation is not possible), and the numerical stability of the approach is yet to be investigated. Very recently, the reconstruction of a function from its noisy projections via an estimation of the orthogonal (Legendre) moments of the 2-D function has been considered [124, 125]. All of the above methods require a computation of the 2-D moments from those of the projections, constituting an inverse problem. An invariant description of the image in the RS, based on a successive application of the FT in the two variables, has been proposed [153]. However, the method disregards phase information and cannot handle geometric scaling[2].

In this chapter, new image invariants based on a set of moment-patterns (MPs) in the RS is investigated. The set of moments (of a certain order) of all the projections constitute a MP (of that order) in the RS[3]. It is shown that appropriately scaled central moments of the projections are invariant to translation and scaling. Rotation may be found out by "matched filtering with circular shift" (circular correlation), or by the use of a formula for orientation. Once the rotation is known,

[1]A hybrid (optical-dsp system) implementation of the algorithm has been reported recently [230].

[2]It is interesting to note that by replacing the application of the FT over the t-variable by the 1-D Mellin transform, invariance to scaling can be achieved [15].

[3]The use of even- and odd-'parity' moments have been considered for orienting the projections to facilitate image reconstruction in electron microscopy [189].

the MPs are suitably centered to produce invariant patterns of moments in the RS itself. An alternative approach involving circular-shift-invariant descriptors of the translation and scale invariant MPs is also proposed. The approach presented in this chapter is particularly useful when the data is available in the RS, in applications such as NDT, medical and radar imaging, to name a few. The major advantage is that the invariant pattern is in the RS, allowing recognition and classification without having to post-process the reconstructed image.

Properties of the RT relevant to this chapter are reviewed in the following Section. The notion of MPs in the RS is introduced in Section 3. A method of rendering them invariant to geometric transformations is described, and a means of extracting the parameters of the geometric transformations is given. An extension of the technique to 3-D is also described. A new image descriptor based on the normalized MPs is presented in Section 4. Simulation results are presented in Section 5, and the chapter is concluded in Section 6.

## 3.2 Relevant properties of the Radon transform

*Translation*: A translation of the object results in angle-dependent translations along the spatial variable of the projections:

$$\mathcal{R}\{f(x-t_x, y-t_y)\} = p_\theta[t-(t_x\cos\theta + t_y\sin\theta)]\} = p_\theta(t-t_\theta) \tag{3.1}$$

*Scaling*: A scaling of the object in the image space results in a scaling of the projections in the spatial variable, as well as in an intensity scaling. Using the superscript $s$ to denote the quantity after scaling, then:

$$\mathcal{R}\{f(\frac{x}{\lambda}, \frac{y}{\lambda})\} \triangleq p^s{}_\theta(t) = \lambda p_\theta(\frac{t}{\lambda}), \quad \forall\theta \tag{3.2}$$

*Rotation*: Let $\phi \in [0, 2\pi)$ be the angle of rotation of the object, $f(x,y)$. It is noted here that $p_{\theta+\pi}(t) = p_\theta(-t)$. Although the RT is completely defined over $\theta \in [0,\pi), \forall t$, due to the above property, it is periodic in $\theta$ with a period of $2\pi$. Using

*tilde* to denote periodicity, $\{p_\theta(t), \theta \in [0, 2\pi)\}$ is one period of $\tilde{p}_\theta(t)$. Mathematically, $\tilde{p}_\theta(t) = \tilde{p}_{\theta+2k\pi}(t), \ \forall k \in I$, so that $p_\theta(t) = \tilde{p}_\theta(t) w_{2\pi}(\theta)$, where, $w_{2\pi}(\theta) = 1, \theta \in [0, 2\pi)$ and 0 elsewhere. A rotation of the object by an angle of $\phi$ results in a linear shift of $\tilde{p}_{\theta+\phi}(t)$ in the variable $\theta$; i.e., $\mathcal{R}\{f_\phi(x, y)\} = \tilde{p}_{\theta+\phi}(t), \ \forall\theta$. Using the superscript $r$ to denote the transform of a rotated object, $p_\theta^{(r)}(t) = \tilde{p}_{\theta+\phi}(t) w_{2\pi}$ is a circularly shifted version of $p_\theta(t)$ in $\theta$ by $\phi$. Thus, a rotation of the object results in a circular shift of the transform in the angle-variable.

## 3.3 Moment-patterns in the Radon space

A projection $p_\theta(t)$ of an image $f(x, y)$ at an angle $\theta$, is a 1-D function in the variable $t$. The moment of order $k$ associated with a projection $p_\theta(t)$ is given by:

$$m_k(\theta) = \int t^k p_\theta(t) dt \tag{3.3}$$

The above moments are referred to simply as the moments, or as the 'usual' or 'regular' or 'geometric' moments. Note that $m_0(\theta) = m_{00}$ (two subscripts denote a 2-D moment associated with the object) is the 'mass' of $f(x, y)$, and is independent of $\theta$. Further, $\bar{t}_\theta \triangleq \frac{m_1(\theta)}{m_0(\theta)}$ is the centroid of the projection $p_\theta(t)$.

The set of moments associated with the set of all projections $\{p_\theta(t), \forall\theta\}$ constitutes a 'moment-pattern' (MP). In particular, the set $\{m_k(\theta), \forall\theta\}$ is referred to as an MP of order k, in the RS.

The MPs involving the usual moments are not invariant to translation, scaling or a rotation of the object $f(x, y)$. However, the MPs can be manipulated into patterns in the RS, invariant to geometric transformations of the 2-D object, as described in the following.

### 3.3.1 Invariant moment-patterns

The usual approach to describe an object in terms of the moments of its projections involves a computation of the 2-D moments from which the 2-D (algebraic) invariants are constructed. In this section, MPs in the RS are rendered invariant to geometric transformations of the 2-D objects, by suitable modifications. The resulting modified MPs are referred to simply as the invariant MPs.

#### Translation-invariance

A translation of the object will produce translations in the projections, the moments of which will turn out be the moments with respect to the associated translations. The use of central moments eliminates the effects of translation. The patterns $\{\mu_k(\theta),\ \forall\theta\}$ in the RS involving the central moments,

$$\mu_k(\theta) = \int (t - \bar{t}_\theta)^k p_\theta(t) dt \tag{3.4}$$

where $\bar{t}_\theta$ is the centroid of $p_\theta(t)$, are therefore translation-invariant. Note that $\mu_0(\theta) = \mu_{00} = m_{00}$ is a constant ($\mu_0$), and $\mu_1(\theta) = 0$, $\forall\theta$. In the subsequent discussion, MPs refer to central MPs unless stated otherwise.

#### Scale-invariance

A scaling of an object will scale the values of the associated moments in the RS. It is shown below that scale-invariance of the moments in the RS can be achieved by an appropriate normalization of the moments. Consider the projection (at a specific angle $\theta$) of an object $f(x, y)$ scaled in terms of the parameter $\lambda$. From (3.2), it can be shown that:

$$\begin{aligned} m^s_k(\theta) &\triangleq \int t^k p^s{}_\theta(t) dt \\ &= \lambda^{2+k} \int \alpha^k p_\theta(\alpha) d\alpha = \lambda^{2+k} m_k(\theta) \end{aligned} \tag{3.5}$$

Thus,
$$m^s_0(\theta) = \lambda^2 m_0(\theta); \qquad m^s_1(\theta) = \lambda^3 m_1(\theta) \tag{3.6}$$

Let $\bar{t}_\theta^s \triangleq \frac{m_1^s(\theta)}{m_0^s(\theta)} = \frac{\lambda^3 m_1(\theta)}{\lambda^2 m_0(\theta)} = \lambda \bar{t}_\theta$. The central moment of order $k$, associated with a projections $p_\theta(t)$ is given by:

$$\begin{aligned} \mu_k^s(\theta) &= \int [t - \bar{t}_\theta^s]^k \lambda p_\theta(\frac{t}{\lambda}) dt \\ &= \lambda \int (\lambda\alpha - \bar{t}_\theta^s)^k p_\theta(\alpha) \lambda d\alpha \\ &= \lambda^{2+k} \mu_k(\theta) \end{aligned} \tag{3.7}$$

From the above, it can be shown that scale-invariance may be achieved by normalizing the central moments as follows:

$$\eta_k(\theta) = \frac{\mu_k(\theta)}{\mu_0^{(k+2)/2}} \tag{3.8}$$

The proof of invariance of $\eta_k(\theta)$ to scaling is given in Appendix-A2. The set $\{\eta_k(\theta),\ \theta \in [0, \pi)\}$ is an MP (of order k) that remains invariant under translation and scaling.

### Rotation-invariance

It is shown in Appendix A-1, that the central MPs of odd orders change sign under a shift by $\pi$, whereas the even-ordered MPs remain invariant. Thus, a rotation of the object induces a circular shift on even-ordered MPs, and a circular shift with a change of sign, on odd-ordered MPs, considered over $[0, \pi)$. Over the interval $[0, 2\pi)$, however, both are (simply) circularly shifted. Hence, the even- and odd-ordered MPs have a period of $\pi$ and $2\pi$ respectively. Since the rotation is over $[0, 2\pi)$, it is possible to find the circular shift suffered by an odd-ordered MP over $[0, 2\pi)$ and use it to 'center' the MPs by an appropriate circular shift. Indeed, all the projections/MPs suffer the same circular shift.

In practice, one can only work with a discrete set of projections, and let $N_p$ denote the number of projections. Thus, an MP of any order consists of $N_p$ discrete values. Let $s(m)$ denote the $(2N_p - 1) \triangleq$L-point sequence corresponding to the

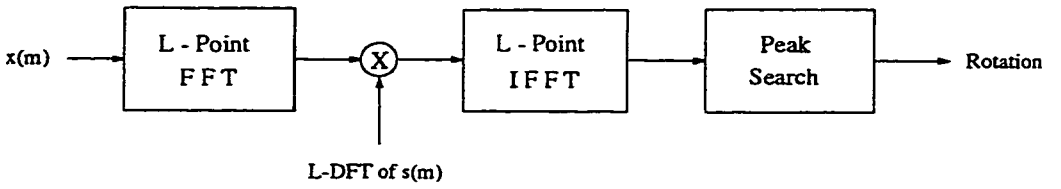


Figure 3.1: Finding the rotation by circular correlation.

reference third order MP and $x(m)$ the corresponding pattern computed from the projections of a rotated object. Let

$$y(n) = \sum_{m=0}^{L-1} s_n(m)x(m), \qquad 0 \leq n \leq L-1 \tag{3.9}$$

where, the suffix denotes (the extent of) circular shift. It is shown in Appendix A-3 that, if $x(m) = s_i(m)$, the point $i$ represents a maximum value in $y(n)$, and that it is unique (except in the case of $s(n)$ being periodic or a constant). Hence, the point corresponding to the maximum value in $y(n)$ will give the circular shift of $x(m)$ with respect to $s(m)$. The above procedure, of circular cross-correlation followed by peak-detection, is referred to as "matched-filtering with circular shifts". Since a circular convolution of two sequences can be obtained by multiplying the respective DFTs [143] the above procedure may be implemented using a 1-D FFT as shown in the block diagram in fig. 3.1.

In the method described above, the number of projections $N_p$ determines the accuracy/resolution of the estimate of rotation, and hence useful when a large number of projections are available. An alternative approach consists of subtracting an estimate of the orientation from the reference orientation. This requires solving for $m_{11}$ from the second-order moments of 3 projections, as shown in Appendix A-4.

Rotation-invariance may be imparted to the MPs by 'centering' them by circular shifts equal to the angle of rotation obtained from the previous step. The resulting 'centered' (denoted by the subscript c), scaled, central MPs,

$$\gamma_k \triangleq \{\eta_{k_c}(\theta),\ \theta \in [0, \pi)\}, \qquad k = 2, 3, ...M \tag{3.10}$$

represent the object $f(x,y)$ invariant to scaling, translation and rotation. $M$ is the order of the highest moment considered. The values of $k \geq 2$ are considered since $\mu_0$ is a constant and $\mu_1$ is zero. The set $\gamma_k$ is referred to as an invariant MP (IMP) of order $k$.

The MPs described above are not invariant under a change of contrast (intensity scaling). However, an intensity scaling of the 2-D object by a factor $c$ preserves the shape of the MPs, but scales them by $c^{-k/2}$. A method of achieving invariance to intensity scaling is described in the next section.

An object $g(x,y)$, representing a geometrically transformed version of a reference object $f(x,y)$, may be compared by computing the IMPs $\{\gamma_k,\ k{=}2,3,...M\}$, and comparing them with the reference IMPs, $\{\gamma_k^r\}$. A normalized mean-square error (NMSE) between each of the 1-D patterns may be employed for the purpose:

$$NMSE_k = \frac{\sum_{j=0}^{N-1} e_k^2(\theta_j)}{\sum_{j=0}^{N-1} \gamma_k^{r^2}(\theta_j)}, \qquad k = 2,3,...M \tag{3.11}$$

where,

$$e_k(\theta_j) = \gamma_k(\theta_j) - \gamma_k^r(\theta_j),\ j = 0,1,2,...N-1, \quad k = 2,3,...M \tag{3.12}$$

A weighted overall measure:

$$E = \sum_{k=2}^{M} w_k\, NMSE_k \tag{3.13}$$

where, the weights $w_k$ are chosen to represent the significance one wishes to attach to a the moment of a certain order, can be used for discrimination. The choice of weights, the number of projections, $N_p$, and the number $M$ of the highest order MP to be considered, depend upon the class/complexity of objects to be represented, the presence of noise, etc. In simple cases, a cursory look at a few low order MPs maybe sufficient for discrimination.

### 3.3.2 Registration

The parameters of geometric transformation of an object in an image are useful features in image analysis and object localization. The process of finding those parameters from a given image of the object is referred to as registration (or localization, if only the position is of interest). The parameters of the geometric transformation can be easily obtained from the moments computed in the RS. Rotation may be estimated by the method described above, or by using the formula involving the moments of 3 projections. Translation is given by the difference in the centroids of the given and the reference images: $(X_c, Y_c) - (X_c, Y_c)_r$. The ordered pair $(X_c, Y_c)$ is the centroid of the object, the coordinates of which are given by the centroids of the horizontal and vertical projections respectively: $X_c = \bar{t}_0$, and $Y_c = \bar{t}_{\pi/2}$. The scale-factor is given by: $\lambda = \sqrt{m_0(0)/m_{0_r}}$. The suffix '$r$' in the above denotes the quantities associated with the reference object.

### 3.3.3 Extension to three dimensions

Consider the RT of a function $f(\mathbf{x})$, $\mathbf{x} \in \mathbf{R}^3$:

$$\mathcal{R}\{f(\mathbf{x})\} = \int f(\mathbf{x})\delta(t - \mathbf{x}\cdot\xi)d\mathbf{x} \triangleq p(t,\xi) \tag{3.14}$$

where, $\xi$ is a unit vector defining the orientation of the plane $t = \mathbf{x}\cdot\xi$ over which integration is carried out. The collection $\{p(t,\xi), \forall t\}$ for a given $\xi$ characterized by $\phi$ and $\psi$, is a projection at that orientation. A projection may be viewed as a parameterized 1-D function $p_\xi(t)$, or $p_{\phi,\psi}(t)$. The set of all projections at various orientations $\phi, \psi \in [0, \pi)$ constitutes the RT.

As in the 2-D case, a translation of the object $f(\mathbf{x})$ results in orientation-dependent translations in the projections of $f(\mathbf{x})$, which can be handled by using central moments. The projection of an object scaled in terms of the parameter $\lambda$ can be shown to be scaled as follows:

$$\mathcal{R}\{f(\frac{1}{\lambda}\mathbf{x})\} \triangleq p^s_\xi(t) = \lambda^2 p_\xi(\frac{t}{\lambda}) \tag{3.15}$$

The central moment of order $k$ associated with the scaled projection $p_\xi(t)$ is related to that associated with the reference object, by:

$$\mu_k^s(\phi,\psi) = \lambda^{3+k}\mu_k(\phi,\psi) \tag{3.16}$$

Hence, the central moments normalized as below, are invariant to scaling:

$$\eta_k(\phi,\psi) = \frac{\mu_k(\phi,\psi)}{\mu_0^{\frac{k+3}{3}}} \tag{3.17}$$

The set $\{\eta_k(\phi,\psi),\ \phi,\psi \in [0,\pi)\}$, is a 2-D MP invariant to scaling and translation of the object. A rotation of $f(\mathbf{x})$ in $\mathbf{R}^3$ results in a 2-D circular shift of the RT considered over $\phi,\psi \in [0,2\pi)$, and a corresponding shift in the MPs. The shift can be determined by a 2-D version of matched filtering with circular shifts. Experiments with simple shapes have confirmed a single peak, and a formal proof of uniqueness of the maximum of circular (auto) correlation would be useful. Alternatively, an expression for the orientation based on the moments of the projections can be formulated.

The above approach would be useful in 3-D tomographic applications. For example, if $f(\mathbf{x})$ is the characteristic function of a bounded region (shape), $p_{\phi,\psi}(t)$ gives the cross-sectional area of the shape at an orientation defined by $\phi$ and $\psi$, at distance $t$ from the origin. In radar scenario, the area-functions of a 3-D object may be obtained from the object's far-field backscattered ramp responses [22].

Registration is accomplished in a manner analogous to that in the 2-D case.

**Remarks:**

1. The definition and analysis of moments are based on integrals of continuous functions. In practice, however, one usually works with digital data and the formulation is replaced by summation for computational ease. Such a formulation leaves the invariance to translation unaffected, while the invariance of the

normalized moments to scaling does not hold good strictly. The effects of discretization, and the improvement possible by employing numerical integration techniques for approximating the moments, are discussed in [212].

2. Moment-based invariants have generally been applied in situations involving no noise, or a level of noise low enough for the effects to be negligible. The presence of noise affects the values of higher order moments more severely, as evident from the associated kernel. Noise also affects the values of the mass and centroid, which in turn affect the normalizations critical to invariance. An analysis of the effects on the invariants is rather involved due to the nature of the relationships involved. Useful properties of moments have resulted in a growing interest in investigations into the effects of noise on moment-invariants [1, 213, 151].

   The effect of additive noise on the 1-D moments considered in this chapter is expected to be similar to that in the 2-D case. The effect on the regular MPs is somewhat uniform. The effect of additive zero-mean white noise independently on each of the projections, is equivalent to the addition of a sequence of uncorrelated RVs of equal variance (depending upon the order) to a regular MP. An analysis of the case involving additive noise on the 2-D data is, however, complicated due to the difficulty in characterizing the RT of a stationary random field (discussed in Chapter 7). In general, higher order moments are vulnerable to the presence of noise as well as discrete approximations involved in processing, which limits the number of moments that can be used, in conflict with the desire to use a large number of moments for better representation [1, 213, 151].

## 3.4 An alternative approach

In the previous sections, MPs in the Radon space were studied, and a method of rendering them invariant to geometric transformations was discussed. The foregoing approach relies on the accuracy of the estimated rotation. Further, the IMPs do not remain invariant under a change in gray-scale. In this section, an alternative set of descriptors based on the MPs are developed. The basic idea is to utilize the circular autoregressive (CAR) modeling [83], that provide features invariant to circular shifts and amplitude scaling of sequences. Specifically, if $s(n)$ is an $N_p$-point sequence, it can be described by a CAR model:

$$s(n) = \alpha + \sum_{i=1}^{m} a_i s(n - n_i) + \sqrt{\beta} w(n), \quad n \in [1, L] \tag{3.18}$$

where, $\{n_i,\ i = 1, 2, ..m\}$ are integers such that the above model is autoregressive, taking into account the periodicity of $s(n)$. The sequence $\{w(n)\}$ consists of independent, identically distributed normal RVs. The parameters $\{a_i,\ i = 1, 2, ..m\}$ and $c = \alpha/\sqrt{\beta}$ are invariant under circular shifts and amplitude scaling of the input sequence. Thus, when each of the MPs is modeled as CAR, the resulting set of features:

$$\{a_{i,k}, c_k : \quad i = 1, 2, ..m,\ \ k = 2, 3, ..M\} \tag{3.19}$$

are invariant descriptors of a given object. *Note that invariance to intensity scaling is also achieved.* In general, the order of the CAR model depends upon the class of objects to be represented. For the purposes of object recognition and classification, it is usually possible to work with low model orders. This results in a parsimonious representation, compared to the invariant MPs discussed in the previous section. Thus, the new approach reduces the size of the feature space required to represent the MPs.

Due to the approximations and digitization, invariance of the MPs and CAR parameters will only be approximate. Consequently, the patterns computed from various instances of scaling, translation and rotation will form close clusters in the

feature space. Hence, suitable schemes based on the principles of statistical pattern recognition and decision theory will have to be devised for object classification.

## 3.5 Simulation

Simulation has been performed with simple gray-level and binary objects for illustrating the proposed techniques. The rotated versions of the images were generated using the nearest-neighbor interpolation[4]. Scaling of the 2-D object has been performed by successive scaling in the two orthogonal directions. The 'interp' function of MATLAB was used for the interpolation required. The projections of the images were computed using SNARK '93. Note that the images and the transformations displayed are amplitude-scaled for clarity. Note that the X-axis associated with the plots of the MPs, is the projection-angle $\theta$.

The first example consists of a simple two-lobed gray-level object of size 255×255 shown in fig. 3.2(a). Reference MPs of the object were computed using 180 projections, as described in Section 3, and stored for comparison. A scaled, rotated and translated version of the object is displayed in fig. 3.2(b). A scaling factor of $\lambda = 2$ was used, and the object was rotated by 45 degrees. figs. 3.2(c) and (d) display the respective RTs. The reference MPs are shown in fig. 3.3(a) and (b). The second and third order normalized central MPs of the modified image are displayed in fig. 3.3(c) and (d), from which, the effect of rotation on the MPs is clear. The rotation estimated by circular correlation was 44 degrees. The small difference may be attributed to the effects of errors in generating the modified version. The IMPs of order 2,3,4 and 5, computed from the projections of the modified image, and overlapped on the corresponding reference MPs, are displayed in fig. 3.3 (e)-(h).

A shape created by a simple thresholding of the object of fig. 3.2, displayed in fig. 3.4(a), is the second example. A modified image with $\lambda = 2$ and a rotation of

[4]In general, better interpolation schemes can be used to minimize errors.

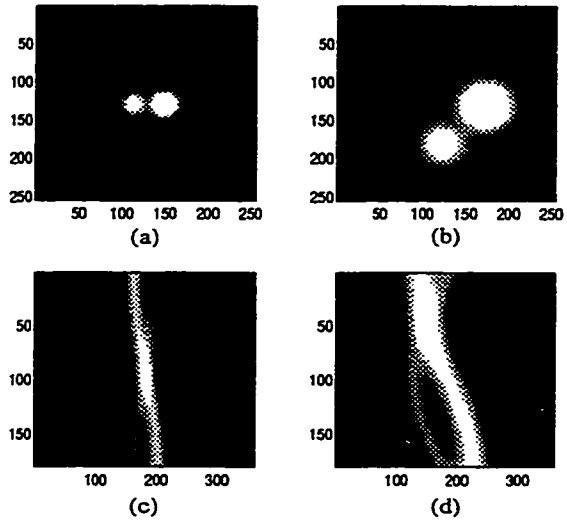


Figure 3.2: (a) Reference object, (b) modified object, (c) RT of the reference object, and (d) RT of the modified object.

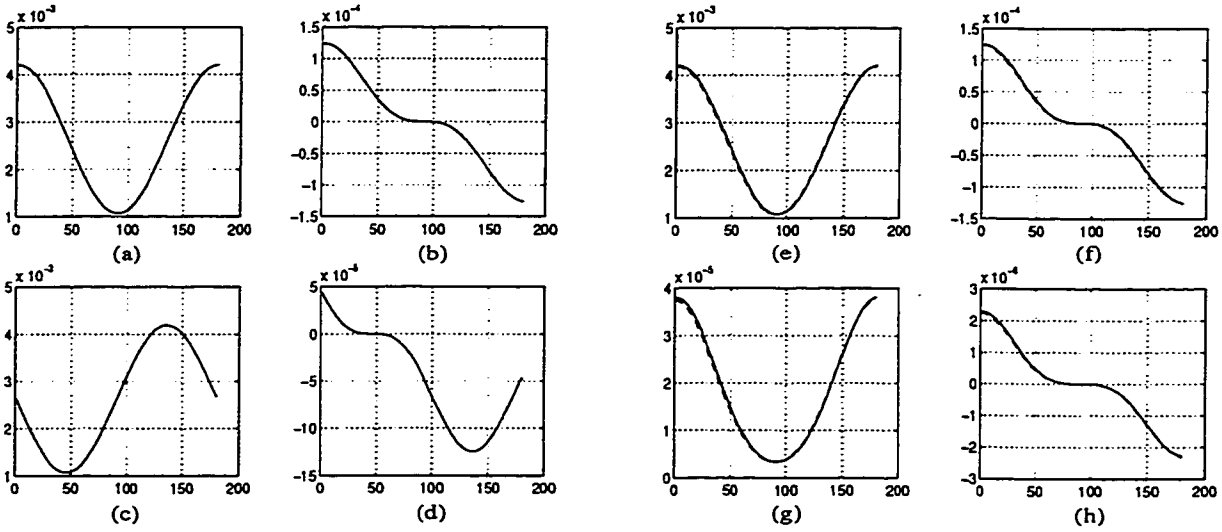


Figure 3.3: (a) Reference second order MP, (b) reference third order MP, (c)-(d): second and third order normalized central MPs of the modified object, showing the effect of object-rotation on the MPs. (e)-(h): Invariant MPs of order 2-5 superimposed on the respective reference MPs.

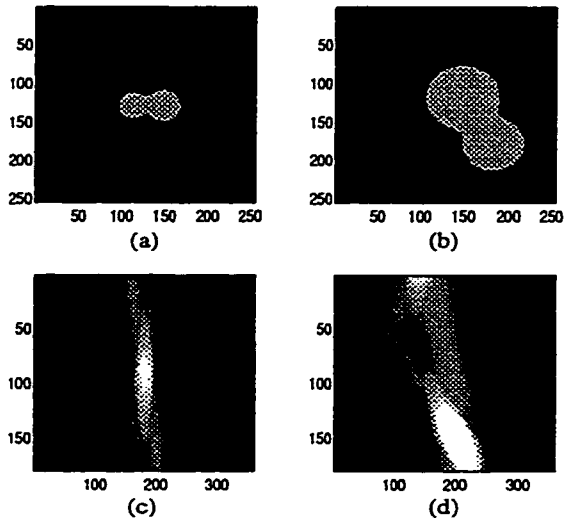


Figure 3.4: (a) Reference object, (b) modified object, (c) RT of the reference object, and (d) RT of the modified object.

120 degrees is shown in fig. 3.4(b). Figs. 3.4 (c)-(d) display the corresponding RTs.

The estimated rotation for this case was 119 degrees. Four of the IMPs are displayed in fig. 3.5, overlapped on the references as before. Note that the third order IMP of the reference image itself is noisy (less smooth) compared to that of the geometrically transformed version. This is because of the effects of digitization in small shapes in comparison with those in bigger versions. Note that, although this object is similar in appearance to the first, its third order MP is quite different, exhibiting the difference in the gray-level content of the objects.

Fig. 3.6 displays a 'plane' image of size $129 \times 129$, the third example. The modified object was obtained by rotating it clockwise by 50 degrees, and translating the result. The estimated rotation was accurate. The results are displayed in figs. 3.7.

Table 3.1 lists the errors (3.13) computed with uniform weights, with 10 MPs considered. The values are scaled by $10^6$. RO refers to the reference objects, and MO to the modified objects. The presence of errors between the MPs of the reference object and the corresponding modified objects is due to the effects of digitization, and simple methods of generating the modified versions, and can be ignored. On the

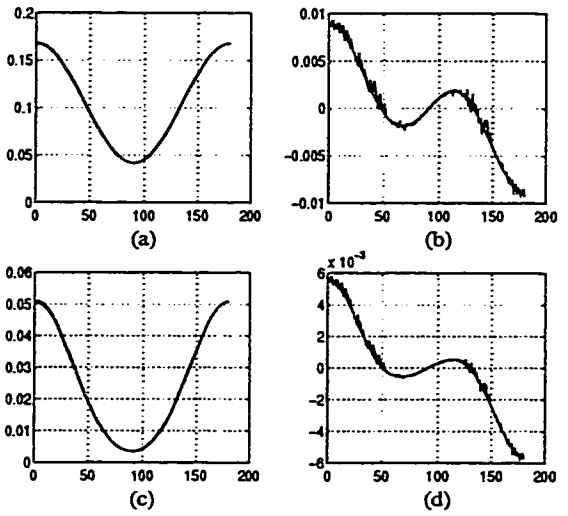


Figure 3.5: (a)-(d): Invariant MPs of order 2-5 superimposed on the respective reference MPs.

other hand, one can appreciate the ability to discriminate in presence of such errors. The relatively high magnitude of the errors associated with the objects 2 and 3 with respect to the object 1 is due to the gray level of object 1 being normalized. The apparent confusion due to the the difference in scale between the error values can be appreciated by considering the binary objects (2 and 3) separately. It is remarked that the errors considered over two patterns were sufficient for discrimination.

Table 3.5 lists the values of the CAR parameters (of order 3) of the third order MPs of the reference and those of the corresponding translated, scaled, rotated and amplitude-scaled versions. Since $\alpha$ is zero for central MPs over $[0, 2\pi)$, so is the invariant $\alpha/\sqrt{\beta}$ for all the cases. In general, CAR parameters were found to be sensitive to the presence of noise. This can be seen from the parameters associated with object 2. It was found that the optimum model order differs from one object to another, and the reference model order will have to be pre-determined.

The MPs illustrated above are smooth, due to a large number of projections being considered, reflecting redundancy. The number projections, and the number

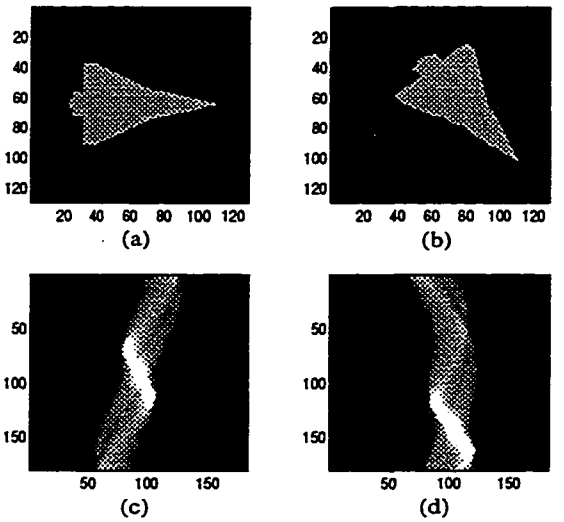


Figure 3.6: (a) Reference object, (b) modified object, (c) RT of the reference object, and (d) RT of the modified object.

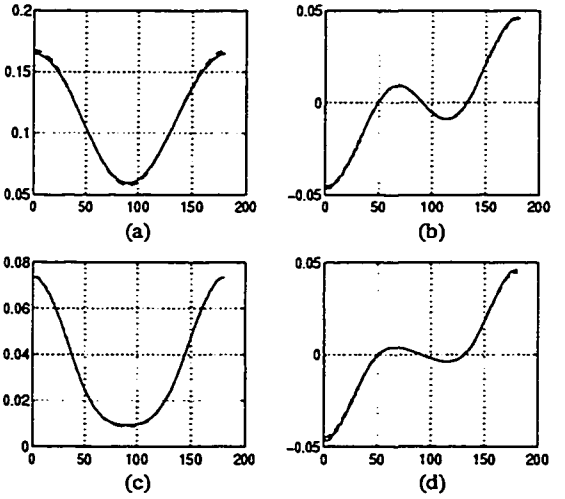


Figure 3.7: (a)-(d): Invariant MPs of order 2-5 superimposed on the respective reference MPs.

| | MO. 1 | MO. 2 | MO. 3 |
|---|---|---|---|
| RO 1 | 1.6711 | 2.2960e+17 | 3.2286e+20 |
| RO 2 | 991.9828 | 3.0603 | 2.2909e+05 |
| RO 3 | 994.5697 | 611.8721 | 3.8666 |

Table 3.1: Errors (3.13), multiplied by $10^6$.

of MPs may be chosen depending upon the complexity of the object and the particular application under consideration. For example, in some simple cases, a visual examination of a few low-order MPs may be sufficient for discrimination. A small number of CAR parameters of a few projections may be sufficient to discriminate objects of another class. On the other hand, the method may not be beneficial over the conventional methods for some classes.

A preliminary simulation has been carried out to study the effects of noise on the MPs. Sequences of uniformly distributed RVs of variance .05 were added to the projections of the 'plane' image. The resulting regular MPs are shown in fig. 3.8(a)-(d), and corresponding invariant MPs are shown in fig. 3.8(e)-(h). The effect on invariant MPs is more severe as the normalizing factors themselves get affected by noise. However, it is interesting to observe that the effect on regular MPs is relatively less severe and somewhat uniform over each pattern.

In the procedure discussed in this chapter, the presence of noise can be accounted for, to some extent, by choosing proper error-weighting function in (3.13). A further analysis of the effects of noise on the MPs would be useful for evolving methods for combating the same. For example, it may be advantageous to construct invariants based on the regular MPs.

| | RO. 1 | MO. 1 | RO. 2 | MO. 2 | RO. 3 | MO. 3 |
|---|---|---|---|---|---|---|
| $a_1$ | 2.1286 | 2.0955 | 0.5519 | 1.3474 | 1.3894 | 1.2752 |
| $a_2$ | -1.2661 | -1.1933 | 0.2886 | 0.2377 | 0.0464 | 0.3679 |
| $a_3$ | 0.1370 | 0.0973 | 0.1549 | -0.5872 | -0.4378 | -0.6453 |

Table 3.2: CAR parameters of the normalized central-MPs of order 3.

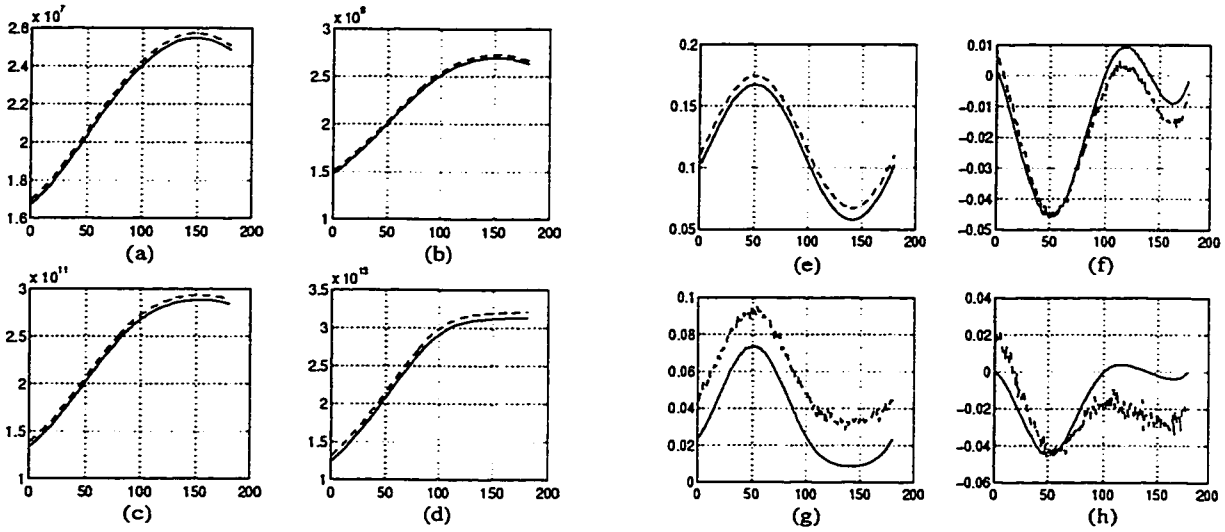


Figure 3.8: (a)-(d): Regular MPs of order 2-5. Solid and the dotted patterns correspond respectively, to the clean and noisy projection data. Figures (e)-(h) display the corresponding invariant MPs.

## 3.6 Conclusion

The notion of MPs in the Radon space has been introduced. A method of rendering the MPs invariant to geometric transformations has been presented. Invariance of the MPs to translation was obtained by employing central moments, and that to scaling by a simple normalization. Invariance to rotation was achieved algorithmically by circularly shifting the MPs suitably by an estimated rotation. Rotation was estimated by circular correlation via the FFT. This approach is useful in the presence of noise, when there are sufficient number of projections. A new formula for rotation involving the second-order moments of three specific projections has been derived. An extension of the invariant MPs to 3-D has been presented. Registration of an object from the information available in the MPs has been indicated. An alternative approach to constructing invariants from the normalized MPs has been proposed. The approach consists of circular-autoregressive modeling of each of a set of normalized central MPs computed from the data. The resulting feature-set is invariant to geometric transformations as well as changes in gray-scale. Further, the new descriptor is generally much smaller in size in comparison with the set of MPs. Simulation results have been presented to illustrate the proposed techniques. In simple cases, a visual inspection of a few MPs can be sufficient for discrimination. Effects of noise on the MPs was discussed.

The proposed method is applicable to CT as well as spatial data. Finally, it is noted that the proposed moment-based invariants serve as a useful image-understanding tool.

# Chapter 4

# Selective Reconstruction from Noisy Projections

This chapter is devoted to an application of the notion of "instantaneous matched filter" (IMF) [160, 159], and involves selective reconstruction of objects from noisy projections. The IMF consists of a combination of the ideas of detection of objects of known shape and location, and an estimation of the associated parameters, based on an inner-product processor. In this sense, a signal of interest is separated from a linear combination of given shapes in white noise. The IMF approach is developed from a discrete viewpoint. Optimal weights are derived for the two-signal case, and some simplifications over the original method are arrived at. The development results in certain new observations. Extension to the case involving colored noise is indicated. A generalized version that does not require an explicit orthogonalization, is presented. The generalized IMF is applied to separate the projections of the object of interest, from which the object is reconstructed. The idea is applicable when the object of interest is of poor contrast, while the densities of the objects change and the projections are noisy, a scenario in which simple subtraction would not be effective. An application, involving a tracking of variations in the density of a selected object, is also presented. Alternatives to the IMF approach are indicated.

## 4.1 Introduction

In a number of applications in CT, an object is of special interest relative to the rest in the cross-section. Often, the object of interest is of poor contrast. The quality of reconstruction of a low-contrast object gets affected by the streaks due to dominant objects in the cross-section [38]. An enhanced visualization of the object is possible by techniques similar to subtraction angiography, when the density functions and their respective positions do not vary. For example, a visual enhancement of the spinal cord is achieved by subtracting the approximate projections of the bone [176]. In NDT, the convex hull of a defect can be estimated from the projections obtained by subtracting the projections of the object under inspection from those of the reference object [209]. However, methods as simple as these may not be very effective when the densities change, and/or in the presence of noise.

In this chapter, selective reconstruction of an object of interest is considered, as an application of the IMF approach [160, 159]. The basic idea consists of separating [1] the projections of the desired object from those of the composite cross-section, from which the image is reconstructed [2]. It is assumed that the composition (objects and their locations) of the cross-section is pre-determined, and that some of the densities change by factors that are not known. Such a situation may arise, for example, in medical imaging while monitoring a patient administered with a contrast material. It is crucial to ensure that the object does not move. The applicability of the approach is hence very restrictive. In applications such as NDT, however, the movement of the object is not an issue. In this context, the IMF is reviewed from a discrete viewpoint. Optimal scaling functions are derived for the two-signal case, and some simplifications are indicated. A generalized version is developed, and used to extract the projections of the individual object of interest, from which the object

[1] In the context of the IMF, separation, selection, or extraction of a signal is in the sense of estimating the associated parameter from an unknown linear combination of given shapes.

[2] The projections of a linear combination of 2-D functions is a linear combination of the projections of the individual functions.

is reconstructed.

The IMF approach is described in the following section. Selective reconstruction of objects from noisy projection data is presented in Section 3. Section 4 concludes the chapter.

## 4.2 The discrete instantaneous matched filter and its generalization

The discrete matched filter (MF) is reviewed and its instant-to-instant implementation, referred to as the discrete IMF, is described in the following. The development is analogous to that in [160, 159] except that it is discrete (vectorial). Indeed, orthogonalization on an instant-to-instant basis is feasible only in the discrete domain. While a sub-optimum approach was followed in [160, 159], optimum scaling functions are derived and a normalization is shown to result in a simpler scheme. Finally, a generalized approach that does not involve an explicit orthogonalization is developed.

### 4.2.1 The discrete instantaneous matched filter

Consider a scaled signal $\Phi$ in the presence of white noise:

$$\mathbf{x} = a\Phi + \mathbf{n} = \mathbf{s} + \mathbf{n} \tag{4.1}$$

where, $\Phi$=$[\phi(1)\ ..\ \phi(N)]'$, $\mathbf{n}$=$[n(1)\ ..n(N)]'$, and $\mathbf{x}$=$[x(1)..x(N)]'$, The solution to the detection problem involves finding a vector $\mathbf{h}$ such that the output SNR of the inner-product processor, $E\{<\mathbf{s},\mathbf{h}>^2\}/E\{<\mathbf{n},\mathbf{h}>^2\}$ is maximized. The vector is the solution of an eigen-equation, and is given by:

$$\mathbf{h} = \alpha\Phi \tag{4.2}$$

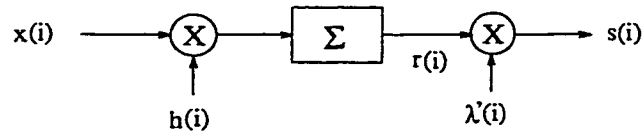


Figure 4.1: Discrete instantaneous matched filter.

where $\alpha$ is any scalar. When the inner-product is realized through a linear filter, the system is a matched filter (MF). However, in conformity with the current practice, the processor will be referred to as a MF. The MF is used to detect the presence of $\Phi$ in the presence of white noise.

Consider the situation when $a$ is a realization of a random variable (RV) $\mathbf{a}$ with $E\{\mathbf{a}^2\} = \bar{a^2}$, and uncorrelated with the noise sequence $n(i)$. The output $r(N)$ can be used to estimate the value of $a$ in the minimum mean-square error sense. Following [160], a post-MF scaling factor $\lambda$ is used for the purpose. However, it is sufficient to minimize the error $\zeta = E\{(\lambda r(N) - a)^2\}$[3]. The scaling factor that minimizes $\zeta$ is $\lambda = \frac{\bar{a^2}}{\bar{a^2}||\mathbf{h}||^2 + {\sigma_n}^2}$. Thus, given $\bar{a^2}$ and ${\sigma_n}^2$, the variance of the white noise sequence, the detection process can be combined with an estimator based on the output of the MF to obtain an estimate $\hat{\mathbf{s}}$ of the signal $\mathbf{s}$. In the case of colored noise, the input will have to be pre-processed by a whitening filter. If $W$ is the matrix representation of the whitening transform, the optimal filter is $\mathbf{h} = W\Phi$i[4]. . The operation by $W$ can be absorbed into $\mathbf{h}$, as $W^T W\Phi$.

The above idea can be applied on an 'instantaneous' basis to obtain $\hat{a}$ right from the beginning [160]. At every instant $i$, an MF with $\mathbf{h}_i = \Phi_i = [\phi(1)\ \phi(2)\ ..\ \phi(i)]'$, $\mathbf{x}_i = [x(1)\ ..\ x(i)]'$, $\mathbf{n}_i = [n(1)\ ..\ n(i)]'$ is implemented, and $\hat{s}(i) = \hat{a}(i)\phi(i)$ is computed. The scaling function associated with the discrete IMF is given by $\lambda(i) = \frac{\bar{a^2}}{\bar{a^2}||\Phi_i||^2 + {\sigma_n}^2}$. A block diagram of the discrete IMF is shown in Fig. 4.1.

The presence of colored noise requires a suitable modification of the filter as

[3]Since $\Phi$ is known, the problem is equivalent to that of parameter estimation. A formulation as a waveform estimation problem results in the scaling factor being proportional to $\Phi$. Indeed, both yield the same result.

[4]This is the corrected version of the erroneous expression in [171].

mentioned above.

Consider the case of two signals in white noise:

$$\mathbf{x} = a_1\mathbf{\Phi_1} + a_2\mathbf{\Phi_2} + \mathbf{n} = \mathbf{s}_1 + \mathbf{s}_2 + \mathbf{n} \tag{4.3}$$

where $a_1$ and $a_2$ are samples of mutually uncorrelated RVs $\mathbf{a}_1$ and $\mathbf{a}_2$ respectively, also uncorrelated with $n(i)$. $E\{\mathbf{a}_1{}^2\} = \bar{a_1}^2$ and $E\{\mathbf{a}_2{}^2\} = \bar{a_2}^2$.

The IMF has been extended to the case of multiple signals by breaking it into a set of single-signal IMF-branches (inner-product processors) [160]. Let $\Phi_{1,i} = [\phi_1(1)\ \phi_1(2)\ ..\ \phi_1(i)]'$ and $\Phi_{2,i}$=$[\phi_2(1)\ \phi_2(2)\ ..\ \phi_2(i)]'$. Following [160], the first processor (branch) is chosen to be associated with $\Phi_{1,i}$ itself, while the second consists of a version of $\Phi_{2,i}$ that is orthogonalized with respect $\Phi_{1,i}$, by the Gram-Schmidt process. Mathematically, the signal can be represented on an 'instantaneous' basis as follows:

$$\mathbf{x}_i = a'_1(i)\mathbf{\Psi}_{1,i} + a_2\mathbf{\Psi}_{2,i} + \mathbf{n}_i \tag{4.4}$$

where, $\mathbf{\Psi}_{1,i} = \Phi_{1,i}$, and $\Psi_{2,i} \perp \Psi_{1,i}$. The parameter $a'_1(i) = a_1 + \rho_{21}(i)a_1$, where $\rho_{21}(i)$ represents the correlation between the vectors $\Phi_{1,i}$ and $\Phi_{2,i}$. The set $\{\Psi_{2,i}, i \in [1, N-1]\}$ can be pre-computed and stored. In [160], a sub-optimum approach was taken to estimate $\mathbf{s}_1$ from (4.3). However, such an approach is not effective, and optimum scaling functions can be found in a manner similar to the single-signal case. Consider the 'first branch'. Forming $r_{o,1}(i) = r_1(i) - \rho_{21}(i)r_2(i)$, and minimizing the error $E\{(\lambda_1(i)r_{o1} - a_1)^2\}$, the scaling function $\lambda_1(i)$ can be shown to be:

$$\lambda_1(i) = \frac{\bar{a_1}^2 c_1(i)}{(\bar{a_1}^2 + \rho_{21}^2\bar{a_2}^2)c_1^2(i) + \rho_{21}^2\bar{a_2}^2c_2^2(i) + \sigma_n{}^2c_1(i) + \rho_{21}^2\sigma_n{}^2c_2(i) - 2\rho_{21}^2\bar{a_2}^2c_1(i)c_2(i)} \tag{4.5}$$

where, $c_1(i) = \|\Psi_{1,i}\|^2$, $c_2(i) = \|\Psi_{2,i}\|^2$. Note that $\Phi_{1,i}$ and $\Phi_{2,i}$ are required to be linearly independent for all values of $i$. This can be ensured by setting $\phi_1(1) = 1$ and $\phi_2(1) = 0$. A block diagram depicting the scheme is given in Fig. 4.2, where $\lambda'_1(i) = \lambda_1(i)\phi_1(i)$. The expression for $\lambda_2(i)$ is much simpler due to orthogonalization:

$$\lambda_2(i) = \frac{\bar{a_2}^2}{\bar{a_2}^2\|\Psi_{2,i}\|^2 + \sigma_n{}^2} \tag{4.6}$$

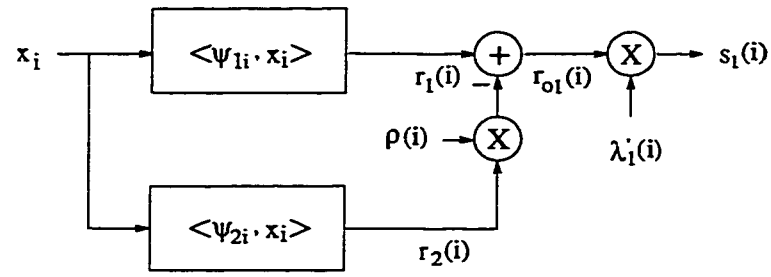


Figure 4.2: IMF for two signals.

It is clear that $s_2$ can be estimated by using only the 'second branch'. This scheme also yielded a better estimate than that obtained by the first. One possible reason is the subtraction by $\rho_{21}r_2$ which makes $\hat{a}_1$ fluctuate when $a_2$ or $\rho_{21}$ is large. It is interesting to note that $\lambda_2$ is independent of the influence of $a_1$, which is the result of orthogonalization. *Thus, $a_2$ can be estimated invariant to fluctuations in $a_1$.* The scheme is depicted in Fig. 4.3, where $\lambda_2'(i) = \lambda_2(i)\phi_2(i)$. Two filters can be employed for separating the two signals, with the knowledge of $\bar{a_1^2}$ and $\bar{a_2^2}$.

In the case involving a single signal, the inner-product is cumulative. However, in the two-signal case, it has to be computed every instant[5].

Expressions (4.5) and (4.6) suggests the use of normalization for further simplification. Specifically, if $\Psi_{1,i}$ and $\Psi_{2,i}$ are replaced by $\Psi_{1n,i}$ and $\Psi_{2n,i}$, where $\Psi_{kn,i} = \Psi_{k,i}/\|\Psi_{k,i}\|$, $c_1(i)$ and $c_2(i)$ are unity for all the values of $i$. The scaling functions simplify to:

$$\lambda_1(i) = \frac{\bar{a_1^2}}{\bar{a_1^2} + (1 + \rho_{21}^2(i))\sigma_n{}^2} \tag{4.7}$$

and

$$\lambda_2(i) = \frac{\bar{a_2^2}}{\bar{a_2^2} + \sigma_n{}^2} = \lambda_2 \tag{4.8}$$

which is independent of $i$; this eliminates the necessity of post-MF scaling. The above expressions lead to a simplified implementation of the discrete IMF for two signals.

[5]The process of orthogonalization changes the reference vector every instant. This has not been noted in [160]. Here, this is made clear by indicating the inner-products explicitly in the block-diagrams.

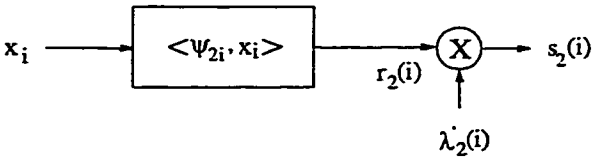


Figure 4.3: Simpler scheme.

Explicit orthogonalization at each instant becomes infeasible as the number of signals/shapes involved increases. A modification involving cumulative computing (via a recursive procedure) has been proposed in [159]. That would take one to recursive least squares, and will not be considered here. The idea here is to work within the framework of the IMF. In the following, a novel approach that does not require an explicit orthogonalization is described. The approach is referred to as generalized IMF (GIMF).

### 4.2.2 The generalized IMF

Consider the case of two signals in white noise as in (4.3). It is possible to find a filter $\mathbf{h}_1$ that maximizes the SNR:

$$SNR_1 = \frac{< \mathbf{h}_1, \Phi_1 >^2}{< \mathbf{h}_1, \Phi_2 >^2 + \|\mathbf{h}_1\|^2 {\sigma_n}^2} \tag{4.9}$$

which can be used as an MF to suppress $\mathbf{s}_2$ and the effect of noise, while emphasizing $\mathbf{s}_1$. It can be shown that the filter is given by [126]:

$$\mathbf{h}_1 = [\Phi_2 {\Phi_2}^T + {\sigma_n}^2 I]^{-1} \Phi_1 \tag{4.10}$$

Let $r_1$ be the output of the MF associated with $h_1$. The parameter $a_1$ may be estimated by multiplying $r_1$ by a scaling factor $\lambda_1$, which can be found by minimizing the error $E\{(\lambda_1 r_1 - a_1)^2\}$. It is shown in Appendix-B that $\lambda_1$ is given by:

$$\lambda_1 = \frac{\bar{a_1}^2 < \mathbf{h}_1, \Phi_1 >}{\bar{a_1}^2 < \mathbf{h}_1, \Phi_1 >^2 + \bar{a_2}^2 < \mathbf{h}_1, \Phi_2 >^2 + \|\mathbf{h}_1\|^2 {\sigma_n}^2} \tag{4.11}$$

Colored noise can be handled by pre-processing by a whitening transform, or by replacing $\sigma_n^2$ by $R_n$ (noise covariance matrix) in (4.10) and $\|\mathbf{h}_1\|^2 {\sigma_n}^2$ in (4.11) by ${\mathbf{h}_1}^T R_n \mathbf{h}_1$ respectively.

The generalized IMF (GIMF) is an instant-to-instant implementation of the above development. Employing the previously defined notations $\Phi_{1,i}$, $\Phi_{2,i}$ and $\mathbf{x}_i$, the scaling function associated with the filter $\mathbf{h}_{1,i}$=$[h(1)\ h(2)\ ..\ h(i)]'$, that minimizes $\zeta_i = E\{[a_1 - r_1(i)\lambda_1(i)]^2\}$, is given by:

$$\lambda_1(i) = \frac{\bar{a_1}^2 < \mathbf{h}_{1,i}, \mathbf{\Phi}_{1,i} >}{\bar{a_1}^2 < \mathbf{h}_{1,i}, \mathbf{\Phi}_{1,i} >^2 + \bar{a_2}^2 < \mathbf{h}_{1,i}, \mathbf{\Phi}_{2,i} >^2 + \|\mathbf{h}_{1,i}\|^2 {\sigma_n}^2} \tag{4.12}$$

Fig. 4.4 shows the block diagram of the GIMF.

The above scheme can be extended to the case involving any (a finite) number of signals (and hence the name generalized IMF). Let $V$ be a real vector space of dimension $N$. Let $\beta = \{\Phi_1\ \Phi_2\ ..\ \Phi_N\}$ be a basis for $V$. Consider the basis split into two sets $\beta_1$ and $\beta_2$. Then, $V$ can be written as the direct sum, $V = S_1 \oplus S_2$, where $S_i = span[\beta_i]$, $i = 1, 2$. The algorithm described above can be used to suppress a signal belonging to one subspace and retrieve that belonging to the other, in presence of noise. The argument is valid for any two proper subspaces of $V$ associated with a direct-sum decomposition. A case of particular interest is that of extracting a shape from a noisy linear combination of multiple shapes. For this case, $\beta_1 = \{\Phi_l\}$ represents the object of interest, and $\beta_2 = \{\Phi_i,\ i \neq l\}$. The filter $\mathbf{h}_l$ to detect $\mathbf{s}_l$ from:

$$\mathbf{x} = \sum_{k=1}^{N} c_k \mathbf{\Phi}_k + \mathbf{n}, \qquad c_k \in \mathbf{R},\ \forall\, k \tag{4.13}$$

is given by:

$$\mathbf{h}_l = [M_l^c M_l^{cT} + {\sigma_n}^2 I]^{-1} \Phi_l \tag{4.14}$$

where, $M_l^c$ is the matrix whose columns are the vectors $\{\Phi_i,\ i \neq l\}$. This filter maximizes the SNR: $\frac{<\mathbf{h}_l, \Phi_l>^2}{\sum_{k \neq l} <\mathbf{h}_l, \Phi_k>^2 + \|\mathbf{h}_l\|^2 {\sigma_n}^2}$. The scaling function $\lambda_l$ is determined by (4.12), with $\Phi_1$ and $\Phi_2$ replaced by those associated with the subspaces $S_1$ and $S_2$, assuming that the values of $\bar{a_1}^2$ and $\bar{a_1}^2$ are available.

The procedure for estimating $\mathbf{s}_l$ consists of two steps - (i) of designing the filter $\mathbf{h}_{l,i}$ and the scaling function $\lambda_l(i)$, and (ii) of implementing the generalized MF on an instant-to-instant basis as above.

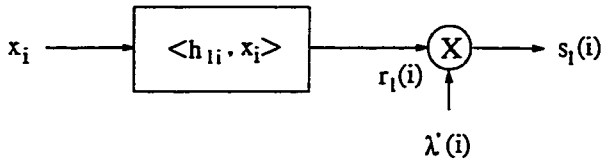


Figure 4.4: Generalized IMF.

The applications considered in this chapter, as well as most of the practical applications, involve one or two fluctuating parameters. In general, the procedure can be used to extract all of the shapes by using a filter for each of them, in parallel. Each filter will be associated with the respective direct-sum decomposition of $V$. The values of the $\{\bar{a_i}^2\}$ associated with the fluctuations are assumed. For mere detection, these are not required, as detection can be achieved independent of the values of the associated linear combiners.

It is interesting to note that the IMF approach is a form of correlation canceling [144].

## 4.3 Selective reconstruction from noisy projections

Consider a situation in CT in which the cross-section consists of two objects $\phi(x, y)$ and $\psi(x, y)$, such that:

$$f(x, y) = a_1\phi(x, y) + a_2\psi(x, y) \tag{4.15}$$

See a pictorial illustration in Fig. 4.5.

The exact values of $a_1$ and $a_2$ are not precisely known, and are subject to fluctuations. However, the values of $\bar{a_1^2}$ and $\bar{a_2^2}$ are assumed to be available. Consider a noisy measurement of the projections of $f(x, y)$:

$$p_{\theta_k}(i) = a_1\phi_{\theta_k}(i) + a_2\psi_{\theta_k}(i) + n_{\theta_k}(i), \quad i \in [1, N], \quad \theta_k \in [0, \pi) \tag{4.16}$$

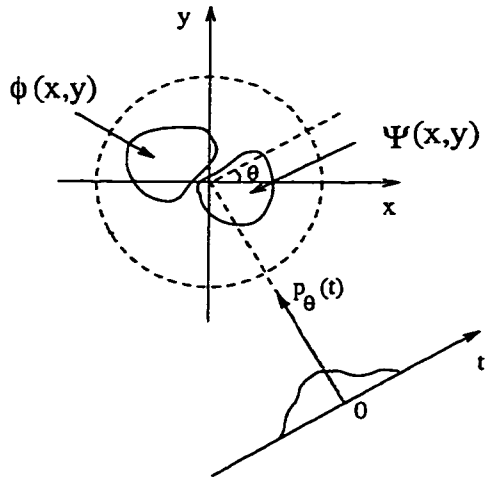


Figure 4.5: A projection of 2 objects.

The white-noise sequences $\{n_{\theta_k}\}$ of variance $\sigma_n^2$, are Gaussian, zero-mean and uncorrelated with $\mathbf{a}_1$ and $\mathbf{a}_2$, and in $\theta_k$ [6]. One can apply the 1-D algorithm developed in the previous section, to each of the projections, to estimate the projections of one of the objects from (4.16). The object may then be reconstructed from the estimated projections. Thus, an object may be selectively reconstructed from the noisy projections of a composite image, i.e., a noisy a linear combination of the projections of the individual objects.

Normalized mean square (reconstruction) error (NMSE), as defined below, may be used as a quantitative measure of comparison:

$$NMSE = \frac{\sum_{i,j}[f(i,j) - \hat{f}(i,j)]^2}{\sum_{i,j} f^2(i,j)} \tag{4.17}$$

It is to be noted that such quantitative measures are not necessarily true indicators of visual quality. In the simulation, results of which are presented below, the value of additive white noise variance was generally based on a visual effect on the projections, as well as the value of $a_1$. No SNR has been used, as it varies over the

[6]Noise in CT data is signal-dependent or multiplicative. However, at high SNRs, the noise in the projections is modeled as additive and Gaussian with zero-mean [228], and this model has been used by various researchers [203]. Noise can also be correlated, in which case, the processing is to be modified as indicated.

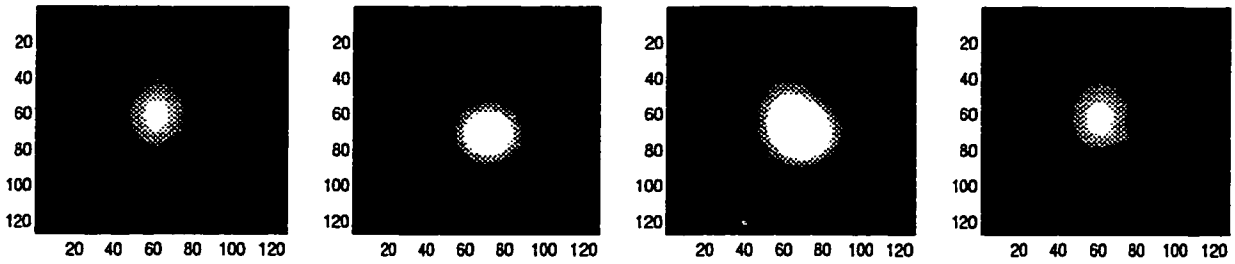


Figure 4.6: (a) Object-1, (b) object-2, (c) superposition, and (d) selective reconstruction of object-1.

projections. The values of $\bar{a_i^2}$ were selected based on the assumed values of mean and variance.

Simulation was performed on different types of objects and their superposition. The first set consists of a superposition of two smooth and spatially overlapping functions of size 127×127. Overlapped objects are chosen for illustration, although physical overlapping does not happen with CT data. The objects (multiplied by factors $a_1 = 3$ and $a_2 = 5$), and their superposition are shown in Fig. 4.6. 180 projections were considered in this example. 1-D GIMFs associated with the projections of the object-1 were designed. The GIMFs were applied on the respective projections of the superposition with additive noise (of variance of $a_1/2$). A reconstruction of the object obtained by CBP with cosine window and Lagrange interpolation, is shown in Fig. 4.6 (d). The NMSE for this case has been found to be 0.0118.

Fig. 4.7(a) shows a simulated test phantom of size 127×127. The object of interest is indicated by the label '1'. 90 equally spaced projections of the object of interest were considered. The GIMFs associated with these projections with respect to the other projections were designed. The value of $a_1$ (associated with object-1) was then reduced from its mean value of 2, to 1.5, while that corresponding to the rest of the objects was increased to 3, from a mean value of 2. The projections of the modified phantom were computed and independent noise (of zero mean and variance equal to 50 times the mean value of $a_1$) was added to each of the projections. The

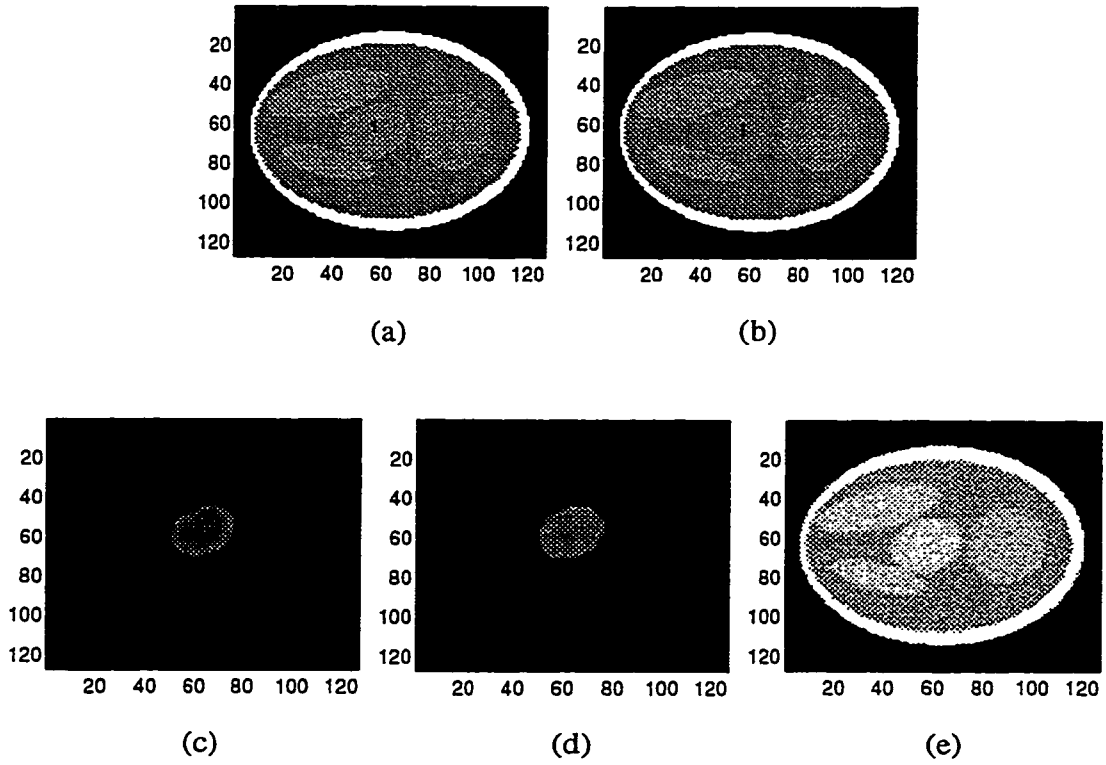


Figure 4.7: (a) Original image, (b) modified image, (c) reconstruction of object-1, (d) selective reconstruction from noisy projections, and (e) reconstruction by subtraction.

respective GIMF was applied to each of the noisy projections of the modified image to retrieve those of the object of interest. A reconstruction using CBP is shown in Fig. 4.7(d), along with the modified phantom, and a reconstruction of the object from known, noise-free projections for reference.

The result of reconstruction from the projections resulting from a simple subtraction of the reference projections of the rest of the objects from the measured projections, is shown in Fig. 4.7(e). Notice that the very objective of subtraction has been futile. Further, object-1 appears to be of higher density, contrary to the actual case. This example, in which the densities of all the objects change is extreme, but highly illustrative and serves to demonstrate the limitations of simple subtraction methods when the densities of the object change relatively.

The utility of selective reconstruction can be appreciated by the example shown

in Fig. 4.8, in which the contrast of the object of interest is very low [7]. $a_1$ was reduced to 1 from a nominal value of 5, whereas that associated with the rest of the objects was increased to 20 from a nominal value of 15, although the assumed variances of $a_1$ and $a_2$ were 2 and 1 respectively. Additive noise variance for this case was 100. The NMSE for this case was found to be 0.0042.

There are several factors that influence the quality of the reconstructed image. Noise level is an obvious one, which deteriorates the reconstruction. A plot of NMSE with respect to additive noise variance is given in Fig. 4.9(a). Another factor is the number of projections. A plot of NMSE in terms of the number of projections is given in Fig. 4.9(b). In general, the number of projections required to selectively reconstruct an object depends upon the nature of the object of interest, and not that of the others composing the scene. However, the degradation in the projections produce more severe reconstruction-errors when the number of projections is small. A third factor that affects the reconstruction quality is the type of the algorithm used. For example, the result obtained by CBP with 90 projections is seen to be very good (unlike in the former example consisting of finely tapered functions, where the errors in reconstruction are visible). However, the errors in the projections start manifesting on the reconstructed image, as the number of projections is reduced, even if the object of interest can be represented by a smaller number of projections. The explanation is that while the CBP is excellent when the number of projections is large, it is not so when the number of projections is small, and/or in presence of significant noise. Methods such as ART, though computationally expensive, would be superior to the CBP under such circumstances.

The approach described above would be practical when the projection data are short in length. Note, however, that it is the filter-design step that is really time consuming, and this need not always be carried out on-line. The scheme can be made

[7]When only one of the objects is of low contrast, it can be displayed by simple thresholding, which, however, is difficult when more than one object of poor contrast are involved. Although this example considers a single object of poor contrast, it is not restrictive.

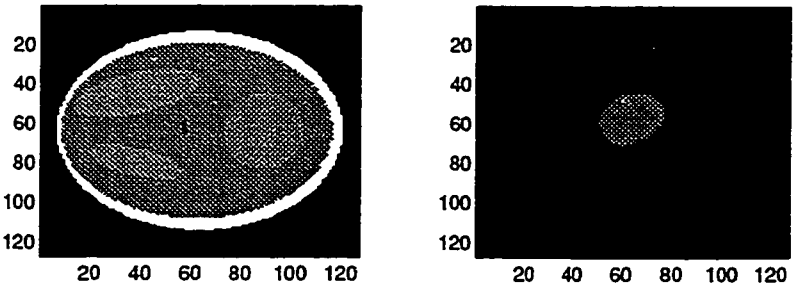


(a) (b)

Figure 4.8: (a) Modified image, and (b) selective reconstruction from noisy projections

more efficient by using a fixed past (window-size or memory). The estimate will then fluctuate with those of noise, resulting in greater errors. A plot of the NMSE (relative to the image reconstructed from projections extracted by the filter using the complete past) as a function of window-size, is shown in Fig. 4.9(c). Additive white noise of variance 100 was considered. It is clear that beyond a certain size, the improvement achieved in terms of NMSE is not significant. However, it should be noted that short windows affect finer details in the reconstructed image, which may not be reflected in the NMSE. Further, longer window lengths are required as the noise strength increases.

### 4.3.1 Discussion

The situation considered so far involved density changes between complete CT scans. If the densities of the objects do not change during scanning, a single projection is sufficient to determine the object densities. Further, in the absence of noise, a few rays (equal to the number of objects whose densities fluctuate) would be sufficient to solve the problem. However, it would be useful to consider many projections and take an average, for robustness.

A natural question that follows is the effect of changes in the density during scanning. Mathematically, such variations would render the RT inconsistent. If the

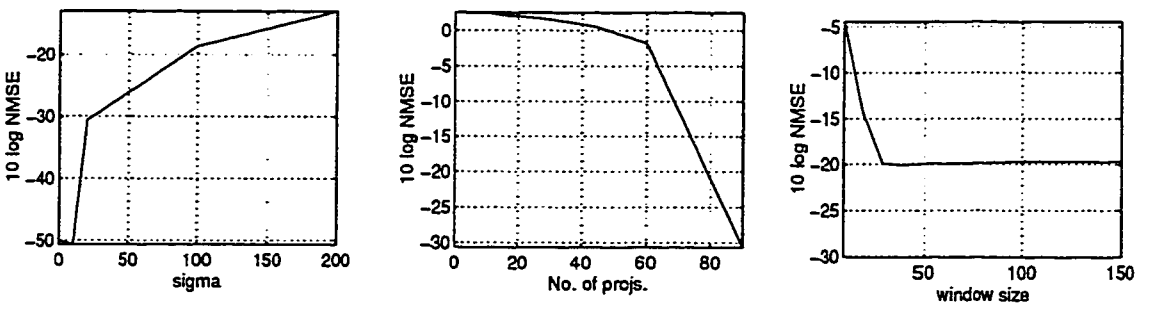


(a) (b) (c)

Figure 4.9: Quantitative measure of reconstruction as a function of: (a) noise variance (sigma), (b) number of projections, and (c) size of the window.

density of the objects fluctuate randomly by a small margin, this is not likely to affect the reconstruction in a significant way. Interestingly, it has been shown experimentally that boundaries of objects in CT reconstructions are not very sensitive to variations in density during scanning [38]. Thus, effects of small variations in density during scanning on selective reconstruction appear to negligible, especially on objects of uniform density.

The problem of separation of signals of known shape and location turns out to be that of parameter estimation. In this chapter, the idea was to apply the IMF approach. However, any of the available methods for the estimation of parameters of known signals in presence of noise can be employed for the purpose. In particular, the problem could be cast into the recursive least squares (RLS) scheme [8] [44]. It is interesting to note that the updating the P-matrix in [159] turns out to be the same as that associated with RLS parameter estimation [44]. RLS is attractive with fast and elegant updation scheme. However, the estimate resulting from the IMF appears to be less sensitive to the fluctuations of the parameter value, in the initial stages.

The approach discussed above can be applied in different ways, as for example, to *track* density variations in selected objects. An example is presented in Fig. 4.10.

[8]To handle noise, the RLS with a 'dead-zone' (a scheme for turning off the updation) is employed.

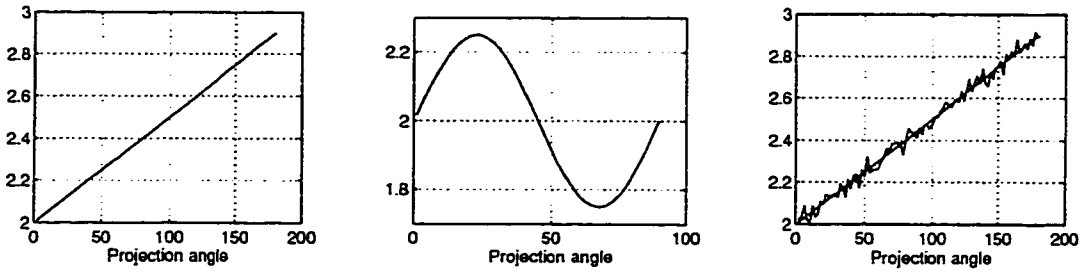


(a) (b) (c)

Figure 4.10: (a) Variation of density in object-1, (b) variation of density in object-2, and (c) estimated variation

Object-1 of the previous example was subject to a variation (in $a_1$) as shown in (a). Simultaneously, the density of the rest was assumed to vary (uniformly, in terms of $a_2$) sinusoidally as in (b). The result of estimating the variation in object-1, from noisy projections of the cross-section, is shown in (c). Estimation was based on the whole block of data as the variation was between the projections only.

The IMF approach would be more appropriate to track variations continuously, i.e., ray-by-ray, possibly in a sequential ray-by-ray scanning. The approach can also be used to study the effects, on the reconstructed image, of variations of density in an object during scanning.

## 4.4 Conclusion

In this chapter, the IMF has been developed from a discrete viewpoint. Some new observations have been made, and a generalized approach that does not require an explicit orthogonalization, has been presented. The generalized algorithm has been applied on noisy projections of the composite image for selective reconstruction. Illustrative simulation results have been presented. Futility of methods involving a simple subtraction when the densities of the objects change, has been illustrated. Issues such as the role of the number of projections and the effect of noise-level were discussed. The importance of the choice of an appropriate reconstruction

algorithm was mentioned. Effect of mild variations of density of the object of interest during scanning on the shape of the object appears to be negligible. An application involving a tracking of the density-variations in a selected object has been presented. Alternatives to the IMF approach have been indicated.

# Chapter 5

# Binary Image Compression

Compression of binary images is considered. The basic idea involved is the fact that binary objects are often represented by few projections. Additional compression is obtained by coding the individual 1-D projections. The application is twofold: (i) in certain situations in CT in which the object may be assumed to be binary, as an alternative to compressing a reconstructed image, and (ii) as a method of coding binary images, wherein the RT is used to convert the problem of coding binary images to that of coding a set of 1-D *non-binary* sequences. The approach is extended to accommodate pictures with closed contours. Illustrative simulation examples are presented. Finally, a new algorithm for reconstructing binary images from their projections is proposed.

## 5.1 Introduction

Data compression is concerned with the minimization of the number of bits for efficient storage and transmission. Basic approaches to data compression have reached a high degree of maturity [78, 70], and may be broadly categorized into those which exploit redundancy in the data, such as predictive coding, and those which employ a transform with a good energy-compaction property. The choice of a particular

approach depends upon various factors such as the nature of data including its dimensionality, and application-specific information. Image data can be categorized into still gray-level and color pictures, sequential pictures as in broadcast TV and remote sensing, and binary (two-tone) images. Further, image data is often available in different forms/domains from which the picture will have to be recovered, as in CT [70, 227]. Inspite of the extensive work that has been carried out, the ever increasing demand for data compression motivates further efforts, such as identifying and exploiting certain application-specific information in conjunction with the basic algorithms. This chapter represents such an effort, involving the compression of binary images in the RS. When the data is available in the RS, the idea is to compress the projections themselves, instead of processing the reconstructed image. On the other hand, the RT can be used as a tool to compress binary images represented by a small number of projections.

Compression of binary images has been a topic of immense interest. Most of the techniques exploit the abundance of the white pixels and the regularity of the black pixels in the image. Prominent among them are run-length coding (RLC), white block skipping, prediction differential quantization (PDQ), relative address coding and predictive coding [72]. These techniques, with the exception of PDQ, do not exploit the inter-dimensional correlation in the 2-D data. A somewhat different approach consists of rectangular-coding [141, 127]. In predictive coding of binary images (eg., [89, 219]), redundancy in the image is reflected in long runs of zeros in the error signal, which are subject to RLC. Algorithms that utilize higher-level information and pattern recognition techniques can yield very high compression [72]. For a detailed description of the approaches, see [200, 6, 59, 70, 72, 135] and the references cited therein. Current techniques are largely based on the ideas developed in the references cited above, and their variants and application-specific improvements. Transform methods have not been applied to binary images, since

a direct application is not feasible[1]. In general, the existing techniques for binary image compression differ significantly from those used for gray-level images.

In a number of applications in CT, the CS can be assumed to be binary [53]. In some situations, objects can be usefully treated as being binary even when they are perceptibly non-homogeneous [131]. One approach to compressing such data is to reconstruct the image and apply 2-D algorithms. Often, a better alternative would be to compress the data in the RS itself and reconstruct the image whenever necessary. The information that binary images are represented by few projections [53, 131, 199], can be exploited for efficient compression [2]. In applications involving only transmission, such a scheme is time-efficient. On the other hand, the RT can be used as a tool to compress binary images [165, 166]. The RT reduces the problem of coding a 2-D binary image to that of coding its projections, a few of which are generally sufficient to represent an object. An additional advantage of such a scheme is that the projections of a binary image are non-binary sequences, which can be compressed using regular 1-D algorithms, including the transform techniques. The procedure for retrieval consists of decoding the projections, followed by a reconstruction of the binary image. The approach can also be extended to compressing closed contours/boundaries of objects, by converting them to the respective characteristic functions.

This chapter addresses binary image compression in the RS, with suitable applications depending upon the domain in which the data is available. In the following section, reconstruction of binary images from projections is discussed briefly, with a specific algorithm. In Section 3, the compression scheme is presented, followed by the application of predictive and transform methods. In Section 4, simulation results are presented. In Section 5, a new algorithm for binary image reconstruction

[1]Efforts towards extending the ideas of wavelet decomposition to binary images have begun very recently [207].

[2]In fact, convex objects can be represented by just two projections [131]. Non-convex objects generally require more projections, and for a given degree of faithfulness of reconstruction, a greater number of projections would be required to represent the shapes of greater intricacy.

is considered. Section 6 concludes the chapter.

## 5.2 Reconstruction of binary images from projections

Reconstruction of binary images from few projections is an interesting topic on its own, and has received considerable attention [17, 53, 90, 199, 131, 123]. Unlike their gray-level counterparts based on closed-form solutions (such as the CBP) binary image reconstruction algorithms are generally iterative in nature, and resemble the ART. Prominent among the existing techniques are the ART-like algorithms of Herman [53], Gilbert (simultaneous iteration reconstruction technique) [42], Soumekh [199], and the approach of Murch and Bates [131]. The approach of [131] is quite different from the usual, and also shows that two projections are sufficient to reconstruct a convex object.

This chapter is concerned with binary image compression in the RS and addresses both continuous CS of CT and digital binary images. A unified treatment to include both the situations is possible with the following assumptions. In CT, the CS is continuous, but practical reconstruction is possible only on a finite set of (grid) points. Without loss of generality, the reconstruction support may be assumed to be a square grid $S_d$ of size N×N. Assuming square pixels of unit area, the continuous support $S$ is a square with a side of length $N$. This corresponds to a flat-top sampled (pixel) model of the CS. Consequently, the projections of the CS are modeled by (2.13). On the other hand, the projections of a digital binary image $f(m,n)$ of size N×N are estimated by (2.13), with the help of the pixel assumption. *Note that the projections of a binary picture are non-binary sequences.* Let $Y_d$ denote the discrete support in the RS. Typically, it corresponds to a small number of projections with uniformly spaced line-integrals. Thus, binary image reconstruction from its projections consists of estimating $f(x,y)$ at the N×N points, or its flat-top

sampled version $f(m,n)$. In the following, the method of Soumekh [199] is reviewed.

Consider the projections of $f(m,n)$, $-M \leq m,n \leq M$, along the horizontal, the vertical, and the two diagonal lines through the lattice points:

$$\begin{aligned} p_0(l) &= \sum_m f(l,m), & -M \leq l \leq M \\ p_{\frac{\pi}{4}}(l) &= \sqrt{2}\sum_m f(m,l-m), & -2M \leq l \leq 2M \\ p_{\frac{\pi}{2}}(l) &= \sum_m f(m,l), & -M \leq l \leq M \\ p_{\frac{3\pi}{4}}(l) &= \sqrt{2}\sum_m f(m,l+m), & -2M \leq l \leq 2M \end{aligned} \tag{5.1}$$

where, the summation is performed over $S_d$ ($N = 2M+1$). The above is a special case of (2.13). The problem of reconstructing $f(m,n)$ from the set of four projections, is formulated as that of solving a set of linear equations. The algorithm is based on the principles of least-squares. Specifically, the points along a ray in the picture space are estimated from their 'noisy versions'[3] in the least-square sense, consistent with the given line integral. The resulting algorithm begins by assuming an initial estimate for $f(m,n)$. In each iteration, $f(m,n)$ is estimated based on the projections at one of the four angles, $\theta = \theta_i$, which forms an initial estimate for that based on the projection at a different angle, $\theta_{i+1}$, as follows:

$$\hat{f}_{\theta_{i+1}}(m,n) = \hat{f}_{\theta_i}(m,n) + \frac{(p_{\theta_{i+1}}(l) - \hat{p}_{\theta_{i+1}}(l))}{n_{\theta_{i+1}}(l)}, \quad m,n \in S_d \tag{5.2}$$

where, $\hat{p}_{\theta_{i+1}}(l)$ is the projection of $\hat{f}_{\theta_i}(m,n)$ at $\theta = \theta_{i+1}$. $n_\theta(l)$ is the number of pixels along the line defined by $\theta$ and $l$, given by[4]:

$$n_\theta(l) = \begin{cases} N, & \theta = 0,\ \frac{\pi}{2} \\ 2(N-|l|), & \theta = \frac{\pi}{4},\ \frac{3\pi}{4} \end{cases} \tag{5.3}$$

The final step in each iteration consists of applying the constraint $0 \leq f \leq 1$. The constrained values of $f(m,n)$ form the basis for the subsequent iteration. The last

[3]Here, as well as in Section 5, 'noisy versions' refers to the previous estimate (based on a different angle), and not to statistical noise.

[4]For a circular support (with square pixels) circumscribing the N×N square, it is approximately $2\sqrt{2N^2-l^2}$ along the horizontal and the vertical, and $2\sqrt{N^2-l^2}$ along the diagonals.

step in the reconstruction algorithm involves setting the values of $f(m,n)$ to 1 if $f(m,n) \geq 0.5$, or to zero otherwise.

**Remark:** Overall convergence of the above algorithm has only been observed by simulation [199].

## 5.3 Binary image compression

The first step in binary image compression consists of determining the type of reconstruction algorithm and the associated number of projections, pertaining to a class of images under consideration. Then, the projections are acquired (in the case of CT) or computed from a digital binary image. The 1-D projections, which are non-binary sequences, are coded for efficient transmission or storage, using a suitable algorithm. Any of the standard methods such as linear predictive coding (LPC) also known as ADPCM (adaptive differential pulse code modulation (DPCM)), transform methods (using the discrete cosine transform (DCT) or the wavelet transform), or by vector quantization techniques. At the receiver, the projections are decoded and the associated image is reconstructed using an appropriate algorithm.

The scheme for binary image compression in the RS is summarized below:

1. Acquire (or compute) an appropriate number of the projections of the binary image.

2. Code each of the projections using a 1-D coding scheme. The coded version is either transmitted or stored for use at a later stage.

3. At the receiver, the projections are retrieved from the coded version and the image is reconstructed using an appropriate algorithm.

The idea of image compression in the RS is illustrated in fig. 5.1.

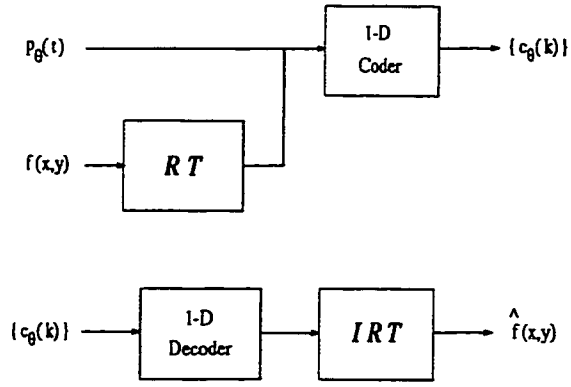


Figure 5.1: Image compression in the Radon space.

With the assumptions of Section 2, the definition of compression ratio (CR) associated with the above scheme is the same for both CT and digital binary images. The CR, defined as the ratio of the number of bits in the original image to that representing the coded image, is given by:

$$CR = \frac{N^2}{\sum_{\theta=0}^{N_p-1} B_\theta} \tag{5.4}$$

where, $N_p$ is the number of projections, and $B_\theta$ is the number of bits required to represent the coded projection at angle $\theta$. The value of $B_\theta$ depends upon the basic compression algorithm used on the projections. It is clear that the value of CR depends upon the number of projections required for a satisfactory reconstruction of the image[5].

An advantage with the RT approach is that the information about the non-zero intervals of each of the projections can be utilized to achieve higher compression. The basic idea is to detect and code the end-points of the interval over which the projections are non-zero, and process only the non-zero portion. The saving achieved

[5]The representation of an N×N binary image by 4 projections as in (5.1) results in compression by a factor of $\frac{N}{6B}$, where $B$ is the bit-rate in the projection domain. If $B = 8$, the gain is $\frac{N}{48}$, which assumes significance for $N > 48$. This can give the impression that CR increases proportionately with the size of the image. However, the number of projections required to represent a picture increases with the size and intricacy. A large picture can be partitioned into suitable sub-blocks before coding.

by discarding the zero-segments generally outweighs the additional number of bits required to carry the end-point information.

Finally, it is remarked that a large image will have to be partitioned into blocks which can be individually coded.

### 5.3.1 Application to closed contours

Many situations in image processing involve closed contours and boundaries of closed objects. It is interesting to note that the foregoing approach can applied to compress closed contours and boundaries of objects by pre-processing. The pre-processing step consists of the closed contour/boundary $C$ to a characteristic function, $c(m,n)$ by the following mapping:

$$c(m,n) = \begin{cases} 1, & (m,n) \text{ inside } C \\ 0, & \text{otherwise} \end{cases} \tag{5.5}$$

A picture with multiple object-boundaries, $\{C_1,\ C_2,\ .\ .\ C_p\}$ can also be coded in a similar way, by converting each of them to the respective characteristic function. The contours are recovered by extracting the edges of the reconstructed image using suitable edge-operators. Alternatively, the approach of Murch and Bates [131] can be used to reconstruct the boundaries directly.

### 5.3.2 Predictive coding

The projections of a binary image can be compressed by standard LPC techniques. Since the projections are non-negative, the mean of each of the projections will have to be subtracted before processing:

$$d_\theta(l) = p_\theta(l) - \mu_\theta \tag{5.6}$$

This is required for reasons of stability [72]. Each of the data sequences $d_\theta(l)$ is modeled as an autoregressive (AR) model of order $M_\theta$.

$$d_\theta(l) = \tilde{d}_\theta(l) + e_\theta(l) \tag{5.7}$$

where,
$$\tilde{d}_\theta(l) = -\sum_{k=1}^{M_\theta} a_\theta(k) d_\theta(l-k) \tag{5.8}$$

is an estimate of $d_\theta(l)$; $\{a_\theta(k),\ k = 1, 2, ..m_\theta\}$ are the model (LP) parameters, and $e_\theta(l) = d_\theta(l) - \tilde{d}_\theta(l)$ is the error (difference) signal. The AR parameters are computed from the data sequence $d_\theta(l)$ using the constrained minimization procedure due to Burg. This guarantees the stability of the inverse prediction-error filter [112]. The computed parameters are used to estimate $\tilde{d}_\theta(l)$ and hence the error signal, $e_\theta(l)$. The sequences $\{e_\theta(l)\}$ are quantized and coded for transmission or storage, along with the parameters $a_\theta(k)$ and the mean $\mu_\theta$. Due to an inherent low variance, each of the segments $\{e_\theta(l)\}$ requires few bits to quantize, which is the principle behind predictive data compression [112, 78]. Hence, the LPC scheme is popularly referred to as DPCM. The quantizer is included within the DPCM loop, to prevent the error from building up [78].

At the receiver, the data sequences $d_\theta(l)$ are retrieved by driving the inverse prediction-error filter by $\{\hat{e}_\theta(l)\}$. The retrieved signal $\hat{d}_\theta(l)$ differs from the original by the quantization error [78]. The projection is obtained by adding the mean to each of them. The binary image is then reconstructed using an appropriate reconstruction algorithm.

Let $N_p$ be the number of projections required to represent the binary image under consideration. Let $B_{a_\theta}$ and $B_\theta$ be the bits per sample assigned to the predictor coefficients and the error segment respectively, associated with $p_\theta(l)$. Then, the CR given by:

$$CR_{LPC} = \frac{N^2}{\sum_{\theta=0}^{N_p-1} M_\theta B_{a_\theta} + N_p B_\theta} \tag{5.9}$$

The contribution of the quantizer step-size information and the mean are neglected. Further simplifications possible with specific information.

### 5.3.3 Transform coding

Standard transforms are not directly applicable to binary images[6]. However, it is possible to use efficient transforms to compress the projections of a binary image. This is possible because of the projections being non-binary sequences. General advantages of transform techniques include higher efficiency and robustness to transmission degradations. The key property of the transforms used for compression is that of energy-compaction. Most of the signal energy will be concentrated close to the origin and compression is achieved by an efficient bit-allocation[7].

The optimum transform coder is defined as one that minimizes the mean-square distortion of the reproduced data for a given number of total bits. This turns out to be the Karhunen-Loeve transform (KLT) [70]. However, the KLT is computationally expensive, and it is replaced in practice by other fast unitary transforms, the most popular among them being the DCT [2, 3, 173]. The performance of the DCT is superior to other fast transforms and is very close to that of the KLT [3, 72]. The DCT pair associated with a sequence $\{s(n),\ 0 \leq n \leq N-1\}$ is given by [72]:

$$C(k) = w(k) \sum_{n=0}^{N-1} s(n) \cos \frac{\pi}{2N}(2n+1)k, \qquad 0 \leq k \leq N-1 \tag{5.10}$$

$$s(n) = \sum_{k=0}^{N-1} w(k) C(k) \cos \frac{\pi}{2N}(2n+1)k, \qquad 0 \leq n \leq N-1 \tag{5.11}$$

where,
$$w(k) = \begin{cases} \frac{1}{\sqrt{N}}, & k = 0 \\ \sqrt{\frac{2}{N}}, & 1 \leq k \leq N-1 \end{cases} \tag{5.12}$$

[6]For example, the inverse DCT of a truncated set of DCT coefficients of a binary sequence will not be binary. However, very recently, a binary wavelet decomposition has been proposed [207].

[7]The variances of the transform coefficients are generally unequal, and therefore each coefficient requires a different number of quantizing bits. For most transforms and non-negative signals, the dc coefficient is non-negative, and the remaining are zero-mean [72]. The bit-allocation criterion is that of minimum (mean-square) reconstruction distortion. Obviously, it depends upon the statistics of the signal under consideration; the theory that deals with such issues is the rate-distortion theory [78]. Similar to the problem of finding the optimal predictor order in LP, bit-allocation is often a matter of art, guided by experience.

The $N$-point forward and inverse DCTs can be computed via a $2N$-point FFT. It is well known that the DCT possesses an excellent energy-compaction property. Compression is achieved by an efficient bit-allocation for the DCT coefficients in a manner that does not seriously degrade the signal under consideration.

The algorithm for binary image compression consists of computing the DCT of each of the projections followed by an appropriate bit-allocation for the DCT coefficients. At the receiver, the decoded coefficients are used to retrieve the projections, which are used to reconstruct the image. The CR afforded by the scheme is:

$$CR_{DCT} = \frac{N^2}{\sum_{\theta=0}^{N_p-1} B_{DCT_\theta}} \tag{5.13}$$

where, $B_{DCT_\theta}$ is the number of bits representing the DCT coefficient associated with the projection at angle $\theta$. Good compression is achieved by sophisticated bit allotments, based on a knowledge of the class of images under consideration.

**Remarks:**

1. In CT, it is often advantageous to code the projections than the reconstructed image. In applications involving on-line transmission, a reconstruction followed by compression is time consuming. An additional advantage is that coding of the reconstruction-errors is avoided, and errors in the decoded projections tend to get distributed over the entire reconstructed image, with a hopefully alleviated visual effect. It should be noted that the concern is the quality of the reconstructed image and not that of the decoded projections.

   It should be pointed out that only lossless compression schemes are in vogue in medicine, due to legal issues [227] (although lossy compression methods have been proposed - see the references cited in [227]). However, the approach presented should be useful as long as the coding errors do not manifest significantly in the reconstructed image.

2. Coding and decoding of the projections can be performed in parallel.

3. The RT approach to coding 2-D binary images can also accommodate gray-level images, with suitable changes in the reconstruction algorithms.

4. Major disadvantages associated with the use of the RT for 2-D binary image compression are: (i) the errors due to projection and reconstruction from projections, and (ii) unsuitability to continuous on-line reconstruction. However, the approach is very useful in applications involving transmission only.

## 5.4 Simulation

Simulation has been performed with computer generated binary phantoms and a text of size $129 \times 129$, shown in fig. 5.2 (a) and (c). Four projections as defined in (5.1) were considered. Reconstructions, after 500 iterations, of the two pictures from four projections, are shown in figs. 5.2 (b) and (d).

The projections were LP-coded with a simple uniform quantizer. The quantizer step-size was computed according to $\Delta = 8\sigma/2^B$, where $B$ is the number of bits per sample, and $\sigma^2$ is the variance of the error-segment associated with a particular projection. The values of $M_\theta$ and $B_\theta$ for each of the projections were chosen so that the CR was 9 in the first case. The second picture being more complicated with abrupt edges in the projection, required a higher bit rate, and the resulting CR was 6.5. The results are shown in figs. 5.3 (a) and (b). In both the examples, the information regarding the end points was utilized only to clean-up the zero-segments. Approaches to improving the CR include the use of adaptive quantizers [78] and the use of a 1-D version of an edge-preserving differential coding scheme proposed by [184]. The results with the DCT are displayed in (c) and (d) of fig. 5.3. The DCT of each of the projections was computed using MATLAB. Only non-zero

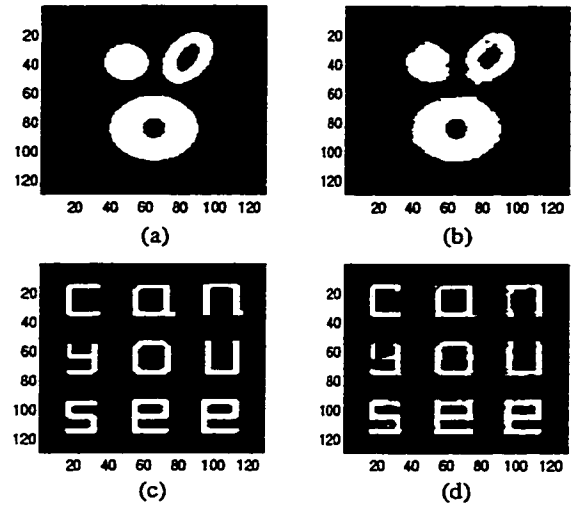


Figure 5.2: (a) A binary phantom, (b) reconstruction of (a) from 4 projections, (c) a binary picture, and (d) reconstruction of (c) from 4 projections.

segments of the projections were processed, and the information regarding the end-points of the interval over which the projections are non-zero, was accounted for in the computation of the CR. The DCT coefficients were partitioned into successively larger blocks, and quantized adaptively by allocating bit-rates that are lower for the blocks away from the origin. A uniform quantizer was used for the purpose. The step-size for each of the blocks was computed as a function of the estimated standard deviation $\sigma$ over that block. Alternatively, one can consider an average over the ensemble of blocks [18]. The resulting CR was 14.5. In general, it is reasonable to expect the performance of the DCT to be better than that of LPC, as the projections, though one-dimensional, have properties similar to those of images. Note that the picture with text is quite complicated to be represented by 4 projections, and the result at CR=14.5 is very interesting and encouraging.

As discussed in the previous section, the proposed approach can be applied to compress pictures with closed contours, by converting them to respective characteristic functions. An example is shown in fig. 5.4.

Note that no attempt has been made to assess the quality of the coded (or

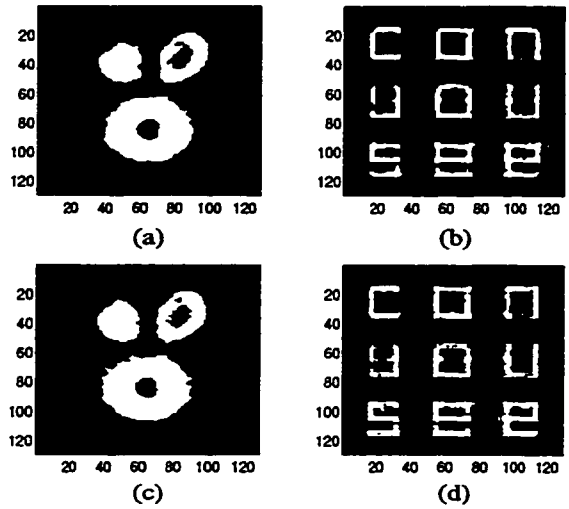


Figure 5.3: Images reconstructed from coded projections: (a) LP coded; CR=9 (b) LP coded; CR=6.5 (c) DCT coded; CR=14.5 (d) DCT coded; CR=14.5.

reconstructed) image by means of quantitative measures such as the mean square error or SNR (which can be defined in various ways) since such measures are not necessarily true indicators of visual quality. An assessment of the quality is left to the viewer.

## 5.5 A new algorithm for the reconstruction of binary images

The algorithm for the reconstruction of binary images from 4 projections, discussed in Section 2, gives good reconstructions. However, the algorithm is applicable to a specific case of four projections associated with the lattice points. As a consequence, the two pairs of projections consist of rays spaced at different intervals (unity for vertical and horizontal, and $\sqrt{2}$ for the diagonals). CT scanning generally involves constant ray-spacing in all directions. Finally, the above algorithm does not address situations involving rays of finite width (strips).

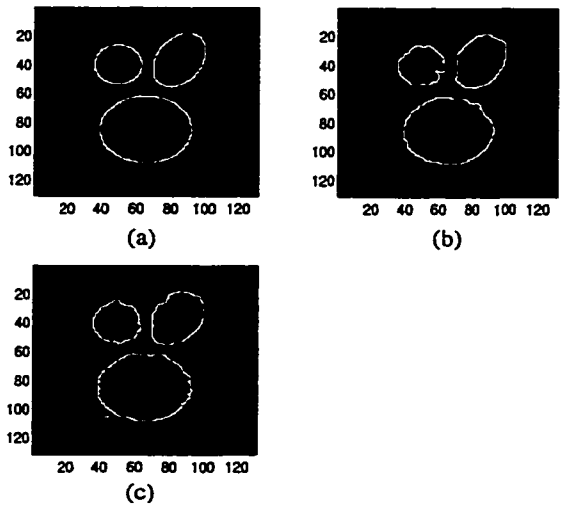


Figure 5.4: (a) Contours; (b) LP coded; CR=9 (c) DCT coded; CR=14.5.

In this section, a generalization of the algorithm of [199] to handle the situations mentioned above, is attempted. The generalization follows naturally from the generality of the operations of projection and backprojection based on the pixel assumption. Let $\epsilon_{\theta_i}(l) = p_{\theta_i}(l) - \hat{p}_{\theta_i}(l)$ be the estimation error-sequences associated with the projections. (5.2) can be written as

$$\hat{f}_{\theta_{i+1}}(m,n) = \hat{f}_{\theta_i}(m,n) + e_{\theta_{i+1}}(m,n) \tag{5.14}$$

where,
$$e_{\theta_{i+1}}(m,n) = \frac{\epsilon_{\theta_{i+1}}(l)}{L_{\theta_{i+1}}(l)}\Delta(l) = \mathcal{B}\{\epsilon_{\theta_{i+1}}(l)\} \tag{5.15}$$

The index $l$ in (5.14) and (5.15) corresponds to the ray at angle $\theta = \theta_{i+1}$, passing through the pixel centered at $(m,n)$. $L_{\theta_{i+1}}(l)$ is the length of the ray, and $\Delta(l)$, its intersection with the pixel centered at $(m,n)$. *It is crucial to recognize that* $e_{\theta_{i+1}}(m,n)$ *is equivalent to (discrete, or weighted) backprojection of the error* $\epsilon_{\theta_{i+1}}(l)$. When projections over a general geometry are considered, the weighting of the error will have to be suitably modified. The modification is based on the following result:

**Theorem:** Let $f$ be an unknown I-element vector, whose inner product $p_0$ with a weighting vector $w$ is known. Let $g$ be a noisy observation of $f$. The elements of $\hat{f}$

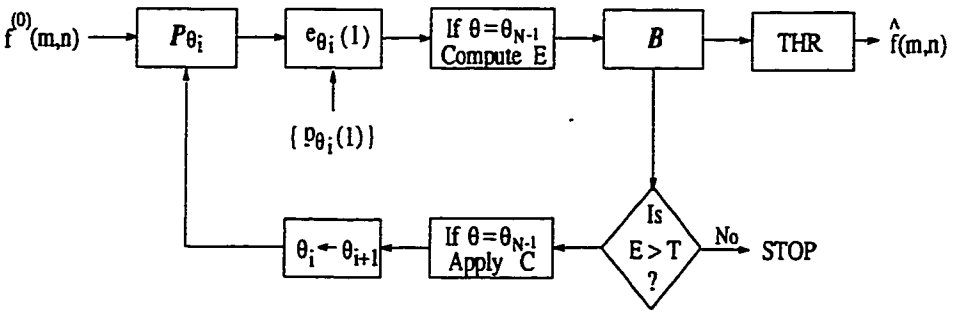


Figure 5.5: Algorithm for the reconstruction of binary images.

that minimize $||g - \hat{f}||^2$ subject to $p_0 =< \hat{f}, w >$ are given by:

$$\hat{f}_i = g_i + \frac{p_0 - < g, w >}{||w||^2} w_i, \quad i = 1, 2, ...I \tag{5.16}$$

The above formula is the very heart of the family of ART [46, 56, 45, 183][8], and the origin of the methodology of the solution is attributed to Kacmarz [81] [183] (a very lucid explanation with a passing mention of the analogy to backprojection is available in [183]). A proof is offered in Appendix-C, where it is also shown that the theorem of [199] is a special case of the above theorem. Relevance to backprojection is obtained by associating $\hat{f}_i$ and $g_i$ to the pixel values, $\{w_i\}$ to the projection-weights, and $p_0$ to the available value of the line integral, respectively, *along the ray under consideration.* The modified estimation algorithm is obtained by replacing $\Delta$ by the weight associated with the pixel, and $L_{\theta_{i+1}}$ by the squared-norm of the vector of weights, along the ray under consideration, in (5.15). Alternatively, the error sequence to be backprojected can be normalized.

Thus, the procedure for reconstruction consists of projecting the estimate at an angle at which a projection is available, backprojecting the error and superposing

[8]ART algorithms generally involve all of the $N^2$ pixels, which are concatenated into a vector, so that $\hat{f}$, $g$ and $w$ are $N^2$-element vectors. The approach developed here is based on an optimization over every ray ($I$ denotes the number of pixels along a ray). From an implementation point of view, some of the methods involve an updation of all of the pixel-values based on every line integral. Methods that incorporate weighted assignments (updation/backprojection) along the particular ray under consideration, boil down to the approach presented, when the weights used are identical.

it on the previous estimate to form the next estimate, and repeating the above to utilize all the available projections. This is the basis of the generalization, depicted in the block-diagram in fig. 5.5. Note that the block $\mathcal{B}$ represents backprojection of the error in the projection under consideration, and summing it to the (previous) image estimate. The final step in each iteration consists of applying the constraint $0 \leq f \leq 1$ (denoted by C) which form the basis of the subsequent iteration. $\mathcal{P}_{\theta_i}$ is the operation of projection at angle $\theta_i$. $E$ is an error-measure in terms of the projections.

Preliminary simulation results of an implementation of the algorithm are shown in fig. 5.6. The test image is shown in (a). Four projections of the image were computed using (2.13). The result of reconstruction by the proposed algorithm after 50 iterations is shown in (b). Some of the errors in the reconstruction can be accounted for by refining the projection and backprojection algorithms used, or by using the routines from SNARK. The performance of the algorithm is yet to be studied in detail.

**Remarks:**

1. The approach developed here has the general form of ART, and may be referred to as binary ART (BART, [53]). Members of the family of ART differ from each other by the type of, and the stages in which, the constraints and tolerances are imposed, and the approximations involved. In particular, any ART can be converted to a BART by incorporating suitable constraints [53]. The algorithm presented above differs from the BART of [53] in terms of constraints, tolerances, updation, and approximations.

2. Further work in the present framework includes incorporating some of the tolerance procedures of [53], studying the effects of the presence of noise in the projection data, and evolving a stopping procedure. It is also relevant to study the performance with true projection data, in view of the remarks of

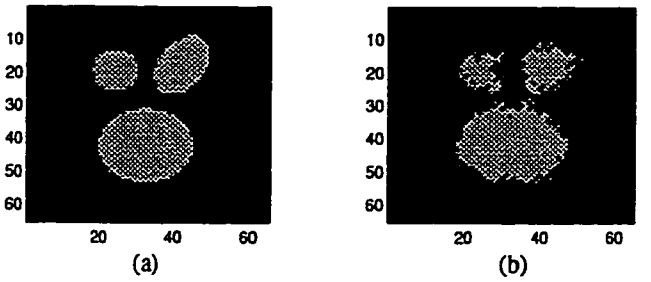


Figure 5.6: (a) A binary phantom, (b) reconstruction of the phantom from 4 projections using the proposed algorithm.

Gilbert [41] on the limitations of ART when the model for the line integral deviates significantly from the true situation. In this context, it would be useful to study algorithms based on a minimization of cost functions that take into account the effect of noise, similar to those considered by Kashyap and Mittal [86].

## 5.6 Conclusion

Compression of binary images in the RS has been addressed. Representation of binary images by few projections is the basis for the approach. Additional compression has been achieved by coding the non-binary projections by predictive and transform methods. A further advantage, arising out of the necessity to process only the non-zero segments of the projections, has been mentioned. Illustrative simulation examples using LPC and the DCT techniques employing uniform quantizer have been presented. Improved CRs are possible by utilizing adaptive quantizers. In the case of the DCT, efficient bit allotments based on the characteristics of the image under consideration will give better results. The approach can be used to compress binary as well as gray-level pictures. While the scheme is very useful for on-line transmission, its inability to reconstruct on-line is a limitation.

A new algorithm has been proposed to overcome the limitations of [199] with

respect to its applicability to a general CT scenario. The algorithm is the result of the observation of the involvement of backprojection in the previous algorithm, and a least squares theorem. The algorithm belongs to the general class of ART, with differences in the type of, and the stages in which, the constraints and tolerances are imposed.

# Chapter 6

# Two-dimensional Spectral Factorization

In this chapter, 2-D spectral factorization in the RS is considered. The RT reduces the 2-D factorization problem to a set of 1-D problems, as a consequence of the central slice theorem involving a 2-D ACF. In this context, the RT of 2-D autocorrelation function, and some of its properties are presented. Spectral factorization in the RS is discussed. An extension to the discrete case through an adequate sampling of the RT, and correlation-match are discussed. Apart from the theoretical development and interpretations, further applications for modeling and processing tomographic data are indicated.

## 6.1 Introduction

Spectral factorization (SF) refers to the determination of a stable, causal and linear shift-invariant (LSI) system of finite order such that the magnitude square of its frequency response matches a given spectral density function (SDF). The stochastic version of the problem corresponds to finding a white-noise driven system that realizes the given SDF. SF techniques are found useful in the design and implementation

of recursive filters, filter stabilization, stochastic realization, spectral-matching and signal classification [187, 82, 32, 33, 71, 172, 100, 72, 144].

In the 1-D case, it is always possible to find stable and causal spectral factors associated with a given rational SDF. This is due to the fundamental theorem of algebra which states that a polynomial of finite degree can always be factored into a product linear factors. In practice, spectra are irrational, and the two major approaches to finding rational approximations that match the SDF, are the Wiener-Doob and linear prediction methods [72].

In 2-D, however, SF is generally not possible due to the lack of a fundamental theorem of algebra. This drawback is regarded as a *fundamental curse* [60]. Researchers have therefore resorted to finding a difference equation representation for the 2-D LSI system that approximately realizes a given SDF. Ekstrom and Woods [32] developed an extension of the Wiener-Doob technique to 2-D [32], based on the fact that the cepstrum and the inverse cepstrum share the same region of support[1]. The approximations involved in computing the cepstrum affect the stability of the resulting system. The method of linear prediction for SF has also been extended to 2-D [117, 71, 172]. Marzetta [117] studied an extension of 1-D LP theory to 2-D, and devised a 2-D analog of Levinson algorithm that yields recursive factors of infinite order on solving an infinite set of equations. Jain [71], and Ranganath and Jain [172] studied causal and semicausal modeling resulting in an algorithm similar to that of Levinson, and developed a procedure to obtain rational approximation [172]. When a finite set of lags of the ACF are given, the method guarantees neither stability nor a correlation match. However, it is a practical procedure in which model stability and improved autocorrelation match follow after some finite model order. Lawton [95] observed the limitations of the quarter-plane (QP) models, and showed [94] that any continuous 2-D spectrum can be uniformly approximated by the squared modulus of a recursively stable finite trigonometric polynomial on a non-symmetric

[1]The basic approach had been indicated by Whittle [226] in 1954 [172].

half-plane (NSHP). Efforts towards obtaining 2-D spectral factors through 1-D techniques include [99, 100, 132]. Le Roux [99] and Le Roux and Dubus [100] consider a factorization based on the *one-projection theorem* [122], in the context of 2-D filter stabilization. A 2-D factorization is obtained by carrying out a single 1-D factorization on a sequence obtained by concatenating the rows of the zero-padded 2-D autocorrelation sequence[2]. However, the associated assumptions are restrictive. Further, the stability of the 1-D spectral factors cannot guarantee that of the 2-D filter obtained by re-ordering. Murray [132] proposed an NSHP SF by considering the 2-D PSD as a parameterized family of 1-D PSDs, resulting in factors that are of infinite order along one direction.

Several techniques, most of which are variants of the approaches outlined above, have emerged over the recent years, the details of which are not considered here. In general, methods of 2-D SF involve obtaining causal finite-support filters that approximately realize a given SDF. The issues involved are the accuracy of approximation, the size and the shape of the filter support, and stability. The cause of the difficulties lie in the lack of polynomial factorization theorem and the notion of causality, in 2-D.

In this chapter, 2-D SF in the Radon space is discussed. The RT of a 2-D ACF, and some of its properties are reviewed. The RT reduces the 2-D problem to a set of 1-D problems, which are easy to handle [3]. Stability is not an issue, and correlation match is guaranteed, though in the RS. In theory (when all the projections of the 2-D ACF are available), exact 2-D SF is possible. In practice, the ACF lags in the RS are required to represent an adequately sampled version of the RT of the 2-D ACF. It should be pointed out that the applications contemplated

[2]Such a sequence is a 'Radon projection' in the sense that its values can be recovered from a slice of the associated 2-D (continuous) FT, at an angle specified by the length of the zero-padding [122]. This result is for the class of bandlimited signals of finite order. The frequency response of the resulting 2-D filter suffer from additional distortions [120, 121].

[3]Although the RT of a 2-D ACF arises in intermediate steps in the derivation of the relations involving power spectra [76, 206], a formal framework of 2-D spectral factorization based on the RT of a 2-D ACF is being presented for the first time.

here are towards processing the data within the RS. For example, SF in the Radon space does not represent a substitute to the current methods of designing 2-D spatial filter masks. Possible applications of factorization in the RS are indicated with an example involving the LPCs. The theory suggests a new method of 2-D spectrum estimation, which forms the topic of the next chapter.

The RT of a 2-D ACF is considered in the following section. In Section 3, it is shown that the 2-D SF problem can be cast as a set of 1-D problems. Applications of the theory are discussed in Section 4, and Section 5 concludes the chapter.

## 6.2 The Radon transform of 2-D autocorrelation function

Consider a 2-D ACF $r(\tau_1, \tau_2)$. Let $r_\theta(\tau)$ represent its projection:

$$r_\theta(\tau) = \int\int r(\tau_1, \tau_2)\delta(\tau - \tau_1 \cos\theta - \tau_2 \sin\theta) d\tau_1 d\tau_2 \tag{6.1}$$

The 2-D ACF on the plane is uniquely determined by the totality of its projections on such a set of 1-D subspaces that cover the 2-D space. From the CST, the FT of a projection of the 2-D ACF at an angle $\theta$, $R_\theta(\omega)$, is a slice of the 2-D FT of $r(\tau_1, \tau_2)$. But the FT of the ACF $r(\tau_1, \tau_2)$ is the 2-D SDF $S(\omega_1, \omega_2)$. Hence, *the FT of the projection $r_\theta(\tau)$, of the ACF $r(\tau_1, \tau_2)$, is a slice of the 2-D SDF $S(\omega_1, \omega_2)$ at angle $\theta$.* i.e.,

$$R_\theta(\omega) = S(\omega\cos\theta, \omega\sin\theta) \triangleq S_\theta(\omega) \tag{6.2}$$

This important result is pictorially depicted in fig. 6.1. Since $r_\theta(\tau) = \mathcal{F}^{-1}\{S_\theta(\omega)\}$, one may conclude that *every projection of a 2-D ACF is also an ACF (in 1-D).* Some of the important properties of $r_\theta(\tau)$ are reviewed below.

1. Every projection of a 2-D ACF is a symmetric, positive (semi-)definite (*psd*) function. This follows from the CST, as a consequence of the (semi-)positiveness of

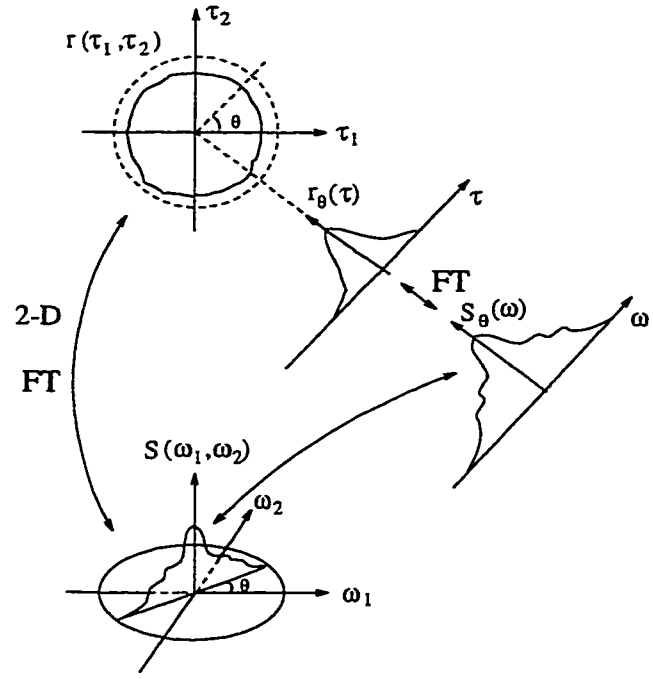


Figure 6.1: CST applied to 2-D autocorrelation function.

the 2-D SDF. If $r(x,y)$ is real, so is $r_\theta(\tau)$. Further, $|r_\theta(\tau)| \leq r_\theta(0), \quad \tau > 0$.

2. If $r(x,y)$ has no periodic components, and $\lim_{x,y\to\infty} |r(x,y)| = 0$, then

$$\lim_{\tau\to\infty} |r_\theta(\tau)| = \lim_{\tau\to\infty} |\int r(\tau\cos\theta - u\sin\theta, \tau\sin\theta + u\cos\theta)du| = 0 \tag{6.3}$$

3. A circularly symmetric ACF of the form:

$$r(\tau_1,\tau_2) = f(|\tau|) \tag{6.4}$$

where, $|\tau| = \sqrt{\tau_1{}^2 + \tau_2{}^2}$, and $f(\tau)$ is an ACF, is fully determined by a single projection. The 2-D function can be obtained by Able-inversion [23].

An n-D symmetric correlation function (normalized ACF) has a lower bound of $-\frac{1}{n}$. This result is due to Bertil Matern [220]. Consequently, every projection $\rho_\theta(\tau)$ of a 2-D correlation function $\rho(\tau_1,\tau_2)$ is lower-bounded by $-1$.

Thus, the RT of 2-D ACF constitutes a set of 1-D ACFs. This is the basis of

2-D SF discussed in the following section.

## 6.3 2-D spectral factorization in the Radon space

Spectral factorization, described in frequency-domain, involves finding a function $H(\omega_1, \omega_2)$ such that

$$S(\omega_1, \omega_2) = \sigma^2 |H(\omega_1, \omega_2)|^2 \tag{6.5}$$

where $\sigma^2$ is a constant. In the space-domain, the problem may be described in terms of a real, symmetric function $r(\tau_1, \tau_2)$, whose FT is positive. In other words, the problem is to determine a function $h(x, y)$ such that:

$$r(\tau_1, \tau_2) = h(\tau_1, \tau_2) * * h(-\tau_1, -\tau_2) \tag{6.6}$$

where, ** denotes 2-D convolution. Since a realization requires $H(\omega_1, \omega_2)$ to be factored (approximated by a minimum phase rational function), a mere existence of such a function does not help, due to the lack of a factorization theorem in 2-D [4]. The 2-D problem, however, maybe reduced to a set of 1-D problems, in the RS, as a consequence of the CST involving 2-D ACFs. Specifically, it can be described in terms of the 1-D slices of the 2-D SDF, $\{S_\theta(\omega), 0 \leq \theta < \pi\}$. Alternatively, the problem may be described in terms of the projections (RT) of the 2-D ACF, $\{r_\theta(\tau), 0 < \theta \leq \pi\}$. To see this, consider the RT of $r(\tau_1, \tau_2)$ in (6.6). The RT of a convolution of 2-D functions is the (1-D) convolution of the individual RTs (i.e., of the respective projections):

$$r_\theta(\tau) = h_\theta(\tau) * h_\theta(-\tau), \qquad 0 \leq \theta < \pi \tag{6.7}$$

where, $h_\theta(\tau)$, is the projection of $h(\tau_1, \tau_2)$. The projections of $h(-\tau_1, -\tau_2)$ are given by $\{h_\theta(-\tau)\}$. The problem now consists of determining a set of 1-D functions $\{h_\theta(t), 0 \leq \theta < \pi\}$ subject to (6.7).

[4]Current approaches obviate the necessity for a factorization of the SDF by using difference equation representation that approximate a given SDF. In this thesis, the emphasis is on the RT and its role in allowing true factorizations of the slices of the 2-D SDF.

In view of the foregoing observation, the problem of 2-D SF can be restated as follows:

- Given a 2-D SDF $S(\omega_1, \omega_2)$ or the corresponding ACF $r(\tau_1, \tau_2)$, find a set of 1-D functions $H_\theta(\omega), 0 \leq \theta < \pi$ such that:

$$S_\theta(\omega) = \sigma_\theta^2 |H_\theta(\omega)|^2 \tag{6.8}$$

  where, $H_\theta(\omega)$ is the filter associated with the slice $S_\theta(\omega) = \mathcal{F}\{r_\theta(\tau)\}$.

Since $H_\theta(\omega)$ and $S_\theta(\omega)$ are the central slices of $H(\omega_1, \omega_2)$ and $S(\omega_1, \omega_2)$ respectively, $H_\theta(0) = H(0,0)$, and $S_\theta(0) = S(0,0)$. Hence, the gain $\sigma_\theta^2$ associated with each of the slices is equal to that of the equivalent 2-D filter, i.e., $\sigma^2$.

Thus, the SF problem on the 2-D Cartesian space has been reduced to a set of 1-D problems in the *Radon space*. The RT splits the 2-D problem into a set of *decoupled* 1-D problems, which can be handled easily by 1-D techniques, ensuring minimum-phase spectral factors. Hence, the necessity of factorizing a 2-D polynomial does not arise. The procedure results in a set of 1-D filters, $H_\theta(\omega)$, $0 \leq \theta < \pi$. The specific relation between the impulse response functions of the resulting set of 1-D filters, and the point spread function of the equivalent 2-D filter is given by the IRT of $\{h_\theta(t)\}$. This follows by comparing (6.7) with (6.6), assuming the uniqueness of the projection domain representation. i.e.,

$$h(x,y) = \mathcal{R}^{-1}\{h_\theta(t), 0 \leq \theta < \pi\} \tag{6.9}$$

The stochastic version of SF in the RS is described in terms of the slices $S_\theta(\omega)$ of the 2-D SDF $S_f(\omega_1, \omega_2)$ of a stationary random field (SRF), $f(x,y)$, or equivalently, in terms of the projections of the 2-D ACF, $r_f(\tau_1, \tau_2)$. Each of the projections of the ACF can be represented by a linear system driven by a process of known SDF. For example, the SDF of a (non-causal) Markovian process described by [220],

$$(\frac{\partial^2}{\partial x^2} + \frac{\partial^2}{\partial y^2} - \alpha^2) f(x,y) = \epsilon(x,y) \tag{6.10}$$

is given by:

$$S_f(\omega_1, \omega_2) = \frac{S_0}{({\omega_1}^2 + {\omega_2}^2 + \alpha^2)^2} \tag{6.11}$$

where, $S_0$ is the spectral height of the white noise field $\epsilon(x, y)$. Note that this function cannot be factorized. However, a slice of the SDF at angle $\theta$, given by $S_\theta(\omega) = \frac{S_0}{(\omega^2+\alpha^2)^2}$, can be factored as:

$$S_\theta(\omega) = \frac{S_0}{[(j\omega + \alpha)(-j\omega + \alpha)]^2} \tag{6.12}$$

The associated model is also (1-D) Markovian [220]:

$$(\frac{\partial^2}{\partial t^2} - \alpha^2) p_\theta(t) = \epsilon(t) \tag{6.13}$$

It should be pointed out, however, that a projection of a 2-D ACF is not the same as the 1-D ACF of the corresponding projection of the associated SRF. The above characterization is interesting in view of the difficulties encountered with the line integral of an SRF [5].

The discussion so far, has been in the continuous domain. In practice, only discrete processing is possible. The foregoing theory extends to the discrete case, as long as the discrete ACF lags in the RS represent an adequately sampled version of the 2-D ACF. The associated 2-D SDF will be on a polar raster [122].

2-D SF in the RS consists of the following steps:

- Specify the discrete projections $r_\theta(l)$ of the 2-D ACF, $r(\tau_1, \tau_2)$ at equispaced angles $\theta$, $0 \leq \theta < \pi$.
- Carry out 1-D SF on each of the projections, $r_\theta(l)$ i.e., obtain the 1-D minimum phase spectral factors corresponding to each $r_\theta(l)$.

The first step involves a computation of the discrete projections $r_\theta(l)$ of 2-D ACF. If one starts from a continuous ACF, this is done by adequately sampling the RT of the ACF. If the 2-D ACF is discrete, then the line integral will have to be suitably approximated. Note that an explicit computation of the ACF may not be required.

[5] Some of these issues are discussed in Chapter 7.

### 6.3.1 Correlation match

Correlation match means that the output ACF/PSD of the system derived by SF matches the given ACF/PSD, implying that the system is consistent with the given PSD/ACF. In practice, a finite set of autocorrelation lags is available, and the output ACF of the system is required to match the given ACF over a certain window, and remain positive-definite (*pd*) beyond the window[6]. In 1-D, correlation match can always be ensured. However, this property does not extend to 2-D because, a *pd* sequence on a rectangular window need not have a *pd* extension with a match on the window [71]. Thus, factorization on a rectangular support need not yield systems that are consistent with the given ACF.

2-D SF discussed in this chapter possesses correlation matching property in the *Radon space*, by virtue of being a set of 1-D problems. An exact match with the given 2-D ACF, although theoretically guaranteed, depends upon how well $\{r_\theta(\tau)\}$ represent the function $r(\tau_1, \tau_2)$. For example, an isotropic SRF is represented adequately by a single projection, and perfect correlation match can be achieved for this case. A general sampling strategy for good correlation match, based on [174], is given below.

Let $r(\tau_1, \tau_2)$ have a finite space-bandwidth product, i.e., $r(\tau_1, \tau_2) \approx 0$, $\tau_1^2 + \tau_2^2 \geq {\rho_c}^2$ and $S(\omega_1, \omega_2) \approx 0$, $\omega_1^2 + \omega_2^2 \geq {\omega_m}^2$. $\rho_c$ is the correlation 'time', and $\omega_m$, the bandlimit. Then, the minimum number of samples that should be considered over each projection, is approximately, $N_m = (2/\pi)\omega_m \rho_c$. The minimum number of projections $M_\theta$, equispaced in angle over $[0, \pi)$, is $M_\theta = [\rho_c \omega_m] + 2$.

**Remarks:**

1. In SF, the SDF/ACF is assumed to be specified/available. For example, in filtering applications, it is specified, and in many image processing applications

[6]This notion also arises in the context of autocorrelation extension in maximum entropy (ME) spectrum estimation problem.

such as restoration and coding, an analytical model for the ACF is used [72, 71].

2. In general, 2-D SF in the RS discussed above, is to be distinguished from SF of the individual projections of 2-D data. The two are equivalent only when the operations of autocorrelation and Radon transformation commute. Applications in which they are equivalent include object recognition and coding involving a modeling of a given class of images. The distinction between the two is best illustrated by the difference between the problem of reconstructing an object from its noisy projections, and that of its reconstruction from the projections of a noisy version. The former is the most commonly encountered and easy to solve wherein each of the projections is simply treated as a 1-D signal in white noise [203], whereas the latter is inherently two-dimensional in nature (eg., involving the 2-D structure of the noise field).

3. The problem of estimating the PSD from observed random field data via parametric models, i.e., *spectrum estimation*, also involves 2-D SF. This forms the topic of the next chapter.

### 6.3.2 Applications

SF is the basis of signal modeling, and arises in a variety of applications such as filtering, restoration, compression, and spectrum estimation. An mentioned in Remark-2 above, SF in the RS is implicit in many of the existing algorithms for processing data in the RS. Further possible applications of 2-D SF in the RS, not considered so far in the literature, are discussed briefly in the following. Application to 2-D spectrum estimation is deferred to the next chapter.

In principle, 2-D spectral factorization in the RS allows 2-D IIR filtering[7], as illustrated in fig. 6.2. The filter $H_{\theta_k}(\omega)$ is obtained by factorizing the respective

[7]The general notion of 2-D filtering via the RT has been proposed in [57, 162, 72].

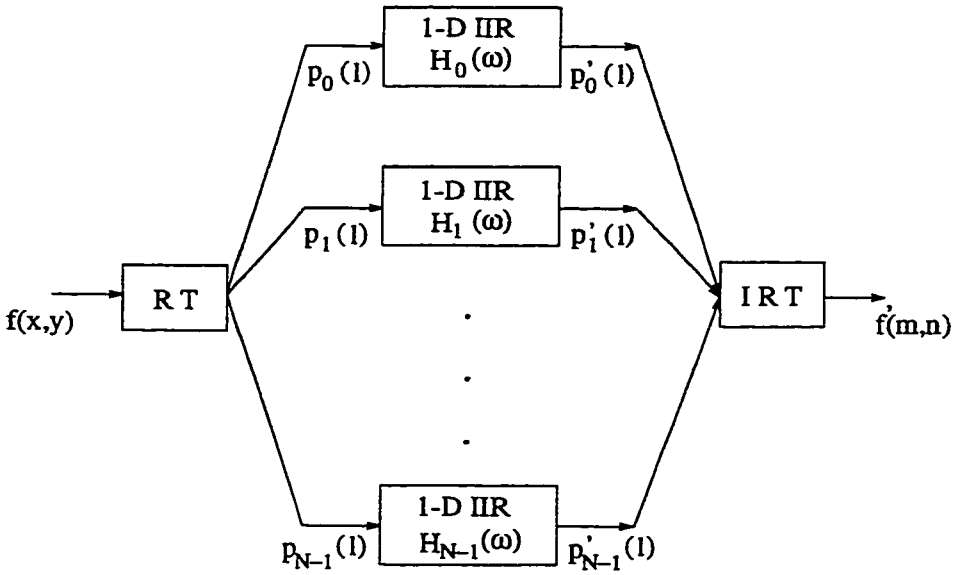


Figure 6.2: IIR filtering in the Radon space.

PSD $S_{\theta_k}(\omega)$. Whenever possible, the reconstruction filter can be absorbed into the filtering operation so that the reconstruction is obtained by backprojection. A perfectly circularly symmetric filter is implemented by choosing all the filters to be identical. With 1-D IIR filters, stability is not an issue, and it is lower in complexity for a given performance. Initialization for improving the performance of an IIR filter for short data segments is considered in [19]. Transient effects can also be countered by forward-backward processing. The complexity of the scheme, and the errors introduced by projection and reconstruction, limit the use of the above scheme as an alternative to filtering 2-D data in the spatial domain. Specific practical situations where the stochastic models and inverse filtering based on the the RT of 2-D ACF can be applied for restoration and compression are to be explored. For example, if a class of (CT) images is known to possess a certain correlation structure and hence a model, the model can be used for processing that class of images.

Consider the matching of 2-D spectra slice-by-slice, by the LP approach. The LP approach has been applied successfully to signal classification problems such as

speech/EEG recognition/classification [157]. Let $\mathbf{a_r} = [a_{r_1} \ldots a_{r_p}]^T$, be the LPC-vector associated with a reference PSD/signal, and $s(n)$ be any sequence whose corresponding LPC-vector is $\mathbf{a} = [a_1 \ldots a_p]^T$. If $R$ is the autocorrelation matrix of $s(n)$, the quantity:

$$d(\mathbf{a}, \mathbf{a_r}) = log\frac{\mathbf{a_r}^T R \mathbf{a_r}}{\mathbf{a}^T R \mathbf{a}} = log\frac{l_r}{l} \tag{6.14}$$

is a measure (named after Itakura [64]), of the distance between the sequences [157]. The rationale behind the above measure is that $d \longrightarrow 0$ as the spectrum approaches the reference spectrum.

The LPCs in the RS, i.e., the set of all LPCs associated with the spectral slices, $\{a_k(\theta_i) : k = 1, .., p;\ \theta_i = (\pi/N)i, i = 0, ..., N-1\}$, are, to a limited extent, features describing a 2-D object. The set $\{a_k(\theta_i) : \theta_i = (\pi/N)i, i = 0, ..., N-1\}$, is an LPC-pattern of order $k$. Invariance of the LPCs to gray-scale, shift, rotation and scaling are the issues to be addressed. Invariance to gray-scale and shift follow from that of the normalized ACF. A rotation of the 2-D spectrum/object results in a circular shift of the LPC-patterns. In the absence of rotation, the LPC distance measures $\{d(\theta_i) = log[l_r(\theta_i)/l(\theta_i)]\}$ can be used as a measure of match. It should be pointed out, however, that $\{d(\theta_i)\}$ cannot be used as an *invariant-pattern*. One approach to handling rotation consists of estimating it using an LPC-pattern of a certain order, using circular correlation as described in Chapter 3. The estimate of rotation can be utilized in appropriately shifting the patterns, facilitating the computation of the LPC distances as above. Alternatively, a CAR model can be used to describe each of the LPC patterns invariant to circular shifts, resulting in an invariant pattern in 2 variables. Finally, it is noted that the peak value of the circular cross-correlation itself can be taken as a measure of the match between two sets of LPC patterns.

Handling scaling, however, is not straightforward, since it is not clear as to how that would affect the LPCs.

Simulation was performed on the 'plane' image considered in Chapter 3, with

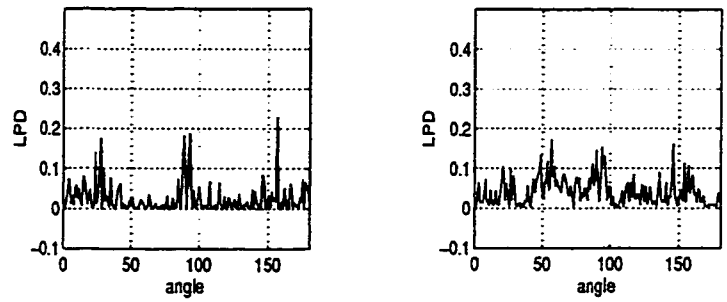


(a) (b)

Figure 6.3: LPC distances of: (a) amplitude-scaled and shifted object, (b) shifted, rotated and amplitude-scaled object.

gray-scale changes, shift, and rotation. Fig. 6.3(a) shows the sequence of LPC distances computed as described above, using the projections of an amplitude scaled and shifted object. The model order used was $p = 5$, for all the projections. The distances with respect to the LPCs of an amplitude-scaled and shifted object, rotated by 50°, is shown in fig. 6.3(b). The rotation estimated via circular correlation involving the second LPC pattern was 49°. Errors due to discretization and the interpolation used in digitally rotating the object, have contributed to the mismatch. However, LPC patterns are not as smooth as the low-order MPs, and are quite sensitive to even small changes. Hence, suitable (overall) statistical distance measures would be required for classification.

**Remark:** In general, the role of orientation has to be taken into account in applications. In some applications such as NDT, rotation may not be an issue.

## 6.4 Conclusion

In this chapter, 2-D spectral factorization in the RS has been considered. The 2-D problem reduces to a set of decoupled problems in the RS, as a consequence of the CST applied to 2-D ACFs. The resulting 1-D spectral factorizations could be carried out independently on each of the projections. By virtue of being a set of

1-D problems, stability is not an issue, and the correlation matching property of the spectral factors can be assured, in the RS. Mathematically, SF in the RS provides a solution to the problem of 2-D SF. The theory, presented in the continuous domain, extends to the discrete case when the discrete RT is obtained from sampling the ACF adequately. Possible applications of SF in the RS have been discussed briefly. The advantages of the proposed IIR filtering scheme with respect to current methods are to be studied with relevance to specific applications. LPC-patterns in the RS have been introduced. The LPCs are invariant to the gray-scale and translation the object. Two approaches to handling rotation have been indicated. The issue of scaling, and the performance with respect to MPs, need to be studied further.

Unfortunately, spectral factorization of the projection of 2-D a autocorrelation function is not equivalent to a factorization of the autocorrelation of the projections of the associated SRF. In other words, the process generated from a projection of the 2-D ACF of an SRF is different from the corresponding projection of the SRF. The problem of estimating the PSD from observed SRF data, i.e, *spectrum estimation*, based on parametric models, also involves 2-D spectral factorization. The theory presented in this chapter suggests a new method of 2-D spectrum estimation, and forms the topic of the next chapter.

# Chapter 7

# Two-Dimensional Spectrum Estimation using the Radon Transform: Some Issues and a New Approach

A review of the existing methods of 2-D spectrum estimation emphasizes the scope for further research on this difficult topic, despite recent advances. Among the recent approaches to 2-D spectrum estimation, the one based on the RT [204] is attractive, due to a reduction in dimensionality it offers. However, there are many issues that arise in applications involving the RT of an SRF, that have not received due attention in the literature so far. In this chapter, a new representation for the RT of an SRF, valid upto second order statistics, is used for analyzing the properties of the transform. Limitations pertaining to the theory and its extension to finite-extent data, are discussed, in the context of the previous approach to 2-D spectrum estimation using the RT. The difficulties in characterizing the RT of an SRF, and their implications on 2-D spectrum estimation provide a motivation for investigating new approaches. A novel approach to 2-D spectrum estimation based on the RT

of 2-D autocorrelation of an SRF, is investigated. Estimation by autoregressive modeling of the projections of 2-D autocorrelation is considered, and an extension to maximum entropy method is proposed. Relevant issues are discussed, and other possible approaches are indicated.

## 7.1 Introduction

Spectrum estimation refers to the problem of estimating the power density spectrum, popularly known as power spectrum density (PSD), of a random process from a finite-extent observation of a sample of the process. It is a topic of importance in many fields of science and engineering and has a rich history [182, 86]. Extensive research that has been carried out highlights the fact that there is more to be done, especially in the multi-dimensional case [119, 29, 71, 116].

Classical methods of spectrum estimation (SE) based on the FT, namely the periodogram and the Blackman-Tukey method, suffer from spectral leakage (smearing) and limited resolution. The implicit assumption that the data/autocorrelation is zero beyond the points of observation results in spectral smearing. The price paid for using a smoothening window is that of frequency resolution. The minimum variance method of Capon [14], fundamentally different from the conventional approach, was the first attempt towards improved resolution. Modern methods try to overcome the limitations of the conventional approach by using finite parametric models for the spectra [86]. The most popular of the parametric models is the autoregressive (AR) model. Its popularity stems from its success in speech processing based on the model for speech production [157, 112, 192], and in geophysics. The all-pole structure of the AR model makes it suitable for representing processes with peaky spectra [1] [2]. The high-resolution capability of the AR model arises from

[1] It is for this reason that the AR model is often used to estimate the PSD of sinusoids in white noise, although the Pisarenko harmonic decomposition is the appropriate approach [86].

[2] In the physical world, it is rather the presence of a frequency component that is appreciated and more easily detected [192].

the implicit extrapolation of the autocorrelation. The linearity of the problem of solving for the predictor coefficients, and the availability of the efficient Levinson-Durbin algorithm that also guarantees stable recursion, is an attractive feature. In contrast, the solution for autoregressive moving-avergae (ARMA) model coefficients is non-linear. Further, an ARMA model can be approximated by an AR model of sufficient order [86]. An additional reason for the attention afforded to the AR model is the equivalence of AR SE and the maximum entropy method (MEM) of Burg [12] [221, 31, 146]. The rationale of the ME principle is elegantly discussed by Jaynes [79]. The concept of maximizing the information theoretic quantity of entropy, defined by $H = \int logS(\omega)d\omega$, subject to correlation-matching constraints, is much broader than those of assuming the correlation lags to be zero beyond a certain point or to obey a certain model. In effect, the ME principle selects the flattest of all possible spectra consistent with the given values of the autocorrelation. On the other hand, it provides an ME extrapolation of the given correlation lags, resulting in high-resolution [3]. In general, estimation of spectra from a finite observation is not possible without additional information or constraints that restrict the class of spectra [139, 48].

The success of high-resolution parametric methods in 1-D led the researchers to consider an extension of the ideas to 2-D involving random field measurements [119, 71, 138, 116]. Initial work in 2-D high-resolution spectrum estimation involved a separable approach [4], of employing 1-D techniques sequentially along each of the dimensions [68, 80, 37, 75]. However, the assumption of separability is not justified [204, 71, 66], and it ignores the 2-D nature of the data [138]. Estimation by 2-D extrapolation of the data [75, 36, 218] provides limited improvement in resolution

[3]The idea of maximum flatness can be confusing, as the terms 'flatness' and 'high-resolution' are mutually conflicting; these aspects are clarified in [113, 133]. In fact, different measures of 'flatness' result in different formulation of the entropy and hence in different classes of spectrum estimators [133, 134].

[4]When the DFT is used along one of the dimensions, the approach is also referred to as hybrid spectrum estimation.

at high SNRs [116]. These observations led to 2-D spectrum estimation algorithms based on 2-D LP models [73, 66, 71, 13, 138]. Cadzow and Ogino [13] proposed the use of quarter-plane (QP) ARMA models. 2-D LP models with causal (NSHP), semi-causal and non-causal regions of support have been studied by Jain [71], and Jain and Ranganath [73]. An extension to m-D was considered by Nikias and Raghuveer [138]. Semi-causal and non-causal models do not guarantee a non-negative PSD. The 2-D QP AR models have received the most attention in the literature, due to the availability of a 2-D Levinson-like algorithm [116]. While causal models do guarantee positive estimates, they do not guarantee stable AR models.

Further advances in 2-D high-resolution spectrum estimation include the use of non-causal AR models [194, 50], the development of an efficient Burg-type algorithm for the solution of 2-D causal AR parameters directly from the data [118, 92], and estimation based on 2-D ARMA model [232]. The method of [194, 50] are based on the assumption of non-causal AR or Gaussian-Markov model for the data, resulting in a non-linear minimization problem that requires numerical techniques for the solution. A recent trend consists of an application of the so called minimum free energy method of parameter estimation for spectrum estimation [155, 198, 154]. Very recently, hybrid [20] and AR [87] methods of 2-D spectrum estimation, based on the minimum free energy criterion, have emerged [5].

There has been considerable effort on 2-D MESE. The form of 2-D MESE had been discovered by Barnard and Burg [7], [229]. Woods [229] showed the existence of the 2-D MESE under the assumption that the available autocorrelation (AC) lags form a part of some positive-definite (*pd*) function. Dickinson [29] pointed out the difficulty in checking whether a given set of AC lags in 2-D is extendable. Specifically, a real-valued function positive-definite on a rectangular grid need not be extendable [186]. When the ME solution exists, it is shown to have a parametric model of the form given in [229, 7, 74]. However, the lack of a factorization theorem

[5]These two methods appeared after the new approach of this chapter had been proposed.

for 2-D polynomials renders the solution non-linear [229, 7]. Lev-Ari [97] has given a characterization of m-D ME covariance and showed that only approximate solutions are possible. Thus, in contrast with the situation in 1-D, 2-D MESE does not have a closed-form solution. Consequently, approaches to 2-D MESE have been largely computational, and attempt to approximate the ME PSD without having to solve for the coefficients of the parametric model [224, 225, 104, 107, 115, 105, 194]. These methods require either iterative algorithms that have trouble converging, or non-linear optimizations that guarantee convergence at the cost of heavy computation [116].

In general, in spectrum estimation techniques involving 2-D parametric models, the choice of the predictor mask, direction of prediction, and non-uniqueness of the resulting estimates, are major issues. Unlike 1-D parametric methods, the 2-D counterpart has remained a difficult task. Further, the equivalence of AR and ME methods does not hold good in 2-D. The difficulties encountered may be attributed to the lack of a fundamental theorem of algebra, as well as the lack of the notion of causality in two dimensions [71, 106, 30].

An RT approach to 2-D spectrum estimation was proposed by Srinivasa et al. [204], to circumvent the difficulties associated with direct 2-D high-resolution methods. The RT was used to reduce the 2-D spectrum estimation problem to a set of 1-D problems, each of which can be solved by a 1-D high-resolution technique. An equivalence of the AR and the ME methods of spectrum estimation in the RS has been discussed in [206]. However, [204] involves the line integral of an SRF, which does not exist in the mean square sense [76]. Further, the approach involves a pre-filtering of the data by a frequency response of $|\omega|^{1/2}$ or equivalently, a post-multiplication of the estimated slices of the 2-D PSD by $|\omega|$. This would emphasize noise, and suppress very low frequencies. Such a filtering would also distort the shape of the spectrum. The RT approach has been applied to estimate the PSD from data available on a discrete polar raster [34]. However, their method is also

based on the RT of an SRF. Further, they assume that a projection of the 2-D ACF and the ACF of the projection of an SRF are the same, contrary to the observations in [76, 72, 204].

In this chapter, some of the issues associated with the representation of the RT of an SRF are highlighted, and a novel approach to 2-D spectrum estimation is investigated. A new representation for the RT of an SRF, based on a 2-D version of the representation of a stationary process as a cosinusoidal function of appropriate random variables (RVs) [145], is developed. This representation is sufficient for all applications involving autocorrelations/power spectra. An expression for the autocorrelation of a projection of an SRF is derived using the above representation, in terms of the projection of the 2-D ACF, resulting in the projection-slice theorem for SRFs. The results agree with the conclusions of Jain and Ansari [76]. However, they worked with the modified transform and then deduced the nature of the transform. Here, an expression for the transform itself is used and the necessity for the modifying transform is pointed out, and its effect is discussed. A preliminary analysis of the RT of an SRF evaluated over a finite support is carried out. A new approach to 2-D spectrum estimation, based on the RT of a 2-D ACF is investigated, and an extension of the approach to 2-D MEM is considered. Although the RT of 2-D ACF has been considered in an intermediate step involving the derivation of the relations involving the power spectra [76, 206], its explicit use is being considered for the first time.

In the following section, a new representation for the RT of an SRF is developed, based on which the projection slice theorem for SRFs is derived. Issues involving the RT of an SRF, and the associated method of spectrum estimation are discussed. In Section 3, a new approach to 2-D spectrum estimation based on the RT of a 2-D ACF is presented, and an extension to 2-D MEM is considered. In Section 4, simulation results are presented. Section 5 concludes the chapter.

## 7.2 The Radon transform of an SRF

Consider a real, zero-mean SRF $f(x,y)$ with a PSD $S(\omega_1,\omega_2)$. In a manner analogous to the 1-D case [145] an SRF with PSD $S(\omega_1,\omega_2)$ may be represented by a cosinusoidal function of RVs, $\Omega_1$ and $\Omega_2$:

$$f(x,y) = a\cos(\Omega_1 x + \Omega_2 y + \Phi) \tag{7.1}$$

where, the joint probability density function $p_{\Omega_1\Omega_2}(\omega_1,\omega_2)$ of the RVs $\Omega_1$ and $\Omega_2$ is chosen to be the normalized PSD $2a^{-2}S(\omega_1,\omega_2)$, and $a^2 = 2\int\int S(\omega_1,\omega_2)d\omega_1 d\omega_2$. The RV $\Phi$ is uniformly distributed in $[-\pi,\pi]$. Clearly, $E\{f(x,y)\} = 0$, and $E\{f(x,y)$ $f(x+\tau_x, y+\tau_y)\}$ equals $r_f(\tau_x,\tau_y)$. Given a function $S(\omega_1,\omega_2)$, an SRF (ensemble) with $S(\omega_1,\omega_2)$ as its PSD can be constructed by (7.1). The RT of $f(x,y)$ is another random field (a function of $t$ and $\theta$) which can be expressed in terms of the RVs $\Omega_1$ and $\Omega_2$, and the uniform phase $\Phi$, as follows:

$$p(\theta,t) = \frac{a}{|\Omega|}\cos(\Omega t + \Phi)\delta(\theta - \theta_\Omega) \tag{7.2}$$

where, $\theta_\Omega = tan^{-1}(\Omega_2/\Omega_1)$, and $|\Omega| = \sqrt{\Omega_1^2 + \Omega_2^2}$. $E\{p(\theta,t)\} = 0$, and the ACF of the RT is:

$$E\{p(\alpha,t)p(\beta,t+\tau)\} = \mathcal{F}^{-1}\left\{\frac{S_\alpha(\omega)}{|\omega|}\right\}\delta(\alpha-\beta) \tag{7.3}$$

where, $S_\theta(\omega) = \mathcal{F}\{r_\theta(\tau)\}$ is a slice of the 2-D PSD at angle $\theta$[6]. See Appendix-D for details. Thus, the RT of an SRF may be expressed in terms of a singular generalized function of the RVs that describe the SRF. From (7.3), the RT can be viewed as a parameterized family of projections $\{p_\theta(t),\ \theta \in [0,\pi)\}$, uncorrelated in the angle variable and stationary in the spatial variable [7].

With the above interpretation, the ACF of a projection at an angle $\theta$ is:

$$E\{p_\theta(t)p_\theta(t+\tau)\} \triangleq r_{p_\theta}(\tau) = \mathcal{F}^{-1}\{\frac{S_\theta(\omega)}{|\omega|}\} \tag{7.4}$$

[6] Assuming that $\frac{S_\theta(\omega)}{|\omega|}$ exists in the limit. The line integral is seen to be an unbounded RV, in general.

[7] Jain and Ansari [76] first showed that the modified transform is whitening, and then concluded that the RT is also whitening in the angle-variable.

and the PSD of the projection is $S_{p_\theta}(\omega) = \mathcal{F}_1\{r_{p_\theta}(\tau)\}$. Indeed, $r_{p_\theta}(\tau)$ may be defined as:

$$r_{p_\theta}(\tau) \triangleq \lim_{\Delta->0} \int_{\theta-\Delta}^{\theta+\Delta} E\{p_\alpha(t)p_\theta(t+\tau)\}d\alpha \tag{7.5}$$

It is clear from the above is that *the autocorrelation of the projection of an SRF is not the same as the projection of the autocorrelation of the SRF*. Note that $\frac{S_\theta(\omega)}{|\omega|}$ does not exist in general, in the ordinary sense. However, if:

$$\tilde{p}_\theta(t) = \mathcal{F}^{-1}\{|\omega|^{1/2}\} * p_\theta(t) \tag{7.6}$$

then, $$E\{\tilde{p}_\theta(t)\tilde{p}_\theta(t+\tau)\} = \mathcal{F}^{-1}\{S_\theta(\omega)\} = r_\theta(\tau) \tag{7.7}$$

The above equation leads to the interpretation that the PSD of a filtered (modified) projection is a slice of the 2-D PSD at the projection-angle.

$$S_\theta(\omega) = S_{\tilde{p}_\theta}(\omega) = |\omega| S_{p_\theta}(\omega) \tag{7.8}$$

where, $S_{\tilde{p}_\theta}(\omega)$ denotes the PSD of the filtered projection at angle $\theta$. The above result agrees with the Jain-Ansari result [76]. Note that (7.8) involves an implicit cancellation of $|\omega|$, which is problematic at the origin.

A difficulty arises in the physical interpretation of the results. From (7.8), it is clear that estimating $S_\theta(\omega)$ from the projections is equivalent to recovering it from $S_{p_\theta}(\omega) = \frac{S_\theta(\omega)}{|\omega|}$. However, it a faithful recovery is impossible due to the nature of the function $|\omega|$. Consider an example. Fig. 7.1(a) shows the 2-D PSD of the data corresponding an SRF with a Gaussian-shaped PSD as considered in [34]. The algorithm given in [197] was used to generate the data of size 5×5. Fig. 7.1(b) displays the PSD of the projection at angles spaced at 1 degree each over $[0, \pi/2)$. The projections were computed by Gaussian interpolation (with a large value of $\sigma$ to obtain a smooth spectrum) as in [34], for the purpose of illustrating the role of $|\omega|$ only[8]. In fig. 7.1(c), the PSD of the projections multiplied by $|\omega|$ is displayed.

[8]It is otherwise not possible to generate such a smooth spectrum. This particular example should not be taken to judge the performance of the RT approach. The use of interpolation with large values of $\sigma$ does not allow the results to be representative. A larger region of support will make the difference between the slices more apparent. Further, a change in the shape of the support changes the shape of the spectrum [169], as explained later in this section.

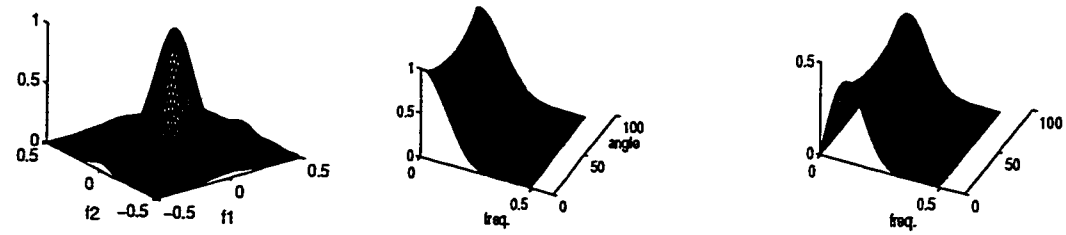


(a) (b) (c)

Figure 7.1: (a) 2-D PSD, (b) PSD of the projections, and (c) modified PSD.

Observe the distortion in the shape of the PSD.

The difficulty discussed above may be attributed to the fact that the derivation of the CST for SRFs was based on representing the RT in terms of generalized functions of RVs. Such representations would be useful as long as the final results (statistics) are in terms of well-behaved functions. However, $S_\theta(\omega)$ and $S_{p_\theta}(\omega)$ are related by (7.8), and spectrum estimation from the projections involves a *deconvolution* of $r_\theta(\tau)$ from $r_{p_\theta}(\tau)$. The nature of the function $\mathcal{F}^{-1}\{\frac{1}{|\omega|}\}$ does not permit a faithful deconvolution. Jain and Ansari [76] derived the result by first using the modified RT $\{\tilde{p}_\theta(t)\}$, and worked backwards to conclude that the RT of an SRF is whitening in the angle-variable. However, the modified RT was obtained by first computing the projections and then filtering them, which is not justified due to the non-existence of $p_\theta(t)$ (of an SRF). Further, a working-back requires the linear transform to be invertible.

An apparent recourse is to work with the RT of $\tilde{f}$; i.e., the SRF filtered by $|{\omega_1}^2 + {\omega_2}^2|^{1/4}$, which has the representation:

$$\tilde{f}(x,y) = a\cos(\Omega_1 x + \Omega_2 y + \Phi) \tag{7.9}$$

where, $p_{\Omega_1\Omega_2}(\omega_1,\omega_2)$ is given by $2a^{-2}|{\omega_1}^2 + {\omega_1}^2|^{1/2}S(\omega_1,\omega_2)$. The quantity $a^2$ is the normalizing factor, which exists when $S(\omega_1,\omega_2)$ is bandlimited. The line integral:

$$\tilde{p}(\theta,t) = a\cos(\Omega t + \Phi)\delta(\theta - \theta_\Omega) \tag{7.10}$$

exists, and is well defined. The projections are uncorrelated in $\theta$, and the PSD of a projection gives a slice of the 2-D PSD of $f(x,y)$ at the projection angle. However, this is simply a 2-D version of the deconvolution problem discussed previously, and involves an implicit attempt to cancel the factor $|\omega|$.

The difficulty discussed above does not manifest when the method is applied to resolving sinusoids in noise, since multiplying the the power spectrum by $|\omega|$ does not affect the resolution (unless one of the sinusoids is relatively weak and close to the origin). The shape of the PSD is not of concern in such an application. However, this is not a justification for assuming that the processes of projection and autocorrelation commute. It is significant to note in this context, that [34] did not use (7.8).

### 7.2.1 Inherent windowing

The discussions of the previous subsection addressed the theoretical case of the SRF over the entire plane. However, in practice, the data is always available over a finite domain. This amounts to an inherent windowing of the data. Being a non-linear operation, windowing the 2-D data is not equivalent to windowing its projections. As an example, consider the constant function $f(x,y) = 1$. The projection, of the function windowed by a uniform circular window (disc):

$$w(x,y) = \begin{cases} 1, & x^2 + y^2 \leq R \\ 0, & \text{otherwise} \end{cases}$$

is given by:

$$p_\theta(t) = \begin{cases} 2\sqrt{R^2 - t^2}, & t \in [-R, R] \\ 0, & t \notin [-R, R] \end{cases}$$

This is different from the RT of $f(x,y)$ (which does not exist) windowed by a uniform 1-D window $w(t) = 1,\ |t| \leq R$ and zero elsewhere. An equivalence is only with respect to the support information, i.e., $f(x,y) = 0,\ \sqrt{x^2+y^2} > R \Longrightarrow p_\theta(t) = 0,$

$|t| > 0$. In general, a window can be any 2-D function within a disc of radius $R$. The values of the projections for $|t| \leq R$ depends upon the shape of the window.

Consider the line integral of an SRF, evaluated over a convex domain $D$:

$$p_\theta(t) = \int_{u_1}^{u_2} f(t\cos\theta - u\sin\theta, t\sin\theta + u\cos\theta)du \tag{7.11}$$

where $u_1$ and $u_2$ are determined by the points of intersection of the line $(L_{\theta,t})$ with the boundary of $D$. The length of intersection $l_{\theta,t} = |u_1 - u_2|$ depends upon the shape of $D$ and the values of $\theta$ and $t$. A rotated coordinate system has been chosen for the ease of interpretation. Note that $p_\theta(t)$ is an RV, whose mean $E\{p_\theta(t)\}$ is $l_{\theta,t}\eta_f$, where, $\eta_f$ is the mean of the SRF. If $\eta_f$ is zero, then the RVs constituting a projection would be zero-mean. However, the variance of the RVs will be different. Consider the autocorrelation of a projection:

$$E\{p_\theta(t_1)p_\theta(t_2)\} = E\{\int_{l_{\theta,t_1}} f(t_1\cos\theta - u\sin\theta, t_1\sin\theta + u\cos\theta)du \int_{l_{\theta,t_2}} f(t_2\cos\theta - v\sin\theta, t_2\sin\theta + v\cos\theta)dv\} \tag{7.12}$$

In general, $l_{\theta,t_2} \neq l_{\theta,t_1}$. The above quantity is a function of $t_1$ and $t_2$, and not merely their difference. Thus, a projection of an SRF over $D$ consists of RVs whose statistical properties depend upon the length of integration, and hence the position (in terms of the variable $t$). Further,

$$E\{p_\theta(t_1)p_\theta(t_2)\} = \int_{l_{\theta,t_1}}\int_{l_{\theta,t_2}} r_f[(t_1-t_2)\cos\theta - (u-v)\sin\theta, (t_1-t_2)\sin\theta + (u-v)\cos\theta]dudv \tag{7.13}$$

Although (7.13) appears to be a function of $(t_1 - t_2)$, a close observation reveals that the limits of integration are functions of $t_1$ and $t_2$, which are in turn dependent on the shape of $D$. In general, the projections of a random field, evaluated over a finite domain, are not homogeneous, even if the random field is. This is in contrast with the 1-D case in which the data may be considered as a sample of a stationary process. *Further, $r_{p_\theta}(\tau)$ is not equal to $r_\theta(\tau)$, and there is no closed-form expression such as (7.4) between the two.* The ACF of the RT in both the variables, although

turns out to be a more complicated expression, reveals the presence of correlation between the projections[9].

It is clear from the above discussions, that the shape of the domain on which the data is available affects the shape of the spectrum estimate. This has also been verified through simulation.

### 7.2.2 Discussion

Some of the issues involving the RT associated with an SRF, and their implications on 2-D SE have been considered. The RT theory for SRFs involves the use of generalized functions. The ACF of a projection was seen to be related to the projection of the 2-D ACF in terms of the function $\mathcal{F}^{-1}\{|\omega|\}$; a slice of the 2-D PSD is related to the PSD of the corresponding projection through a multiplication by $|\omega|$ function vide (7.8). This was seen to lead to a difficulty in interpreting the result, and questions regarding its generality remain. A preliminary analysis of the RT evaluated over a finite support revealed some fundamental aspects such as non-stationarity of the projections, the lack of a simple relation between the ACF of the RT and the RT of the 2-D ACF, and the presence of correlation between the projections.

The foregoing observations highlight the difficulties in characterizing the RT of an SRF especially over a limited support, motivating the search for alternative approaches/interpretation. In the following section, a new approach to 2-D spectrum estimation based on the Radon transform of 2-D autocorrelation function of an SRF, instead of that of the random field itself, is presented. A motivation for the approach is the fact that it is the projection of the 2-D ACF that provides a slice of the 2-D PSD at the angle considered. An actual investigation of the RT of ACF and an extension to MEM are novel features of the work.

[9]This can be appreciated by observing a merger of the spectral peaks as the size of the data is reduced, in the case of sinusoids in white noise. A simple example showing the correlation between the integrals of lines passing through the origin is given in [210].

## 7.3 Spectrum estimation based on the Radon transform of 2-D autocorrelation

Consider an SRF with ACF $r(\tau_1, \tau_2)$. Let $r_\theta(\tau)$ be a projection of $r(\tau_1, \tau_2)$. From the CST applied to the RT of a 2-D ACF,

$$r_\theta(\tau) \overset{\mathcal{F}}{\Longleftrightarrow} S(\omega\cos\theta, \omega\sin\theta) \tag{7.14}$$

where, $S(\omega\cos\theta, \omega\sin\theta) \overset{\Delta}{=} S_\theta(\omega)$, a slice of the 2-D PSD $S(\omega_1, \omega_2)$ at angle $\theta$. As discussed in the previous chapter, a projection of a 2-D ACF is also an ACF. An example of 2-D ACF of cosinusoids in white noise, relevant to the context of spectrum estimation is given below.

- **Example:** Consider a 2-D signal consisting of $p$ cosinusoids in additive zero-mean white noise $w(x, y)$ with a flat PSD of height $N_2$.

$$f(x, y) = \sum_{k=1}^{p} A_k cos(u_k x + v_k y + \psi_k) + w(x, y) \tag{7.15}$$

where, $\psi_k$ are independent RVs, uncorrelated with $w(x, y)$, and uniformly distributed over $(-\pi, \pi)$. The ACF of $f(x, y)$ is given by:

$$r_f(\tau_x, \tau_y) = \sum_{k=1}^{p} \frac{A_k^2}{2} cos(u_k \tau_x + v_k \tau_y) + N_2 \delta(\tau_x, \tau_y) \tag{7.16}$$

The RT of $r_f(\tau_x, \tau_y)$ is obtained by inserting the RT of a cosinusoid [2] and that of a 2-D Dirac delta:

$$r_\theta(\tau) = \sum_{k=1}^{p} \frac{A_k^2}{2|\omega_k|} cos(\omega_k \tau)\delta(\theta - \phi_k) + N_2 \delta(\tau) \tag{7.17}$$

where, $\omega_k = \pm\sqrt{u_k^2 + v_k^2}$, and $\phi_k = tan^{-1}(v_k/u_k)$. Thus, a projection of the ACF of 2-D cosinousoids in white noise also corresponds to the ACF of a signal consisting of cosinusoids in white noise. Taking FT on both the sides of (7), the PSD $S_\theta(\omega)$ results:

$$S_\theta(\omega) = \sum_{k=1}^{p} \frac{A_k^2}{2|\omega_k|} [\delta(\omega + \omega_k) + \delta(\omega - \omega_k)]\delta(\theta - \phi_k) + N_2 \tag{7.18}$$

Thus, $S_\theta(\omega)$, which is a slice of the 2-D PSD $S_f(\omega_1, \omega_2)$, is a 1-D PSD corresponding to pure sinusoids in additive zero-mean white noise. The height of the flat PSD due to the noise component is the same as that of the 2-D white noise field. The factor $\delta(\theta - \phi_k)$ in the expression (7.18) accounts for the presence or absence of a peak in a particular slice, depending upon the angle made by the sinusoids in the 2-D frequency plane.

The approach to 2-D spectrum estimation considered here is based on the CST applied to 2-D ACFs. As a consequence of the CST, the problem of 2-D spectrum estimation can be reduced to a set of independent 1-D problems. It was seen that the projections of a 2-D ACF are 1-D ACFs. The basic idea consists of applying 1-D spectrum estimation method based on correlation lags, to each of the projections, to form the respective slice of the 2-D PSD. By considering a set of projections spaced uniformly over $[0, \pi)$, the 2-D PSD can be built-up in terms of its 1-D slices. The resulting PSD will be on a polar grid. It is pointed out that it is possible to consider the projection at any angle.

In applications such as radio/radar astronomy where the projections of the 2-D ACF are available, the method is straightforward. In applications involving finite extent samples of 2-D SRFs, however, the 2-D autocorrelation has to be estimated from the available data. One then obtains the estimates of the slices of the 2-D PSD, from the projections computed from the estimated 2-D autocorrelation.

Let $f(m,n)$ be the data available over $0 \leq m,n \leq N-1$. The 2-D autocorrelation is estimated from the available data as follows:

$$r(k,l) = \begin{cases} \frac{1}{N^2} \sum_{m=0}^{N-1-k} \sum_{n=0}^{N-1-l} f(m,n) f(m+k, n+l), & k,l \geq 0 \\ \frac{1}{N^2} \sum_{m=0}^{N-1-k} \sum_{n=0}^{N-1} f(m,n) f(m+k, n+l), & k \geq 0, \quad l < 0 \end{cases} \tag{7.19}$$

The values of $r(k,l)$ over the rest of the support $|k| \leq N-1, |l| \leq N-1$ is obtained by $r(k,l) = r(-k,-l)$, $k \leq 0, \forall\, l$. The biased estimate given above is the most

widely used, as unbiased estimates do not in general yield *pd* lags [116]. An efficient algorithm for computing the 2-D autocorrelation is given in [179].

The discrete projections $r_{\theta_i}(\tau_j)$ of the 2-D discrete autocorrelation $r(k,l)$ are computed as described in Chapter 2. In particular, the procedure involving Gaussian interpolation has been used in the examples presented in this chapter, due to a better performance they yielded with respect to that based on the pixel assumption, in the context of spectrum estimation. Due to symmetry, the projections may in general be sampled at $\tau_j = 0,..,J$ where $J = \sqrt{2}(N-1)$. In spectrum estimation via AR modeling, however, the projections need be computed over $\{0 \leq \tau_j \leq p\}$, where $p$ is the order of the AR model, which can often be much smaller than $J$. Since the 2-D ACF can be estimated only over a finite support, the line integrals will not be accurate, from a 2-D perspective. This is the major difference between methods based on the RT, and the direct 2-D methods. One approach to alleviate the above problem is to consider the RT in which each of the projections consists of integrals over lines of same length $L_I$. This results in considering the more reliable central portion of the 2-D correlation, but amounts to an inefficient use of the available information. Further, the integration can be carried over a narrow strip of width $\Delta$ to improve accuracy. An alternative approach is to use spectrum estimation methods that tend to accommodate inaccurate estimates of the correlation lags, as described at a later stage.

The AC lags $r_{\theta_i}(\tau_j)$ computed from the above step are used to obtain estimates of $S_{\theta_i}(\omega)$. The 2-D spectral space is filled by computing the PSDs of the various projections. Due to symmetry, the projections over $\theta \in [0,\pi)$ need be considered. The algorithm for spectrum estimation from observed 2-D data is summarized below:

1. Estimate the 2-D autocorrelation $r(k,l)$ from the available samples of the 2-D SRF.

2. Compute the projections $\{r_{\theta_i}(\tau_j)\}$ of the 2-D ACF $r(k,l)$, for $\theta_i = \frac{\pi}{N}i,\ i = 0,1,...N-1$, where $N$ is the number of projections.

3. Compute the 1-D spectrum estimates $S_{\theta_i}(\omega)$, using the autocorrelation sequences $\{r_{\theta_i}(\tau_j)\}$, $\theta_i = \frac{\pi}{N}i,\ i = 0,1,...N-1$.

In general, any procedure for computing the 1-D PSD from AC lags can be used. In fact, the approach has the flexibility of allowing one to tailor the 2-D PSD by using different models and techniques to compute difference slices. In this thesis, the application of AR modeling of the AC lags is considered, for spectrum estimation. Several reasons for the choice of AR modeling were described in Section 1[10]. In the following, 2-D spectrum estimation using AR models for the projections of the 2-D autocorrelation is presented. Further, a procedure for an ME extension of the projections of the 2-D autocorrelation is described.

For the sake of notational simplicity in the subsequent development, the suffix $i$ will be dropped off from $\theta_i$.

### 7.3.1 Estimation by AR modeling and extension to MEM

Given a set of AC lags $\{r(j),\ j = 0,1,..p\}$, the problem of AR spectrum estimation reduces to that of determining the AR parameters $\{a_k,\ k = 1,..p\}$ $(a_0 = 1)$, by solving the Yule-Walker equations [112]

$$R\,\mathbf{a} = -\mathbf{r} \tag{7.20}$$

where, $R$ is the symmetric Toeplitz autocorrelation matrix formed from the lags $\{r(j),\ j = 0,1,..p-1\}$, $\mathbf{a}$ is the vector of AR (prediction) coefficients $[a_1\ a_2\ ..\ a_p]^T$,

[10]It is interesting and important to note that correlation matching property of the all-pole models does not readily extend to pole-zero models [114]. Further, it is not always possible to find a pole-zero model of order $(p,q)$ that matches the given $pd$ correlation lags $\{r_k,\ 0 \le L\}$ for $p \le L$, irrespective of the value of $q$.

r is the AC vector, $[r(1)\ r(2)\ .\ .r(p)]^T$, and $p$ is the order of the AR model[11]. The gain of the filter $G$ is given by $G^2 = r(0) + \sum_{k=1}^{p} a_k r(k)$. The solution is accomplished by the well known and efficient Levinson-Durbin algorithm [112]. The spectrum estimate is proportional to the inverse of the squared magnitude of the frequency response of the prediction-error filter (PEF):

$$S(\omega) = \frac{G^2}{|1 + \sum_{k=1}^{p} a_k \exp^{-jk\omega}|^2} \tag{7.21}$$

where, $G$ is the gain of the filter, given by $G^2 = r(0) + \sum_{k=1}^{p} a_k r(k)$.

The above procedure is used to estimate the 2-D PSD, by AR modeling of the projections $r_{\theta_i}(\tau_j)$. Specifically, a slice of the 2-D PSD at angle $\theta_i$ obtained by computing the AR parameters via the Levinson-Durbin algorithm based on $\{r_{\theta_i}(j),\ j = 0, 1, ...p_i\}$, is given by:

$$S_{\theta_i}(\omega) = \frac{{G^2}_{\theta_i}}{|1 + \sum_{k=1}^{p_i} a_{\theta_k} \exp^{-jk\omega}|^2} \tag{7.22}$$

where, $p_i$ is the order of the AR model associated with the projection at angle $\theta_i$. Note that it is possible to use different model-orders $p_i$ for different slices. An appropriate criterion for model-order selection may be used for that purpose.

When the true values of the projections of the 2-D ACF are available (as in some situations in radio/radar astronomy) the proposed method of AR modeling of $r_{\theta_i}(\tau_j)$ yields slices of the 2-D ME PSD. The method is then straight-forward. In spectrum estimation involving 2-D data over a finite support, the estimated ACF will also be over a finite extent, the line integrals will not be accurate. However, when the estimated AC lags in the RS are positive definite, an ME spectrum exists and is unique. The AR approach is equivalent to MESE, and it provides an ME

[11]The choice of an appropriate model-order is essential for obtaining good spectrum estimates. A very low order will not provide good resolution, whereas too large a model-order gives rise to spurious peaks. Many criteria have been proposed for the selection of the model-order, such as, the final prediction error (FPE) [4], the Akaike information criterion (AIC) [5], the minimum description length (MDL) criterion of Rissanen [180], and the criterion autoregressive transfer (CAT) due to Parzen [148]. However, none of the criteria work well in a general situation, especially for short data [116], and model-order selection has remained an art, based on experience. For more details, see [116] or [85]

extrapolation of the autocorrelation consistent with the lags available in the RS. This establishes the equivalence of the AR and ME methods in the RS. This is by virtue of having reduced the 2-D problem to a set of 1-D problems by the use of the RT.

As noted above, the line integrals computed from 2-D AC lags over a finite support will not be accurate - a consequence of inherent windowing. Similar problems do arise in the approach of [204, 34]. However, the errors in autocorrelation values appear to be of greater concern than those in the projection data. The standard MEM based on inaccurate AC lags will therefore not be fully consistent with the ME principle in 2-D. Although the above method provides an ME extrapolation of the autocorrelation consistent with the lags available in the RS (inaccurate from a 2-D viewpoint), the question is whether it gives a 2-D extrapolation consistent with 2-D AC lags. This is somewhat tricky, because, a projection of a reconstruction of the set of 1-D autocorrelations extended in the RS, will not be equal to the originally available lags. In fact, *an extension of the 1-D AC lags assumes that the values of the 2-D ACF are zero beyond the 2-D support in the direction perpendicular to that in which extension is carried out.* Hence, the MESE using AR modeling in the RS is only an approximate MESE. On the other hand, the projections of the ACF available on a support can be used to reconstruct the function on that support, whereas the extensions alone can be used to reconstruct the hollow 2-D extension. Their superposition constitutes the extended 2-D ACF in the plane. The method, therefore does provide *a pd extension of a 2-D pd function in the Radon space, provided the inherent window preserves the pd nature of the AC lags.* A practical procedure is to attenmpt to preserve the *pd* nature of the AC lags by computing the projections of a biased estimate of the 2-D autocorrelation, via Gaussian interpolation. Its significance arises from the fact that such a result does not hold good on a rectangular raster in 2-D.

One approach to alleviating the effects of inaccurate AC estimates to some

extent, involves modeling the inaccurate correlation lags as windowed and noisy version of the true lags, as in [136][12]. This results in a modified MEM, as described below.

Consider the following modification of the MESE problem formulation:

- Maximize: $H = \frac{1}{2\pi}\int_{-\pi}^{\pi} lnS(\omega)d\omega$

  Subject to: $\sum_{k=-p}^{p} w(k)|\int_{-\pi}^{\pi} S(\omega)e^{-j\omega k}d\omega - r(k)|^2 \leq \sigma^2$

where, $\{r(k)\}$ are the available correlation lags. $\sigma$ is a correcting factor for noise, and $w(k)$ is a measure of the degree of confidence on lag $k$. The sequence $\{w(k)\}$ should be positive and symmetric.

The modified formulation of MESE is applied independently to each of the projections $r_\theta(\tau_j)$. Specifically, the problem is to find the slices $S_\theta(\omega)$ that maximize the entropy subject to the respective modified correlation-matching constraints associated with $r_\theta(\tau_j)$. Let $w_\theta(j)$ be the weight one wishes to attach to $r_\theta(\tau_j)$. The value of $\sigma_\theta$ should be a measure of noise that is used to model the inaccurate autocorrelation estimates at angle $\theta$. The solution to the above formulation amounts to working with the 'corrected' or 'derived' autocorrelation:

$$\tilde{r}_\theta(j) = r_\theta(j) + \sigma_\theta \frac{b_\theta(j)}{\sqrt{\sum_m b^2{}_\theta(m)/w_\theta(m)}}, \quad j = -p, ..., p \tag{7.23}$$

The sequence $b_\theta(j)$ is given by:

$$b_\theta(j) = \sum_{k=0}^{p-j} \gamma_\theta(k+j)\gamma_\theta(k), \quad j = 0, ..., p \tag{7.24}$$

The $\gamma_\theta$ coefficients are solved from:

$$\sum_{j=0}^{p} \gamma_\theta(j)\tilde{r}_\theta(j-k) = \frac{1}{\gamma_\theta(0)}\delta_{k,0}, \quad k = 0, ..., p \tag{7.25}$$

[12]At this juncture, it is relevant to quote Dickinson [29]: "There are some other possibilities that seem to be worth some research effort. ... We could also consider relaxing the requirement that the fitted model match the estimated AC lags exactly. Newman [136] has reported a time series version of such an estimator ... . It might also be possible to avoid the non-existence problem if the estimate were required to be positive definite on some non-rectangular region." This also explains the phrase 'extension to MEM'.

where, $\delta$ is the Kronecker delta function. The first step consists of evaluating the $\gamma$-coefficients with $\sigma_\theta = 0$. (This is equivalent to standard MEM). The $\gamma$-coefficients are used to compute the sequence $b_\theta(j)$, which will then give the corrected AC lags, $\tilde{r}_\theta(j)$. The AC lags $r_\theta(j)$ may be (justifiably) assumed to be symmetric in $j$. Then, the equations (7.25) reduce to the Yule-Walker equations with the corrected AC lags, where $a_{\theta_k} = \gamma_{\theta_k}/\gamma_{\theta_0}$, $G_\theta^2 = 1/\gamma_{\theta_0}^2$. The coefficients can be solved by the Levinson-Durbin algorithm, and the PSD is computed using (7.22). Thus, the PSD is estimated from the corrected AC lags.

The set $\{\tilde{r}_\theta(j)\}$ for each $\theta$ constitutes a form of an ME fit to inaccurate autocorrelation data, and an AR modeling of the same is equivalent to ME extrapolation. This amounts to extending the 2-D correlation over the entire plane. Consequently, the method is a practical procedure for 2-D MESE using the RT. If the given estimates $\{r_\theta(n)\}$ are *nnd*, an ME spectrum exists for each $\theta$ and is unique.

The value of $\sigma_\theta$ should be a measure of the variance of the noise that is used to model the given AC lags. If the given AC sequence is *nnd*, an ME spectrum exists and is unique, and only equality in the modified autocorrelation constraint need be employed [136]. When a choice of $\sigma_\theta$ cannot be made *a priori*, an iterative scheme with increasing values of $\sigma_\theta$ can be set up. Such a scheme converges when the AC lags are *nnd*. If the estimates are not *nnd*, the existence of the spectrum can still be assured by choosing a sufficiently large value of $\sigma_\theta$ [136], although a precise criterion is not known in general. However, the overall spectrum estimation method will then turn out to be complex. This emphasizes the need to develop a suitable criterion for the choices of the value of $\sigma_\theta$, and the weighting sequences $\{w_\theta(j)\}$. In general, these criteria will be dictated by the type of the autocorrelation and the shape and the size of the support on which it is available.

Thus, the method discussed above tends to accommodate the 2-D correlation lags in a direction perpendicular to that in which extension is carried out, that is otherwise unaccounted for by the standard MEM. On the practical side, a proper

choice of $\sigma_\theta$ and $w_\theta(j)$ would serve to improve the estimates. This is in spirit with the ME principle, of assuming the least possible about the 2-D correlation lags while performing an extension.

It is remarked at this juncture, that a correlation-match requires a sufficient number of projections to be considered.

**A note on Pisarenko harmonic decomposition:**

Pisarenko harmonic decomposition (PHD) is a special approach to analyze pure sinusoids in white noise [156, 86]. The approach is based on the fact that pure sinusoids in white noise can be represented as a symmetric ARMA process of order equal to the number of sinusoids. The solution to the problem of estimating the parameters of the process reduces to that of solving an eigenvalue problem. The frequencies of the sinusoids is obtained by solving for the roots of the polynomial associated with the ARMA parameter vector [86].

An extension of the PHD to 2-D is an interesting problem, which is, however, not straight-forward due to the lack of a fundamental theorem of algebra. Lang and McLellan [103] attempted a generalization of the method to m-D, by avoiding polynomial factorization, but reported that the method suffers from potential uniqueness problems.

In principle, the PHD can be extended to 2-D, based on an eigen-decomposition of the matrices $R_\theta$ formed by the projections $r_\theta(\tau_k)$. The significance of this observation arises from the impossibility of a direct extension of the method to 2-D on $\mathbf{R}^2$. In practice, however, the 2-D ACF is estimated from a finite-extent sample of an SRF, and the line integral estimated from it will not be accurate. It has been found from experiments that the PHD is very sensitive to such errors, and to a deviation of the data from the assumed model of pure sinusoids in white noise.

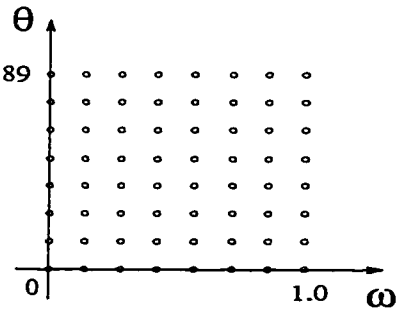


Figure 7.2: Display grid.

## 7.4 Simulation results

Data consisting of sinusoids in white noise is a standard test signal in spectrum estimation. In this section, results of simulation studies on the examples of the data consisting of sinusoids in additive white Gaussian noise, considered in [204, 87] are presented. The estimated PSD is on a polar raster, which is displayed on a rectangular geometry with the angle and (normalized) radial frequency as the two axes, as shown in fig. 7.2. Peak locations on this grid are defined by the angle-radial frequency pair $(\theta, \omega)$. True peaks are indicated by the mark 'x'. Since the examples considered here consist of with frequencies in the angular range $0 \leq \theta \leq 89$, the display is limited to that range. The 2-D autocorrelation of the data maybe computed using (7.19), or obtained by utilizing the built-in program of MATLAB. Projections of the 2-D discrete autocorrelation lags were computed from (2.14) using Gaussian interpolation (with $\sigma = 0.5$), for $\theta_i = \frac{\pi/2}{N} i$, $i = 0, 1, ...N-1$, where $N = 90$.

Consider the following data, corresponding to the first example in [204]:

$$f(m,n) = \cos(0.4688\pi m)\cos(.5313\pi n) + \cos(0.5938\pi m)\cos(.6563\pi n) + w(m,n),$$
$$1 \leq m, n \leq 31; \quad \sigma_w^2 = .25 \ \ (SNR = 0)$$

The true spectral peaks associated with the above data are the at the points $(47.8, 0.88)$ and $(48.6, 0.71)$. The 2-D autocorrelation of the above data, and its 90 equally spaced projections were computed. For every $\theta_i$, the correlation lags $r_{\theta_i}(\tau_j)$, $\tau_j = 0, 1, ..p$ were used to compute the AR (prediction) coefficients $\{a_{\theta_i}(k), \ \tau_j = 0, 1, ..p\}$ by

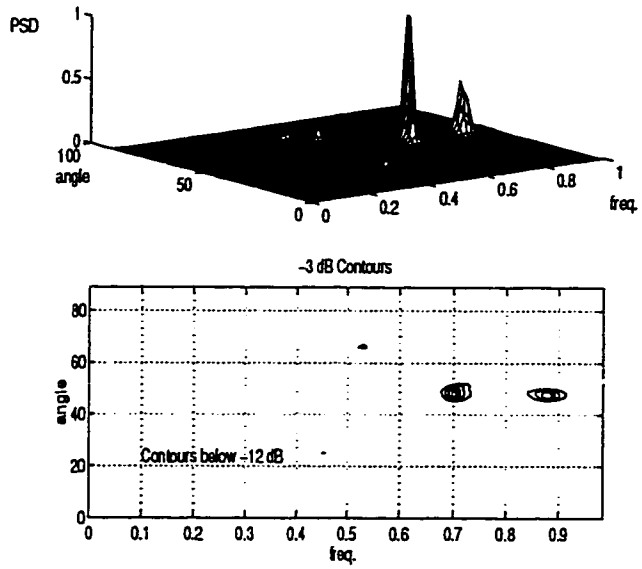


Figure 7.3: Spectrum estimate for the data of example-1.

using the Levinson algorithm. A model order of $p = 8$ was used in this case. The resulting AR PSD is shown in fig. 7.3. Note that the locations of the peaks are close to the actual locations.

The second example consists of the data considered in [87], with $n = 31$.

$$f(m,n) = \cos(0.1\pi m + .3\pi n) + \cos(0.15\pi m + .25\pi n) + w(m,n),$$
$$1 \leq m,n \leq 31; \quad \sigma_w^2 = .5 \ (SNR = 0)$$

This example is the same as those considered in [13, 194], at an SNR of $10dB$. The true locations of the spectral peaks associated with the above data are $(59, 0.29)$ and $(71.5, 0.32)$. The AR spectrum estimate with $p = 6$ is shown in fig. 7.4. Note again, the closeness of the peaks in the estimated spectrum with their true locations.

In the third and fourth examples, very short data records of closely spaced sinusoids in white noise are considered. The third example consists of a $9 \times 9$ version of the data of example-2 of [204], at an SNR of 3 dB.

$$f(m,n) = \cos(0.1464\pi m + .2249\pi n) + \cos(0.2889\pi m + .0778\pi n) + w(m,n),$$

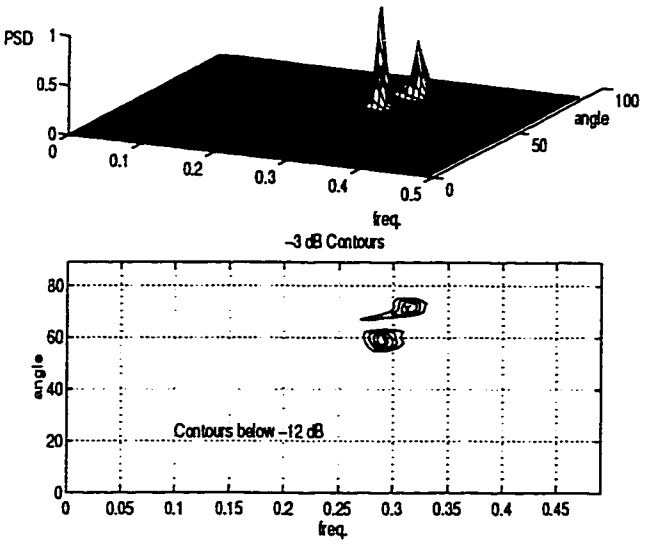


Figure 7.4: Spectrum estimate for the data of example-2.

$$1 \leq m, n \leq 9; \quad \sigma_w^2 = .5 \ (SNR = 3\,dB)$$

The true locations of the spectral peaks associated with the above data are $(18.8, 0.299)$ and $(57, 0.268)$. The last example consists of sinusoids of same frequencies as in example-2 above, for $9 \times 9$ data.

The result of AR spectrum estimation on the data in the third example, with $p = 5$ is shown in fig. 7.5. The result of the modified MEM on the data of the fourth example with $p = 8$ and $\sigma = .003$ is displayed in fig. 7.6. The weighting functions used were the respective projections of the (discrete) characteristic function of the 2-D autocorrelation support. The modified MEM helped locate the peaks only slightly better than the AR method.

In case of very short data records, the method does not seem to perform well, especially in comparison with the recent results presented in [87]. The results shown for the short-data case were not, in all the cases, easily arrived at, with respect to the choice of the values of $p$ and $\sigma_\theta$. Sometimes, although they were well resolved, the locations of the peaks were not good. In general, for short data, the approach

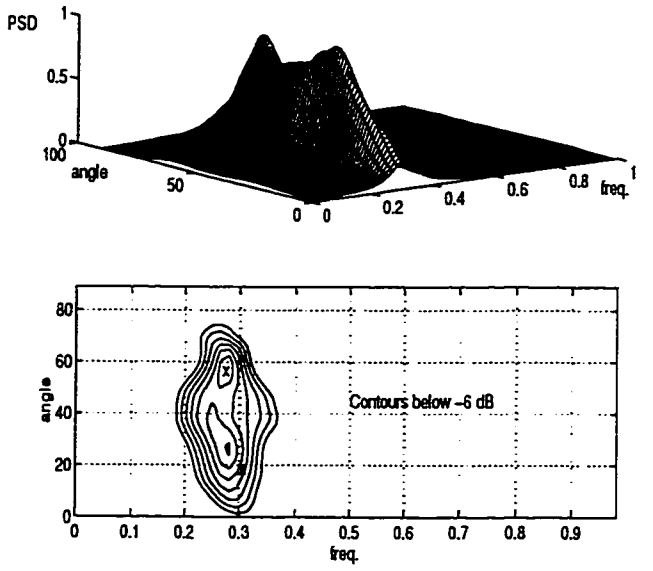


Figure 7.5: Spectrum estimate for the data of example-3.

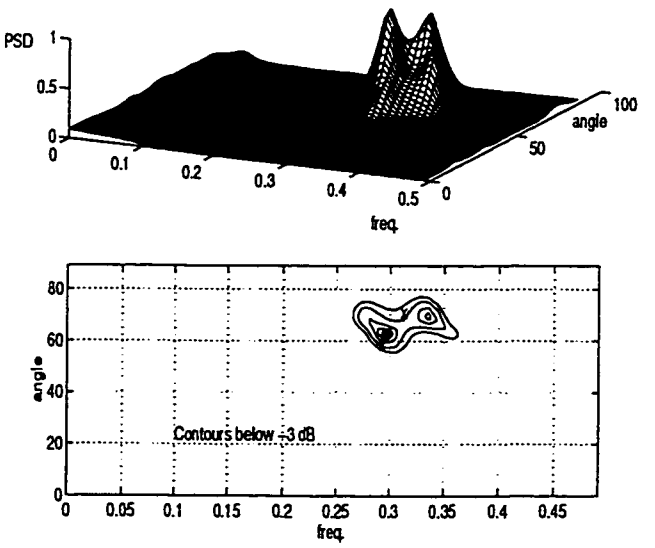


Figure 7.6: Spectrum estimate for the data of example-4.

exhibited a bias in the location of the peaks (frequency-estimates). This can be seen in the results displayed. Some anomalies with respect to the location and the shape of the peaks have also been observed, on some occasions. However, data records of the size under consideration are generally difficult to handle. Further, in 2-D, the resolution also depends upon the orientation of one component with respect to the other. Some of the anomalies and issues involved in resolving 2-D sinusoids in white noise and the behavior of specific estimators are discussed in [233]. An easier approach to studying the effect of rotation on QP AR models by the use of a polar-coordinate coefficient mask has been considered by [188].

In general, the method of corrective MEM tends to allow larger model orders, as the parameter $\sigma_\theta$ has a smoothening effect. This can be used to alleviate the undesired effects of high model-orders, to some extent. In some cases, its effect was to merge split-peaks. In the above simulations, a single value of $\sigma_\theta$ had been used for all the slices. Sometimes, an increase in the value of $\sigma_\theta$ had the effect of drawing one of the peaks closer to its true location, while having an opposite or no effect on the other. This can be avoided by using different values of $\sigma_\theta$ for different slices.

Experiments with certain criteria for the selection of the model-order resulted in good results in a few instances. However, the results are not representative. In general, appropriate criteria for (i) the selection of $\sigma_\theta$ for each of the slices (ii) the selection of model-order, and (iii) the choice of the windowing sequence, associated with the modified MEM are some of the issues to be addressed. With a proper choice of $\sigma_\theta$ that can tolerate high model order, one can perhaps dispense with the requirement for a good model-order selection criterion.

**Remarks:**

1. The use of interpolation for the computation of the projections introduces smoothing. Its effect can be minimized by reducing the value of the variance of the Gaussian interpolating function. The value used in this chapter was 0.5,

which yielded projections close to those obtained from SNARK, for a 31×31 (unity) picture.

2. The computational complexity of the new approach, i.e., AR modeling of the 2-D autocorrelation, is comparable to that of [204]. The corrective MEM, however, is more expensive.

3. The spectrum estimates obtained by the proposed approach are smoother (have less spurious peaks) than those obtained in [204].

## 7.5 Conclusion

The RT of SRFs has been discussed, and the CST (for SRFs) has been obtained, based on a new representation for the line integral, valid upto second-order statistics. The CST for SRFs states that the projections of an SRF are uncorrelated in angle and stationary in the spatial variable. Further, it expresses the ACF of a projection of an SRF, in terms of the corresponding projection of the 2-D ACF, in a closed-form. Difficulties due to the nature of the function involved in the closed-form relation have been pointed out. Further, it has been shown that, when the integration over a finite support is considered, as is the case in practice, no closed-form relation exists, and that the projections are not stationary.

The difficulties in characterizing the RT of SRFs have motivated an investigation into a new approach to 2-D spectrum estimation, based rather on RT of a 2-D ACF. A justification for the approach is the CST involving a 2-D ACF. Consequently, an algorithm based on the projections of the 2-D autocorrelation computed from the data has been proposed. Estimation of the PSD by AR modeling of the projections of the 2-D autocorrelation has been considered. The use of a biased estimate of the 2-D autocorrelation, and the computation of its projections via Gaussian

interpolation has arisen out of the desire to preserve positive-definiteness of the autocorrelation lags. When the projections are positive definite, an ME extension of each of them exists and is unique. However, the line-integral evaluated from an estimate of the 2-D ACF are only approximate, as a consequence of inherent windowing. An interesting 'extension' of the method to 2-D MEM, using the concept of 'derived' autocorrelation has been proposed, in an effort to alleviate the effects the errors in the AC lags and inherent windowing. Simulation results presented are encouraging. However, further efforts are needed to handle short data records. The proposed extension to MEM imparts a flexibility to the approach. Further work includes finding a criterion for selecting the window for the corrected MEM, and making the algorithm robust. The proposed approach may be extended to higher dimensions.

# Chapter 8

# Conclusion

This thesis has considered new algorithms/schemes for image analysis, compression, and 2-D spectrum estimation in the Radon space.

In Chapter 3, the notion of moment-patterns in the Radon space has been introduced. Two new approaches to constructing invariant features based on the moment-patterns have been presented. In contrast to algebraic invariants based on the 2-D moments, the new feature-sets are patterns, within the Radon space. The first approach has been to render the moment-patterns invariant to translation, scaling and rotation. Invariance to translation is achieved by the use of central moments, and that to geometric scaling is achieved by a normalization in the Radon space. Invariant moment-patterns are obtained by circularly shifting the normalized, central moment-patterns by an estimated rotation. A method of estimating the rotation via circular correlation of the second-order moment-pattern has been proposed. A formula for rotation based on an expression for the orientation in terms of the second order moments of three projections has also been given. An extension of the technique of extracting the invariant moment-patterns, to 3-D case, has been presented, and its application to radar target shape classification has been mentioned. The fact that the normalized and centered central moment-patterns are not invariant to

changes in gray-scale, motivated an alternative approach. The alternative set of invariants consists of circular-autoregressive parameters of a set of normalized central moment-patterns, and is invariant to geometric transformations as well as contrast. This descriptor has the additional feature of being parsimonious. Simulation results have been presented to illustrate the new techniques. The effect of noise on the moment-patterns, and one possible avenue for combating the same, have been indicated. The proposed feature-sets can be used for representing tomographic as well as spatial data. The invariant descriptors based on the moment-patterns constitute a useful contribution towards image-understanding. Further work on invariants in the Radon space consists of the following.

- An investigation of the conditions under which, and recognizing the practical situations in which, the approaches based on the moment-patterns have an edge over those based on 2-D moments obtained from the projections.
- Application of the proposed techniques to specific practical scenarios including spotlight-mode SAR and 3-D CT.
- An investigation into other possible invariants in the Radon space.

Chapter 4 has been devoted to an application of the instantaneous matched-filter [160], and considered selective reconstruction of an object of interest from noisy projections of multiple objects. The estimation or selection of a signal by the instantaneous matched-filter approach [160] is in the sense of detecting a shape and estimating the associated parameter from an unknown linear combination of given shapes, using an inner-product processor. A development of the instantaneous matched-filter from a discrete viewpoint, new observations and improvements over the original approach, and a generalization that does not require an explicit orthogonalization, have been presented. The generalized version has been applied on noisy projections of a composite image for selective reconstruction. The restricted applicability of the approach has been mentioned. A limitation of simple subtraction-based

approaches when the density of an object varies has been discussed. Alternatives to the instantaneous matched-filter approach have been indicated. Scope of further work in this direction is outlined below.

- Imaging cross-sections with objects of changing densities and of low-contrast is a challenging problem with a vast scope for the application of digital processing techniques [77]. While subtraction-based methods serve the purpose in many situations in radiology [77], they may not be effective when the contrast of objects in a certain neighborhood are similar, and/or vary quickly, often in a correlated manner. Optimum reconstruction in the situations outlined above, constitutes an interesting topic for further research.

Compression of binary images in the Radon space, investigated in Chapter 5, is a new direction in data compression. The basic idea involves exploiting the *a priori* information of a cross-section in CT being binary, and that of the representation of a binary image by few projections. The non-binary projections can be compressed using any of the available 1-D techniques. Two basic methods of data compression, namely predictive and transform techniques, have been applied. In particular, transform techniques have been shown to be applicable, and the DCT has been seen to be effective. An extension of the approach to compress pictures with closed contours has been dicussed. With the proposed scheme, it is possible to take advantage of the projections being non-zero over short intervals. Illustrative examples have been presented. The proposed scheme is useful for on-line transmission of CT data involving binary cross-sections, although it cannot handle on-line reconstruction. The proposed scheme can handle binary as well as gray-level images.

An attempt to generalize the approach of [199] for binary image reconstruction has resulted in a variant of the well known family of algebraic reconstruction techniques. The interesting projection-backprojection implicit in the algorithm of [199] combined with its good performance, has been the motivation for the new development. The development offers new possibilities in binary image reconstruction

methodologies. Other problems to be addressed in this area are listed below.

- Application of other compression techniques such as the wavelet transform, vector quantization, and lossless compression schemes (eg., [137]).
- A performance-comparison with the current techniques for binary image compression, with the objective of classifying the type of images that benefit from the proposed method.
- A study of the algorithm for binary image reconstruction with different approximations of the operations of projection and backprojection, and different constraints, and their performance in the presence of noise.

Two-dimensional spectral factorization in the Radon space has been discussed in Chapter 6. The 2-D problem reduces to a set of 1-D problems, of factorizing the 1-D slices of the 2-D spectral density function, as a consequence of the central-slice theorem involving a 2-D autocorrelation function. Hence, the virtues of 1-D spectral factorization are preserved, although within the Radon space. The development has been in the continuous domain, and an extension to the discrete case is through an adequate sampling the 2-D autocorrelation. Apart from investigating a solution to the 2-D spectral factorization problem via the Radon transform, the purpose has been to provide a formal framework that highlights the basis of many of the existing algorithms involving a mathematical modeling of the projections, with the desire to motivate further applications from a new perspective. Indeed, further possible applications, such as 2-D IIR filtering and restoration have been indicated, and an example of LPC-based invariants in the Radon space has been presented. The theory motivated a new approach to 2-D spectrum estimation using the Radon transform, which has been considered in Chapter 7. It has been clarified that spectral factorization of the projections of 2-D autocorrelation is not equivalent to a factorization of the autocorrelation of the projections of a stationary random

field (SRF). An interesting topic for further investigation, not mentioned in Chapter 6, is indicated below.

- Two-dimensional spectral factorization based on the discrete Radon transform, with applications to 2-D filter analysis and design, and analysis of discrete random fields.

In Chapter 7, the Radon transform of an SRF has been reviewed in the context of 2-D spectrum estimation, and a new approach based on the Radon transform of 2-D autocorrelation has been investigated. In the context, a new mathematical representation for the Radon transform of an SRF, valid upto second-order statistics, has been developed. The new representation has been used to derive the so called central-slice theorem for SRFs. Although the final result has turned out to be the same as that of Jain and Ansari [76], the new representation is interesting in its own right, and has served to bring out some issues that are not evident in [76]. In the sequel, some of the difficulties associated with the Radon transform of SRFs, which have been ignored in the literature so far, have been highlighted. The role of the function relating a projection of 2-D autocorrelation and the autocorrelation of the respective projection of the associated SRF, has been discussed. Being non-invertible, it gives rise to a difficulty in interpreting the results. Consequently, an extension of the results associated with an infinite-extent SRF, to handle the sample of a random field over a finite-extent, is not straight-forward. Further, it has been shown that, in the finite-extent case, a projection of a 2-D autocorrelation of an SRF and the autocorrelation of the corresponding projection of the SRF do not possess a closed-form relation. Finally, it has been shown that the projections consisting of integrals of an SRF considered over a finite-extent support are not even stationary, in general.

Owing to the difficulties in characterizing the Radon transform of an SRF, a

new approach based on the Radon transform of 2-D autocorrelation has been investigated. The use of the Radon transform of the 2-D autocorrelation estimated from the data, has been considered for the first time. When the projections of the 2-D autocorrelation are positive-definite, a maximum entropy extension of each of them exists and is unique. The result is a closed-form solution to the 2-D maximum entropy spectrum estimation problem. The use of a biased estimate of the autocorrelation, and the computation of its projections through Gaussian interpolation have been suggested to preserve positive-definiteness. However, the line integral computed from the autocorrelation available over a finite support are not true values of the line integral of the 2-D autocorrelation. As an alleviative procedure, constituting an interesting extension to 2-D MEM, using the concept of 'derived' autocorrelation has been presented. This approach provides a flexibility of accommodating errors in the autocorrelation and the effects of windowing, to some extent. However, it is an approximate MEM from a 2-D viewpoint. Possible modifications of the approach for improved performance, and the scope of of 1-D techniques other than those considered, have been indicated. This includes finding a criterion for selecting the window for the corrected MEM, and devising robust algorithms especially for short data records. It is appropriate to remark at this juncture, that 2-D maximum entropy spectrum estimation continues to be an interesting field of research. Scope for future work involving the Radon transform associated with random fields is outlined in the following.

- Application of other techniques such as the minimum-norm method of Kumaresan and Tufts [216], on the Radon transform of autocorrelation. The proposed extension of the method of [216] to 2-D [91] has left many issues unresolved. Although this approach is regarded a frequency-estimator [116], the associated spectrum estimate is interpreted as AR estimate [217]. One

could also explore the applications of different approaches based on eigen-decomposition of the autocorrelation matrix, such as multiple signal classification [144]. Finally, it would be particularly interesting to try the procedure involving AR and ARMA modeling of the windowed correlation data [67].

- Investigation of methods based on the Radon transform of the data, while taking into account the effects of integrating over line segments of different lengths. An alternative approach is to use a common length of integration. It would also be interesting to extend the ideas of local integration of SRFs indicated in [220], for a definition and analysis of the Radon transform of SRFs. Finally, one could study the family of line integrals scaled by the inverse of the length of integration.

- Spectrum estimation is only one among the contexts in which the Radon transform of an SRF arises. The ever increasing utility of the Radon transform as a tool in m-D signal processing emphasizes the scope for further investigation into the characterization of the transform of random fields.

In summary, this thesis has considered applications of signal processing techniques in the Radon space. New algorithms for image analysis, compression and spectrum estimation have been presented. The techniques of signal processing in the Radon space have gathered momentum over the recent past. The vast number of physical situations in which the data is available in the Radon space, and the potential of the Radon transform as a tool in multi-dimensional signal processing, enrich the scope of this relatively new direction. The advent of dedicated hardware for the computation of the forward and the inverse Radon transform, and the availability of optical means of computing the Radon transform, provide a strong motivation for further efforts involving signal processing in the Radon space. General directions for future work in this area include: (i) a further analysis of, and approximations to the Radon transform of random fields, (ii) an identification of new areas in which

the Radon transform-based techniques can be applied, and (iii) further efforts in the development of dedicated hardware for fast computation of the forward and the inverse Radon transform.

# Appendix A

# Properties of the moment-patterns

### Appendix-A1

The behaviour of the moments under a shift in the variable $\theta$ by $\pi$ is examined in this appendix. Consider:

$$\mu_k(\theta+\pi) = \int (t - \bar{t}_{\theta+\pi})^k p_{\theta+\pi}(t) dt$$

Noting that $p_{\theta+\pi}(t) = p_\theta(-t)$, and $\bar{t}_{\theta+\pi} = -\bar{t}_\theta$,

$$\begin{aligned} \mu_k(\theta+\pi) &= \int (t + \bar{t}_\theta)^k p_\theta(-t) d(-t) \\ &= \int (-t + \bar{t}_\theta)^k p_\theta(t) dt \\ &= (-1)^k \mu_k(\theta) \end{aligned} \tag{A.1}$$

As a consequence, the following property results:

$$\mu_k(\theta+\pi) = \begin{cases} \mu_k(\theta), & \text{k-even} \\ -\mu_k(\theta), & \text{k-odd} \end{cases} \tag{A.2}$$

Thus, even-ordered MPs are periodic in $\theta$ with a period of $\pi$. Due to the change of sign, the odd ordered MPs remain periodic with a period of $2\pi$. The above property also shows that actual computation of the moments need to be only over $\theta \in [0, \pi)$.

## Appendix-A2

Consider the projection $p^s{}_\theta(t) = \lambda p_\theta(\frac{t}{\lambda})$, of a scaled object, where $\lambda$ is the scaling factor. The normalized central moment of order $k$, of $p^s{}_\theta(t)$ is given by:

$$\eta^s{}_k(\theta) = \frac{\mu^s{}_k(\theta)}{[\mu^s_0(\theta)]^{(k+2)/2}} \tag{A.3}$$

From (3.7), the function $\mu^s_k(\theta)$ is given by $\lambda^{2+k}\mu_k(\theta)$, where, the quantities without the superscript $(s)$ denote those associated with the unscaled object. Substituting this in the above equation,

$$\begin{aligned} \eta^s{}_k(\theta) &= \frac{\mu^s{}_k(\theta)}{[\lambda^2\mu_0(\theta)]^{(k+2)/2}} \\ &= \frac{\mu^s{}_k(\theta)}{\lambda^{k+2}[\mu_0(\theta)]^{(k+2)/2}} \\ &= \frac{\mu_k(\theta)}{[\mu_0(\theta)]^{(k+2)/2}} \end{aligned}$$

which is invariant to the scaling factor, $\lambda$.

## Appendix-A3

Let $s(j)$, $0 \leq j \leq L-1$, denote the reference third order MP in the RS, where $L$ is the number of projections. This pattern may be viewed as an $L$-point vector:

$$v = [s(0)\ s(1) \ldots s(L-1)]' \tag{A.4}$$

where, $'$ denotes transpose. Let $S = \{v_i,\ 0 \leq j \leq L-1\}$ be the set of all possible circularly shifted versions of the reference vector (the elements of the vectors also undergo the same circular shift or rotation). The subscript $i$ denotes the number

of points (extent) of the circular shift. For example, $v_0 = v$, $v_2 = [s(L-2)\ s(L-1)\ s(0)\ s(1)\ ..s(L-3)]'$. From (3.9), $y(n) = v_n' v_i,\ \forall n$. Thus, $y(n)$ is a projection (not the line integral) of the vector $v_n$ onto the vector $v_i$, and

$$v_n' v_i \ \leq \ v_i' v_i \ = \ \| v \|^2 \tag{A.5}$$

Since the vectors $v_i$ in the set $S$ are distinct (unless the vector $v$ corresponds to the trivial case of all the elements being identical, or to that where the elements are periodic with a period smaller than $L$), there exists only one maximum in the set $y = \{v_n' v_i,\ n = 0, 1, 2, ...L-1\}$. Note that the lengths of all the vectors in $S$ are the same. Barring such trivialities, the point corresponding to the peak in $y$, representing $y(n)$ in (3.9), is unique.

## Appendix-A4

The *orientation* of an object, defined as the angle made by its bounding rectangle/ellipse, is related to its 2-D moments as follows [58, 211]:

$$\psi = \tan^{-1} \frac{2\mu_{11}}{\mu_{20} - \mu_{02}} \tag{A.6}$$

The 2-D moments in (A.6) above can be found in terms of the moments of just three projections. Clearly, $\mu_{20} = \mu_2(0)$, $\mu_{02} = \mu_2(\pi/2)$. The expression for $\mu_{11}$ in terms of the usual moments as:

$$\mu_{11} = m_{11} - \frac{m_{10} m_{01}}{m_{00}} \tag{A.7}$$

It is straightforward to see that $m_{10} = m_1(0)$ and $m_{01} = m_1(\pi/2)$, which can be computed from two perpendicular projections. An expansion of $m_2(\pi/4)$ yields the relation required to compute $m_{11}$ [43]:

$$m_{11} = m_2(\pi/4) - 0.5(m_2(0) + m_2(\pi/2)) \tag{A.8}$$

resulting in the following expression for the orientation:

$$\psi = \frac{1}{2} \tan^{-1} \frac{2\{m_2(\pi/4) - 0.5[m_2(0) + m_2(\pi/2)] - [m_1(0) m_1(\pi/2)/m_0]\}}{\mu_2(0) + \mu_2(\pi/2)} \tag{A.9}$$

The ambiguity due to the inverse tangent relation can be resolved by making use of the signs of the numerator and the denominator of the argument [211]. The sign of $\mu_3(0)$ can be employed to determine the axis. The rotation of an object is the difference between the reference and the computed orientations. The sign of $\mu_3(0)$ can be employed to determine the axis. The above procedure is applicable only to non-negative distributions, as is the case with images [211].

The expression (A.9) is new, and is yet to be implemented.

# Appendix B

# Expression for the scaling factor

Let $r =< \mathbf{h}_1, \mathbf{x} >$. From (4.3),

$$r = a_1 < \mathbf{h}_1, \Phi_1 > + a_2 < \mathbf{h}_1, \Phi_2 > + < \mathbf{h}_1, \mathbf{n} > \tag{B.1}$$

The problem is to find $\lambda_1$ such that $\zeta = E\{[\lambda_1 r - a_1]^2\}$ is minimized.

$$\zeta = E\{\lambda_1{}^2 r^2 + a_1{}^2 - 2a_1\lambda_1 r\} \tag{B.2}$$

Expanding and taking expected values noting that $a_1$ and $a_2$ are uncorrelated mutually as well as with noise, the expression for $\zeta$ simplifies to:

$$\zeta = \lambda_1{}^2[\bar{a_1}^2 < \mathbf{h}_1, \Phi_1 >^2 + \bar{a_2}^2 < \mathbf{h}_1, \Phi_2 >^2 + \|\mathbf{h}_1\|^2\sigma_n^2] + \bar{a_1}^2 - 2\lambda_1\bar{a_1}^2 < \mathbf{h}_1, \Phi_1 > \tag{B.3}$$

Setting $\frac{\delta}{\delta\lambda_1}\zeta$ to 0,

$$2\lambda_1[\bar{a_1}^2 < \mathbf{h}_1, \Phi_1 >^2 + \bar{a_2}^2 < \mathbf{h}_1, \Phi_2 >^2 + \|\mathbf{h}_1\|^2\sigma_n^2] - 2\bar{a_1}^2 < \mathbf{h}_1, \Phi_1 >= 0$$

The expression for $\lambda_1$ is given by:

$$\lambda_1 = \frac{\bar{a_1}^2 < \mathbf{h}_1, \Phi_1 >}{\bar{a_1}^2 < \mathbf{h}_1, \Phi_1 >^2 + \bar{a_2}^2 < \mathbf{h}_1, \Phi_2 >^2 + \|\mathbf{h}_1\|^2\sigma_n{}^2}$$

# Appendix C

# Proof of the least-squares theorem

Given a noisy observation $g$ of a vector $f$, and the inner product $p_0$ of $f$ with respect to a weighting vector $w$, the problem is to find $\hat{f}$ such that $J = ||g - \hat{f}||^2$ is minimized, subject to $< w, \hat{f} >= p_0$.

The above problem of constrained minimization can be reduced to one of unconstrained minimization by formulating a new cost function:

$$J_1 = ||g - \hat{f}||^2 + \lambda(p_0 - w^T \hat{f}) \tag{C.1}$$

where $\lambda$ is a Lagrange multiplier. Setting $\frac{\partial J_1}{\partial \hat{f}} = \theta$, where $\theta$ is the zero-vector,

$$\hat{f} = g + \frac{\lambda}{2} w \tag{C.2}$$

Multiplying both sides of the above equation by $w^T$ and using the constraint,

$$\lambda = 2\,\frac{p_0 - w^T g}{w^T w} \tag{C.3}$$

Substituting for $\lambda$ in the expression for $\hat{f}$ above,

$$\hat{f} = g + \frac{p_0 - < w, g >}{||w||^2}\, w \tag{C.4}$$

Replacing the weighting vector $w$ by $u = [1\ 1\ ..1]^T$, and observing that $u^T u = N$, the theorem of Soumekh results:

$$\hat{f} = g + \frac{s_0 - \sum_i g_i}{N} u \tag{C.5}$$

where $s_0$ is the given value of the sum of the unknown sequence.

# Appendix D

# Radon transform of an SRF

Consider the representation (7.1) of an SRF:

$$f(x,y) = a\cos(\Omega_1 x + \Omega_2 y + \Phi) \tag{D.1}$$

Using the RT of a cosinusoid [72], the RT of $f(x,y)$ is:

$$p(\theta,t) = \frac{a}{|\Omega|}\cos[(\Omega_1\cos\theta + \Omega_2\sin\theta)t + \Phi]\delta(\theta - \theta_\Omega) \tag{D.2}$$

where, $\theta_\Omega = tan^{-1}(\Omega_2/\Omega_1)$, and $\Omega = \pm\sqrt{\Omega_1^2 + \Omega_2^2}$. (D.2) can be written as:

$$p(\theta,t) = \frac{a}{|\Omega|}\cos(\Omega_\theta t + \Phi)\delta(\theta - \theta_\Omega) \tag{D.3}$$

Using the property $f(\theta)\delta(\theta - \theta_\Omega) = f(\theta_\Omega)\delta(\theta - \theta_\Omega)$, and noting that $\Omega_1\cos\theta_\Omega + \Omega_2\sin\theta_\Omega$ reduces to $\Omega$,

$$p(\theta,t) = \frac{a}{|\Omega|}\cos(\Omega t + \Phi)\delta(\theta - \theta_\Omega) \tag{D.4}$$

Now, $E\{p(\theta,t)\} = 0$, and the ACF $E\{p(\alpha,t)p(\beta,t+\tau)\}$ is given by:

$$\begin{aligned} & \frac{a^2}{2}E\{\frac{1}{\Omega^2}\cos(\Omega\tau)\delta(\alpha - \theta_\Omega)\delta(\beta - \theta_\Omega)\} \\ = & \int\int \frac{S(\omega_1,\omega_2)}{({\omega_1}^2 + {\omega_2}^2)}\cos(\sqrt{{\omega_1}^2 + {\omega_2}^2}\tau)\delta(\alpha - \theta_\omega)\delta(\beta - \theta_\omega)d\omega_1 d\omega_2 \end{aligned}$$

where, $\theta_\omega$ is $tan^{-1}(\omega_2/\omega_1)$. Substituting $\omega_1 = \omega\cos\theta$, $\omega_2 = \omega\sin\theta$, $\theta_\omega$ reduces to $\theta$, and the expression for the ACF reduces to:

$$= \left[\int_{-\infty}^{\infty} \frac{S_\alpha(\omega)}{|\omega|}\cos(\omega\tau)d\omega\right]\delta(\alpha-\beta) \tag{D.5}$$

$$= \mathcal{F}^{-1}\left\{\frac{S_\alpha(\omega)}{|\omega|}\right\}\delta(\alpha-\beta) \tag{D.6}$$

where, $S_\theta(\omega) = \mathcal{F}\{r_\theta(\tau)\}$ is a slice of the 2-D PSD at angle $\theta$. Note that the above derivation brings out the unbounded nature of the line integral of an SRF.

# Bibliography


[1] Y.S. Abu-Mostafa and D. Psaltis, "Recognitive Apsects of Moment Invariants", IEEE Trans. Pattern Anal. Mach. Intell., Vol. PAMI-6, No. 6, pp: 698-706, Nov. 1984.

[2] N. Ahmad et al., "Discrete Cosine Transform", IEEE Trans. Comput., Vol. C-23, pp: 90-93, Jan. 1974.

[3] N. Ahmad and K.R. Rao, "Orthogonal Transforms for Digital Signal Processing", Berlin: Springer-Verlag, 1975.

[4] H. Akaike, "Power Spectrum Estimation through Autoregressive Model Fitting", Ann. Inst. Stat. Math., Vol. 21, pp: 407-419, 1969.

[5] H. Akaike, "A New Look at the Statistical Model Identification", IEEE Trans. Automat. Contr., Vol. AC-19, pp: 716-723, Dec. 1974.

[6] R.B. Arps, "Bibliography on Binary Image Compression", Proc. IEEE Vol. 68, No. 7, pp: 922-924, July 1980.

[7] T. Barnard and J.P. Burg, "Analytical Studies of Techniques for the Computation of High Resolution Wavenumber Spectra", Advanced Array Research Report #9, Texas Instruments Inc., May 1969.

[8] R.H.T. Bates et al., "Overview of Computerized Tomography with Emphasis on Future Developments", Proc. IEEE Vol. 71, No. 3, pp: 356-372, Mar. 1983.

[9] M.G. Belanger et al., "Automated Scene Analysis of CT Scans", Computerized Tomography, Vol. 3, pp: 201-211, 1979.

[10] S.O. Belkasim et al., "Pattern Recognition with Moment Invariants: A Comparative Study and New Results", Pattern Recognition, Vol. 24, No. 12, pp: 1117-1138, 1991.

[11] R.N. Bracewell, "Image Reconstruction in Radio Astronomy", in [54].

[12] J.P. Burg, "Maximum Entropy Spectral Analysis", Proc. 37Th Meeting Soc. of Exploration Geophysicists, Oklahoma City, Okla., Oct. 1967.

[13] J.A. Cadzow and K. Ogino, "Two-Dimensional Spectral Estimation", IEEE Trans. Acoust. Speech Signal Processing, Vol. ASSP-29, No. 3. pp: 396-401, June 1981.

[14] J. Capon, "High-Resolution Frequency Wavenumber Spectrum Analysis", Proc. IEEE, Vol. 57, pp: 1408-1418, Aug. 1969.

[15] D. Casasent and D. Psaltis, "Position, Rotation and Scale Invariant Optical Correlation", Appl. Opt., Vol. 15, No. 7, pp: 1795-1799, July 1976.

[16] L.W. Chang and E.S. Angel, "The Karhunen-Loeve Transform in Computerized Tomography", Math. Bio., Vol. 77, pp: 189-200, 1985.

[17] S.K. Chang and G.L. Shelton, "Two-Algorithms for Multiple-View Binary Pattern Reconstruction", IEEE Trans. Syst. Man Cybern., Vol. SMC-1, No. 1, pp: 90-94, Jan. 1971.

[18] W. Chen and H. Smith, "Adaptive Coding of Monochrome and Color Images", IEEE Trans. Communications, Vol. COM-25, No. 11, pp: 1285-1292, Nov. 1977.

[19] E.S. Chornoboy, "Initialization for Improved IIR Filter Performance", IEEE Trans. Signal Processing, Vol. 40, No.3, pp: 543, Mar. 1992.

[20] D.K. Cooper and J.M. Pimbley, "A Miniumum Free-energy Hybrid Algorithm for 2-D Spectral Estimation", IEEE Trans. Signal Processing, Vol. 39, No. 6, pp: 1348-1359, June 1991.

[21] A.C. Copeland et al., "Localized Radon Transform-Based Detection of Ship Wakes in SAR Images", IEEE Trans. Geosci. and Remote Sensing, Vol. 33, No. 1, pp: 35-45, Jan. 1995.

[22] Y. Das and W.M. Boerner, "On Radar Target Shape Estimation Using Algorithms for Reconstruction from Projections", IEEE Trans. Antennas Propagat., Vol. AP-26, No.2, pp: 274-279, Mar. 1978.

[23] S.R.Deans, *The Radon Transform and Some of its Applications*, NY: John Wiley & Sons, 1983.

[24] R. Deklerck et al., "Segmentation of medical images", Image and Vision Computing, Vol. 11, No. 8, pp: 486-503, Oct. 1993.

[25] D.J. DeRosier and A. Klug, "Reconstruction of Three dimensional Structures from Electron Micrographs", Nature, Vol. 217, pp: 130-134, 1968.

[26] D.J. DeRosier, "The Reconstruction of Three-dimensional Images from Electron Micrographs", Contemp. Phys, Vol. 12, pp: 437-452, 1971.

[27] M.D. Desai and W. K. Jenkins, "Convolution Backprojection Image Reconstruction for Spotlight Mode Synthetic Aperture Radar", IEEE Trans. Image Processing, Vol. 1, No. 4, pp: 505-517, Oct. 1992.

[28] A.J. Devaney, "Geophysical Diffraction Tomography", IEEE Trans. Geosci. Remote Sensing, Vol. GE-22, pp: 3-13, Jan. 1984.

[29] B.W. Dickinson, "Two-Dimensional Markov Spectrum Estimates Need Not Exist", IEEE Trans. Inform. Theory, Vol. IT-26, No. 1, pp: 120-121, Jan. 1980.

[30] D.E. Dudgeon and R.M. Mersereau, *Multidimensional Digital Signal Processing*, Prentice-Hall Signal Processing Series, A.V. Oppenheim, ed., 1984.

[31] J.A. Edward and M.M. Fitelson, "Notes on Maximum-Entropy Processing", IEEE Trans. Inform. Theory, Vol. IT-19, No. 2, pp: 232-234, Mar. 1973.

[32] M.P Ekstrom and J.W. Woods, "Two-Dimensional Spectral Factorization with Applications to Recursive Digital Filtering", IEEE Trans. Acoust. Speech Signal Processing, Vol. ASSP-24, pp: 115-128, Apr. 1976.

[33] M.P. Ekstrom et al., "Two-Dimensional Recursive Filter Design: A Spectral Factorization Approach", IEEE Trans. Acoust. Speech Signal Processing, Vol. ASSP-28, No. 1, pp: 16-26, Feb. 1980.

[34] W. Fang and A.E. Yagle, "Two-Dimensional Linear Prediction and Spectral Estimation on Polar Raster", IEEE Trans. Signal Processing, Vol. 42, No. 3, pp: 628-641, Mar. 1994.

[35] D. Fraser et al., "Principles of Tomography in Image Data Compression", Opt. Engg., Vol. 24, No. 2, pp: 298-306, 1985.

[36] O.L. Frost, "High Resolution 2-D Spectral Analysis at Low SNR", Proc. ICASSP 80, Denver, Colorado, Apr. 1980, Vol. 2, pp: 580-583.

[37] O.L. Frost and T.M. Sullivan, "High-resolution Two-Dimensional Spectral Analysis", Proc. ICASSP 79, Washington, DC, Apr. 1979, pp: 673-676.

[38] K.L. Garden et al., "Computerized tomography imaging is insensitive to density variation during scanning", Image and Vision Computing, Vol. 2, No. 2, pp: 76-84, May 1984.

[39] I.M. Gel'fand et al., *Generalized Functions*, Vol. 5, New York Press, 1966.

[40] I. Gertner, "A New Efficient Algorithm to Compute the Two-Dimensional Discrete Fourier Transform", IEEE Trans. Acoust. Speech Signal Processing, Vol. 36, No. 7, pp: 1036-1050, July 1988.

[41] P.F.C. Gilbert, "Iterative Methods for the Three-Dimensional Reconstruction of an Object from Projections", J. Theor. Biol. 36, No. 1, pp: 105-117, July 1972.

[42] P.F.C. Gilbert, "An Iterative Method for Three-Dimensional Reconstruction from Electron Micrographs", Proc. Fifth European Congress on Electron Microscopy", 1972, pp: 602-603.

[43] G.R. Gindi and A.F. Gmitro, "Optical feature Extraction via the Radon Transform", Opt. Engg., Vol. 23 No. 5, pp: 499-506, Oct. 1984.

[44] G.C. Goodwin and K.S. Sin, *Adaptive Filtering, Prediction, and Control*, Englewood Cliffs, NJ: Prentice-Hall, 1984.

[45] R. Gordon, "A Tutorial on ART", IEEE Trans. Nucl. Sci., Vol. NS-21, pp: 78-93, June 1974.

[46] R. Gordon et al., "Algebraic Reconstruction Techniques (ART) for Three Dimensional Electron Microscopy and X-ray Photography", J. Theor. Biol. Vol. 29, No.3, 471-481, Dec. 1970.

[47] X.U. Gu et al., "Application of a Multilayer Decision Tree in Computer Recognition of Chinese Characters", IEEE Trans. Pattern Anal. Mach. Intell., Vol. PAMI-5, No. 3, pp: 83-89, 1983.

[48] R.R. Gutowski et al., "Spectral Estimation: Fact or Fiction", IEEE Trans. Geosci. Electron., Vol. GE-16, No. 2, pp: 80-83, Apr. 1978.

[49] G. Hall et al., "Transputer Implementation of the Radon Transform for Image Enhancement", Proc. ICASSP 89, Glasgow, Scotland, May 1989, Vol. 3, pp: 1548-1551.

[50] R.R. Hansen and R. Chellappa, "Noncausal 2-D Spectrum Estimation for Direction Finding", IEEE Trans. Inform. Theory, Vol. 37, No. 1, pp: 108-125, Jan. 1989.

[51] H.P. Hiriyannaiah, "X-Ray Computed Tomography for Medical Imaging", IEEE Signal Processing Magazine, pp: 42-59, Mar. 1997.

[52] H.P. Hiriyannaiah and K.R. Ramakrishnan, "Moments Estimation in the Radon Space", Pattern Recognition Letters, Vol. 15, No. 3, pp: 227-234, 1994.

[53] G.T. Herman, "Reconstruction of Binary Patterns from a Few Projections", in A. Gunther et al. (eds.) International Computing Symposium 1973, North Holland Publishing Co., 1974, pp: 371-379.

[54] G.T. Herman, Ed., "Image Reconstruction from Projections: Implementation and Applications", *Topics in Applied Physics*, Vol 32, NY: Springer-Verlag, 1979.

[55] G.T. Herman et al., "On the noise in images produced by Computed Tomography", Comput. Graph. Image Processing, Vol. 12, No.3, pp: 271-285, Mar. 1980.

[56] G.T. Herman et al., "ART: Mathematics and Applications", J. Theor. Biol. Vol. 42, No. 1, pp: 1-32, Nov. 1973.

[57] E.B. Hinkle et al., "$P^3E$: New Life for Projection-based Image Processing", J. Par. Dist. Comput. 4, pp: 45-78, 1987.

[58] M.K. Hu, "Visual Pattern Recognition by Moment Invariants", IRE Trans. Inform. Theory, Vol. IT-8, pp: 179-187, Feb. 1962.

[59] T.S. Huang, "Coding of Two-tone Images", IEEE Trans. Communications, COM-25, Vol. 11, No. 11, pp: 1406-1424, Nov. 1977.

[60] T.S. Huang et al., "Image Processing", Proc. IEEE, Vol. 59, No. 11, pp: 1586-1609, Nov. 1971.

[61] O. Ibikunle, "Projection Allocation for Image Recsontruction", Proc. ICASSP 89, Glasgow, Scotland, May 1989, Vol. 3, pp: 1445-1448.

[62] O. Ibikunle, *Projection Domain Compression of Image Information*, Ph.D. Thesis, Imperial College of Science and Technology, 1987.

[63] O. Ibikunle et al., "Numerical Recognition Using the Radon Transform And Relaxation Matching", Digital Processing of Signals in Communications, Loughborough, I.E.R.E. Pub. No. 62, Apr. 1985, pp: 22-26.

[64] F. Itakura, "Minimum Prediction Residual Principle Applied to Speech Recognition", IEEE Trans. Acoust. Speech Signal Processing, Vol. ASSP-23, pp: 67-72, 1975.

[65] L.B. Jackson, *Digital Filters and Signal Processing*, Kluwer Academic Publishers, MA, 1986.

[66] L.B. Jackson and H.C. Chien, "Frequency and Bearing Estimation by Two-Dimensional Linear Prediction", Proc. ICASSP 79, Washington, DC, Apr. 1979, pp: 665-668.

[67] L.B. Jackson et al., "AR, ARMA and AR-in-Noise Modeling by Fitting Windowed Correlation Data", IEEE Trans. Acoust. Speech, Signal Processing, Vol. 37, No. 10, pp: 1608-1612, Oct. 1989.

[68] P.L. Jackson et al., "Application of Maximum Entropy Frequency Analysis to Synthetic Aperture Radar", Proc. RADC Spectrum Estimation Workshop, Rome, NY, May 1978, pp: 217-225.

[69] A.K. Jain, "A Sinusoidal Family of Unitary Trasnforms", IEEE Trans. Pattern Anal. Mach. Intell., Vol. PAMI-1, No. 4, pp: 356-365, Oct. 1979.

[70] A.K. Jain, "Image Data Compression: A Review", Proc. IEEE, Vol. 69, No. 3, pp: 349-389, Mar. 1981.

[71] A.K. Jain, "Advances in Mathematical Models for Image Processing", Proc. IEEE, Vol. 69, No. 5, pp: 502-528, May 1981.

[72] A.K. Jain, *Fundamentals of Digital Image Processing*, Englewood Cliffs, NJ: Prentice-Hall, 1989.

[73] A.K. Jain and S. Ranganath, "Two-Dimensional Spectrum Estimation", Proc. RADC Spectrum Estimation Workshop, Rome, NY, May 1978, pp: 151-157.

[74] A.K. Jain and S. Ranganath, "High-Resolution Spectrum Estimation in Two-Dimensions", Proc. First ASSP Workshop on Spectrum Estimation, Hamilton, Ontario, Canada, Aug. 1981, pp: 3.4.1-3.4.5.

[75] A.K. Jain and S. Ranganath, "Extrapolation Algorithms for Discrete Signals With Application in Spectral Estimation", IEEE Trans. Acoust. Speech Signal Processing, Vol. ASSP-29, pp: 830-845, Aug. 1981.

[76] A.K. Jain and S. Ansari, "Radon Transform Theory for Random Fields and Optimum Reconstruction from Noisy Projections", Proc. ICASSP 84, San Diego, California, Mar. 1984, Vol. 1, pp: 12A.7.1-12A.7.4.

[77] A.E. James, J.H. James and C.B. Higgins, *Digital Image Processing in Radiology*, Williams and Wilkins, Baltimore, MD, 1985.

[78] N.S. Jayanth and P. Noll, *Digital coding of waveforms : principles and applications to speech and video*, Englewood Cliffs, NJ: Prentice-Hall, 1984.

[79] E.T. Jaynes, "On The Rationale of Maximum Entropy Methods", Proc. IEEE, Vol. 70, No. 9, pp: 939-952, Sept. 1982.

[80] L.S. Joyce, "A Separable 2-D Autoregressive Spectral Estimation Algorithm", Proc. ICASSP 79, Washington, DC, Apr. 1979, pp: 677-680.

[81] S. Kacmarz, "Angenaherte Auflosung von Systemen linearer Gleichingen", Bull. Acad. Polon. Sci. Lett. A., pp: 355-357, 1937.

[82] T. Kailath, "A View of Three Decades of Linear Filtering Theory", IEEE Trans. Inform. Theory, Vol. IT-20, No. 2, pp: 146:181, Mar. 1974.

[83] R.L. Kashyap and R. Chellappa, "Stochastic Models for Closed Boundary Analysis: Representation and Reconstruction", IEEE Trans. Inform. Theory, Vol. IT-27, No. 5, pp: 627-637, Sept. 1981.

[84] R.L. Kashyap and M.C. Mittal, "Picture Reconstruction from Projections", IEEE Trans. Comput., Vol. C-24, No. 9, pp: 915-923, Sept. 1975.

[85] S.M. Kay, *Modern Spectral Estimation: Theory and Application*, Englewood Cliffs, NJ: Prentice-Hall, 1988.

[86] S.M. Kay and S.L. Marple, "Spectrum Analysis-A Modern Perspective", Proc. IEEE, Vol. 69, No. 11, pp: 1380-1419, Nov. 1981.

[87] P. Kiernan, "Two-Dimensional AR Spectral Estimation Using a Two-Dimensional Minimum Free Energy Method", IEEE Trans. Signal Processing, Vol. 43, No. 12, pp: 3075-3081, Dec. 1995.

[88] V.V. Klyuev et al., "Computational Tomography - A New Radiation Method of Non-destructive Testing I, II", Soviet J. Nondestruct. Test., Vol. 16, pp: 180-193, 1980.

[89] H. Kobayashi and L.R. Bahl, "Image Data Compression by Predictive Coding I: Prediction Algorithms", IBM J. Research and Development, Vol. 18, No. 2, pp: 164-171, Mar. 1974.

[90] A. Kuba, "Reconstruction of Measurable Plane Sets From Their Two Projections Taken in Arbitrary Directions", Inverse Problems 7, pp: 101-107, 1991.

[91] R. Kumaresan and D.W. Tufts, "A Two-Dimensional Technique for Frequency-Wavenumber Estimation", Proc. IEEE, Vol. 69, No. 11, pp: 1515-1517, Nov. 1981.

[92] G.R. Kuduvalli and R.M. Rangayyan, "An algorithm for Direct Computation of 2-D Linear Prediction Coefficients", IEEE Trans. Signal Processing, Vol. 41, No. 2, pp: 996-999, Feb. 1893.

[93] V. Kulkarni et al., "Impedence imaging in upper arm fractures", J. Biomed. Engg., Vol. 12, pp: 219-227, May 1990.

[94] W.M. Lawton, "Solution to the Two-Dimensional Factorization Problem", Proc. IEEE, Vol. 73, No. 2, pp: 370-371, Feb. 1985.

[95] W.M. Lawton, "A Complete Spectral Characterization of Quarter-Plane Autoregressive Models", IEEE Trans. Acoust. Speech Signal Processing, Vol. ASSP-33, No. 6, pp: 1617-1619, Dec. 1985.

[96] V.F. Leavers, "Use of the Radon transform as a method of extracting information about the shape in two dimensions", Image and Vision Computing, Vol. 10, No. 2, pp: 90-98, 1992.

[97] H. Lev-Ari, "Multidimensional Maximum Entropy Covariance Extension", Proc. ICASSP 85, Tampa, Florida, Vol. 2, pp: 816-819.

[98] R.M. Lewitt and R.H.T. Bates, "Image reconstruction from projections: General theoretical considerations", Optik 59, No. 1, pp: 19-33, 1978.

[99] J. Le Roux, "2-D Spectral Factorization and Stability Test for 2D Matrix Polynomials based on the Radon Projection", Proc. ICASSP 86, Tokyo, Japan, 1986, Vol. 2, pp: 1041-1044.

[100] J. Le Roux and F. Dubus, "On the Relationship Between 1-D and 2-D Spectral Factorization-Application to the Analysis of the Stability of 2-D Transfer Functions", Signal Processing, Vol. 16, No. 3, pp: 219-232, Mar. 1989.

[101] H. Li et al., "Object Recognition in Brain CT-Scans: Knowledge based Fusion of Data from Multiple Feature Extractors", IEEE Trans. Med. Imaging, Vol. 14, No. 2, pp: 212-229, June 1995.

[102] Z. Liang, "Unification of the Inverse Radon Transform in Odd and Even Dimensions", IEEE Trans. Med. Imaging, Vol. 14, No. 4, pp: 757-758, Dec. 1995.

[103] S.W. Lang and J.H. McLellan, "Extension of Pisarenko Harmonic Decomposition Method to Multiple Dimensions", Proc. ICASSP 82, Paris, France, May 1982, Vol. 1, pp: 125-128.

[104] S.W. Lang and J.H. McLellan, "Multidimensional MEM Spectral Estimation", IEEE Trans. Acoust. Speech Signal Processing, Vol. ASSP-30, pp: 880-887, Dec. 1982.

[105] S.W. Lang and T.L. Marzetta, "Image Spectral Estimation", in *Digital Image Processing Techniques*, M.P. Ekstrom, Ed., Academic Press Inc., Orlando, Fla., 1984.

[106] J.S. Lim, *Two-Dimensional Signal and Image Processing*, Englewood Cliffs, NJ: Prentice-Hall, 1990.

[107] J.S. Lim and N.A. Malik, "A New Algorithm for Two-Dimensional Maximum Entropy Spectral Estimation", IEEE Trans. Acoust. Speech Signal Processing, Vol. ASSP-29, No. 3, pp: 401-413, June 1981.

[108] J.S. Lim and A.V. Oppenheim, eds., *Advanced Topics in Signal Proccessing*, Englewood Cliffs, NJ: Prentice-Hall, 1988.

[109] A.K. Louis and F. Natterer, "Mathematical Problems of Computed Tomography", Proc. IEEE, Vol. 71, No. 3, pp: 379-389, Mar. 1983.

[110] A. Macovski, "Physical Problems of Computerized Tomography", Proc. IEEE, Vol. 71, No. 3, pp: 373-389, Mar. 1983.

[111] S. Maitra, "Moment Invariants", Proc. IEEE, Vol. 67, No. 4, pp: 697-699, Apr. 1979.

[112] J. Makhoul, "Linear Prediction: A Tutorial Review", Proc. IEEE, Vol. 63, No. 4, pp: 561-580, Apr. 1975.

[113] J. Makhoul, "Maximum Confusion Spectral Analysis", Proc. Third ASSP Workshop Spectral Estimation, Modeling, Boston, MA, Nov. 1986, pp: 6-9.

[114] J. Makhoul and A.O. Steinhardt, "On Matching Correlation Sequences by Parametric Models", IEEE Trans. Signal Processing, Vol. 39, No. 1, pp: 214-216, Jan. 1991.

[115] N.A. Malik and J.S. Lim, "Properties of Two-Dimensional Maximum Entropy Power Spectrum Estimates, IEEE Trans. Acoust. Speech Signal Processing, Vol. ASSP-30, pp: 788-797, Oct. 1982.

[116] S.L. Marple Jr., *Digital Spectral Analysis With Applications*, Englewood Cliffs, NJ: Prentice-Hall, 1987.

[117] T.L. Marzetta, "Two-Dimensional Linear Prediction: Autocorrelation Arrays, Minimum Phase Prediction Error Filters, and Reflection Coefficient Arrays", IEEE Trans. Acoust. Speech Signal Processing, Vol. ASSP-28, No. 6, pp: 725-733, Dec. 1980.

[118] B.F. McGuffin and B. Liu, "An Efficient Algorithm for Two-Dimensional Autoregressive Spectrum Estimation", IEEE Trans. Acoust. Speech Signal Processing, Vol. 37, No. 1, pp: 106-117, Jan. 1989.

[119] J.H. McLellan, "Multidimensional Spectral Estimation", Proc. IEEE, Vol. 70, No. 9, pp: 1029-1039, Sept. 1982.

[120] R.M. Mersereau and D.E. Dudgeon, "The Representaion of Two-Dimensional Sequences as One-Dimensional Sequences", IEEE Trans. Acoust. Speech Signal Processing, Vol. ASSP-22, No. 5, pp: 320-325, Oct. 1974.

[121] R.M. Mersereau and D.E. Dudgeon, "Two-Dimensional Digital Filtering", Proc. IEEE, Vol. 63, No. 4, pp: 610-623, Apr. 1975.

[122] R.M. Mersereau and A.V. Oppenheim, "Digital Reconstruction of Multidimensional Signals From Their Projections", Proc. IEEE, Vol. 62, No. 10, pp: 1319-1338, Oct. 1974.

[123] P. Milanfar, "Reconstructing Binary Polygonal Objects from Projections: A Statistical View", CVGIP: Graphical Models and Image Processing, Vol. 56, No. 5, pp: 371-391, Sept. 1994.

[124] P. Milanfar, "Recovering the moments of a function from its Radon-transform projections: Necessary and Sufficient Conditions", LIDS Tech. Rep. LIDS-P-2113, Mass. Inst. Tech., Lab. for Information and Decision Systems, June 1992.

[125] P. Milanfar et al., "A Moment-Based Variational Approach to Tomographic Reconstruction", IEEE Trans. Image Processing, Vol. 5, No. 3, pp: 459-470, Mar. 1996.

[126] J.M.V. Miller et al., "Spatially Invariant Image Sequences", IEEE Trans. Image Processing, Vol. 1, No. 2, pp: 148-161, Apr. 1992.

[127] S.A. Mohammad and M.M. Fahmy, "Binary Image Compression Using Efficient Partitioning into Rectangular Regions", IEEE Trans. Communications, Vol. 43, No. 5, pp: 1888-1893, May 1995.

[128] W. Munk and C. Wunsch, "Ocean Acoustic Tomography: A scheme for Large Scale Monitoring", Deep Sea Research, Vol. 26A, pp: 123-161, 1979.

[129] D.C. Munson et al., "A Tomographic Formulation of Spotlight-Mode Synthetic Aperture Radar", Proc. IEEE, Vol. 71, No. 8, pp: 917-925, Aug. 1983.

[130] L.M. Murphy, "Linear Feature Detection and Enhancement in Noisy Images Via the Radon Transform", Pattern Recognition Letters, Vol. 4, No. 4, pp: 279-284, 1986.

[131] R.D. Murch and R.H.T. Bates, "Image reconstruction from projections IX: Binary images", Optik., Vol. 85, No. 4, pp: 167-172, Sept. 1990.

[132] J.J. Murray, "Matrix Two-Dimensional Spectral Factorization", IEEE Trans. Circ. Syst.-II, Vol. 40, No.8, pp: 509-511, Aug. 1993.

[133] C. Nadeu, "Maximum Flatness Spectral Modeling", IEEE Tran. Acoust. Speech Signal Processing, Vol. ASSP-38, No. 11, pp: 2006-2008, Nov. 1990.

[134] C. Nadeu and M. Bertran, "A Flatness Based Generalized Optimization Approach to Spectral Estimation", Signal Processing, Vol. 19, No. 4, pp: 311-320, 1990.

[135] A.N. Netravali and B.G. Haskell, *Digital Pictures: Representation, Compression, and Standards*, 2nd ed., NY: Plenum Press, 1995.

[136] W.I. Newman, "Extension to the Maximum Entropy Method", IEEE Trans. Inform. Theory, Vo l. IT-23, No. 1, Jan. 1973.

[137] Y.W. Nijim et al., "Lossless Compression of Seismic Signals Using Diffraction", IEEE Trans. Geosci. Remote Sensing, Vol. 34, No. 1, pp: 52-56, Jan. 1996.

[138] C.L. Nikias and M.R. Raghuveer, "Mutlidimensional Parametric Spectral Estimation", Signal Processing, Vol. 8, No. 2, pp: 191-205, Apr. 1985.

[139] R. Nitzberg, "Spectral Estimation: An Impossibility?", Proc. IEEE, Vol. 67, No. 3, pp: 437-438, Mar. 1979.

[140] N. Ohayama et al., "Discrete Radon Transform in Continuous Space", J. Opt. Soc. Am. A, Vo l. 4, No. 2, pp: 318-324, Feb. 1987.

[141] T. Ohtsuki, "Minimum Dissection of Rectangualr Regions", Proc. ISCAS '82, Rome, May 1982, Vol. 3, pp: 1210-1213.

[142] M. Onoe et al., "Computed Tomography for Measuring Annular Rings of a Live Tree", Proc. IEEE, Vol. 71, pp: 907-908, July 1983.

[143] A.V. Oppenheim and R.W. Schafer, "*Digital Signal Processing*", Englewood Cliffs, NJ: Prentice-Hall, 1991.

[144] S.J. Orfanidis, *Optimum Signal Processing*, McGraw-Hill, 1990.

[145] A. Papoulis, *The Fourier Integral and its Applications*, McGraw-Hill, 1962.

[146] A. Papoulis, "Maximum Entropy and Spectral Estimation: A Review", IEEE Trans. Acoust. Speech Signal Processing, Vol. ASSP-29, pp: 1176-1186, Dec. 1981.

[147] H.B. Park and C.W. Lee, "Image Compression by Vector Quantization of Projection Data", IEICE Trans. Inf. and Syst., Vol. E75-D, No. 1, pp: 148-155, Jan. 1992.

[148] E. Parzen, "Some Recent Advances in Time Series Modeling", IEEE Trans. Automat. Contr., Vol. AC-19, pp: 723-730, Dec. 1974.

[149] M.A. Pavel, "A Unified Setting for Projections in Pattern Recognition", Pattern Recognition, Vol. 10, pp: 249-254, 1978.

[150] T. Pavlidis, "Computer Recognition of Figures through Decomposition", Information and Control 12, pp: 526-537, 1968.

[151] T. Pawlak, "On the Reconstruction Aspects of Moment Descriptors", IEEE Trans. Inform. Theory, Vol. 38, No. 6, pp: 1698-1708, Nov. 1992.

[152] J.V. Pendrell and D.E. Smylie, "The Maximum Entropy Principle in Two-Dimensional Spectral Analysis", Astron. Astrophys., Vol. 112, pp: 182-189, 1982.

[153] F. Peyrin and R. Goutte, "Image Invariant via the Radon Transform", IEE Int. Conf. Image Proc. and its Applications, 1992, pp: 458-461.

[154] J.M. Pimblay, "Recursive Autoregressive Spectral Estimation by Minimization of Free Energy", IEEE Trans. Signal Processing, Vol. 40, No. 6, pp: 1518-1527, June 1992.

[155] J.M. Pimblay and S.D. Silverstein, "Recursive Minimum Free Energy Spectral Estimation", Proc. 23rd Asilomar Conf. Signals, Syst. Comput., 1989, Vol. 2, pp: 1051-1055.

[156] V.F. Pisarenko, "The Retrieval of Harmonics from a Covariance Function", Geophys. J. R. Astr. Soc., Vol. 33, pp: 347-366, 1973.

[157] L.R. Rabiner and R.W. Schafer, *Digital Processing of Speech Signals*, Englewood Cliffs, NJ: Prentice-Hall, 1978.

[158] J. Radon, "Uber die Bestimmung von Funktionen durch ihre Integralwerte langs gewisser Mannigfaltigkeiten", Berichte Sacgsische Academie der Wissenschaften, Leipzig, Math. Phys., Kl., 69, 262-267 (An English Translation of the paper is available in [23]).

[159] Rajeev Agarwal, *Enhancement and Suppression of Short-Duration Narrowband Signals with application to ABR Audiometry*, Ph.D. Thesis, Dept. of Electrical and Computer Engg., Concordia University, Montreal, Canada, 1995.

[160] Rajeev Agarwal, E.I. Plotkin and M.N.S. Swamy, "Statistically Optimal Null Filters for Processing Short Record Length Signals", Proc. ISCAS '95, Seattle, Washingotn, Vol. 3, pp: 2277-2280.

[161] Ramesh G.R., *Filtering and Linear Predictive Coding in the Radon Space*, M.Sc. (Engg.) Thesis, Dept. of Electrical Engineering, Indian Institute of Science, Bangalore, India, Sept. 1989.

[162] Ramesh G.R., N. Srinivasa and K. Rajgopal, "An Algorithm for Computing the Discrete Radon Transform with Some Applications", 6th Scandinavian Conf. on Image Analysis, University of Oulu, Oulu, Finland, June 1989.

[163] Ramesh G.R., N. Srinivasa and K. Rajgopal, "A Radon Transform Approach to Linear Predictive Coding of Images", IEEE Int. Conference on Image Processing (ICIP '89), Singapore, Sept. 1989.

[164] Ramesh G.R. and K. Rajgopal, "On the Applications of Tomographic Modeling of Spotlight-Mode Synthetic Aperture Radar for Ground Target Feature Analysis", Proc. 1989 Int. Symp. on Noise and Clutter Rejection in Radar and Imaging Sensors (ISNCR-89), Japan, pp: 744-749.

[165] Ramesh G.R. and K. Rajgopal, "Linear Predictive Coding of Binary Images: A Radon Transform Approach", Second International Symp. Signal Processing and its Applications (ISSPA 90), University of Queensland, Gold Coast, Australia, Aug., 1990.

[166] Ramesh G.R. and K. Rajgopal, "Binary Image Compression Using the Radon Transform", Proc. Annual Convention of the IEEE India Council and Bangalore Chapter (ACE-90), Bangalore, India, Jan. 1991, pp: 178-182.

[167] Ramesh R. Galigekere, E.I. Plotkin, and M.N.S. Swamy, "Two-Dimensional Spectral Factorization in the Radon Space", Proc. Seventh SP Workshop on Statistical Signal and Array Processing, Quebec City, June 1994, pp: 15-18.

[168] Ramesh R. Galigekere, E.I. Plotkin, and M.N.S. Swamy, "A Modified Approach to 2-D Spectrum Estimation Using the Radon Transform", Proc. 1995 Europian Conference on Circuits and System Design, Istanbul Turkey, Aug. 1995, Vol. 2, pp: 1007-1010.

[169] Ramesh R. Galigekere and E.I. Plotkin, "On Some Intrinsic Properties of the Radon Transform of an SRF with Applications to 2-D Spectrum Estimation", Proc. Canadian Conference on Electrical and Computer Engg., Montreal, Canada, Sept. 1995, Vol. 2, pp: 882-885.

[170] Ramesh R. Galigekere and E.I. Plotkin, "Moment Based Invariants in the Radon Space", Proc. International Conf. Signal Processing and Application Technology (ICSPAT 95), Boston, MA, Oct. 1995, pp: 1137-1141.

[171] Ramesh R. Galigekere and E.I. Plotkin "Selective Reconstruction of Objects from the Radon Transform Using the Generalized Instantaneous Matched-Filtering Approach", Proc. ICECS'96, Rodos, Greece, Oct. 1996, Vol. 1, pp: 57-60.

[172] S. Ranganath and A.K. Jain, "Two dimensional Linear Prediction Models-Part I: Spectral Factorization and Realization", IEEE Trans. Acoust. Speech Signal Processing, Vol. ASSP-33, No. 1, pp: 280-299, Feb. 1985.

[173] K.R. Rao and P. Yip, "Discrete Cosine Transform: Algorithms, Advantages, Applications", San Diego, CA: Academic Press, 1990.

[174] P.A. Rattey and A.G. Lindgren, "Sampling the 2-D Radon Transform", IEEE Trans. Acoust. Speech Signal Processing, Vol. ASSP-29, No.5, pp: 994-1002, Oct. 1981.

[175] S.S. Reddi, "Radial and Angular Moment Invariants for Image Identification", IEEE Trans. Pattern Anal. Mach. Intell., Vol. PAMI-3, No. 2, pp: 240-242, Mar. 1981.

[176] I.S. Reed et al., "X-Ray Reconstruction of the Spinal Cord, Using Bone Supression", IEEE Trans. Biomed. Engr., Vol. BME-27, No. 6, pp: 293-298, June 1980.

[177] A.P. Reeves et al., "Three-Dimensional Shape Analysis Using Moments and Fourier Descriptors", IEEE Trans. Pattern Anal. Mach. Intell., Vol. PAMI-10, No. 6, pp: 937-940, Nov. 1988.

[178] S.T. Reiderer et al., The Noise Power Spectrum in Computed X-ray Tomography", Phys. Med. Biol., Vol. 23, pp: 446-454, 1978.

[179] R. Rinaldo et al., "Techniques for the Efficient Evaluation of Two-Dimensional Autocorrelation Functions", IEEE Trans. Signal Processing, Vol. 40, No. 1, pp: 2854-2857, Nov. 1992.

[180] J. Rissanen, "A Universal Prior for Integers and Estimation by Minimum Description Length", Ann. Stat., Vol. 11, pp: 417-431, 1983.

[181] E.A. Robinson, "Spectral Approach to Geophysical Inversion by Lorentz, Fourier and Radon Transforms", Proc. IEEE Vol. 70, No. 9, pp: 1039-1054, 1986.

[182] E.A. Robinson, "A Historical Perspective of Spectrum Estimation", Proc. IEEE, Vol. 70, pp: 885-907, 1982.

[183] A. Rosenfeld and A.C. Kak, *Digital Picture Processing*, Vol. 1, Second Edition, NY: Academic Press, 1992.

[184] M.C. Rost and K. Sayood, "An Edge Preserving Differential Image Coding Scheme", IEEE Trans. Image Processing, Vol. 1, No. 2, pp: 250-256, Apr. 1992.

[185] S.W. Rowland, "Computer Implementation of Image Reconstruction Formulas", in [54].

[186] W. Rudin, "The Extension Problem for Positive-Definite Functions", Ill. J. Math., Vol. 7, pp: 532-539, 1963.

[187] R. Saeks, "The Factorization Problem - A Survey", Proc. IEEE, Vol. 64, No. 1, pp: 90-95, Jan. 1976.

[188] M. Sakurai and N. Hamada, "Two-Dimensional Line Spectrum Estimation by Polar Coordinate AR Models", Electronics and Communications in Japan, Part 3, Vol. 77, No. 1, pp: 104-112, 1994.

[189] D.B. Salzman, "A Method of General Moments for Orienting 2D Proejctions of Unknown 3D Objects", Comput. Vision, Graphics, and Image Processing, Vol. 50, No. 2, pp: 129-156, May 1990.

[190] J.L.C. Sanz and I. Dinstein, "Projection Based Geometric Feature Extraction for Computer Vision: Algorithms in Pipeline Architectures", IEEE Trans. Pattern Anal. Mach. Intell., Vol. PAMI-9, No. 1, pp: 160-168, Jan. 1987.

[191] D.J. Scheibner, "The Discrete Radon Transform With Some Applications to Velocity Estimation", EE Tech. Report, Mar. 1981, Rice University, Houston, Texas.

[192] M.R. Schroeder, "Linear Prediction, Entropy and Signal Analysis", IEEE ASSP Magazine, pp: 3-11, July 1984.

[193] P.G. Selfridge and J.M.S. Prewitt, "Organ Detection in Abdominal Computerized Tomography Scans: Applications to the Kidney", Comput. Graph. Image Processing, Vol. 15, No. 3, pp: 265-278, March 1981.

[194] G. Sharma and R. Chellappa, "Two-Dimensional Spectrum Estimation Using Non-causal Autoregressive Models", IEEE Trans. Inform. Theory, Vol. IT-32, No. 2, pp: 268-275, Mar. 1986.

[195] T. Shen et al., "Fast Algorithm for 2-D Image Moments Via the Radon Transform", Proc. ICASSP 96, Atlanta, Georgia, Vol. 3, pp: 1327-1330.

[196] E. Shieh et al., "High Speed Computation of the Radon Transform and Backprojection Using an Expandable Multiprocessor Architecture", IEEE Tran. Circuits Syst. Video Technology, Vol. 2, No.4, pp: 347-360, Dec. 1992.

[197] M. Shinozuka, "Digital Simulation of Random Processes and Its Applications", J. Sound and Vibrations, 25 (1), pp: 111-128, 1972.

[198] S.D. Silverstein and J.M. Pimbley, "Minimum-free-energy Method of Spectrum Estimation: Autocorrelation Sequence Approach", J. Opt. Soc. Amer. A, Vol. 7, No. 3, pp: 356-372, Mar. 1990.

[199] M. Soumekh, "Binary Image Reconstruction from Four Projections", Proc. ICASSP 88, New York City, Vol. 2, pp: 1280-1283.

[200] *Special Issue on Digital Encoding of Graphics*, Proc. IEEE, Vol. 68, No. 7, July 1980.

[201] *Special Issue on Tomography*, Proc. IEEE, Vol. 71, No. 3, Mar. 1983.

[202] *Special Issue on Medical Imaging Modalities*, IEEE Signal Processing Magazine, Jan. 1997.

[203] N. Srinivasa, *Applications of Linear Prediction and Filtering in the Radon Space*, Ph.D. Thesis, Dept. of Elec. Engg., Indian Institute of Science, Bangalore, India, Aug. 1988.

[204] N. Srinivasa et al., "Two-Dimensional Spectral Estimation: A Radon Transform Approach", IEEE J. Oceanic Engg., Vol. OE-12, No. 1, pp: 90-96, Jan. 1987.

[205] N. Srinivasa et al., "Detection of Edges from Projections", IEEE Trans. Med. Imaging, Vol. 11, No. 1, pp: 76-80, Mar. 1992.

[206] N. Srinivasa et al., "On Multidimensional Maximum Entropy Spectral Estimation", IEEE Trans. Acoust. Speech Signal Processing, Vol. 40, No. 1, pp: 241-244, Jan. 1992.

[207] M.D. Swanson and A.H. Tewfik, "A Binary Wavelet Decomposition of Binary Images", IEEE Trans. Image Proc., Vol. 5, No. 12, pp: 1637-1650, Dec. 1996.

[208] N. Ta et al., "Fast Computation of Two-Dimensional Discrete Cosine Transforms Using Fast Discrete Radon Transform", Electronics letters, Vol. 26, No. 8, pp: 82-84, Apr. 1990.

[209] K.C. Tam, "The Construction and Use of Convex-Hulls in Limited Angle Computerized Tomography", J. Nondestructive Evaluation, Vol. 6, No. 4, pp: 189-204, 1987.

[210] M. Tasto, "Reconstruction of Random Objects from Noisy Projections", Comput. Graphics and Image Processing, Vol. 6, No. 2, pp: 103-122, Apr. 1977.

[211] M.R. Teague, "Image Analysis via the General Theory of Moments", J. Opt. Soc. Am., Vol. 70 , No. 8, pp: 920-930, Aug. 1980.

[212] C. Teh and R.T. Chin, "On Digital Approximation of Moment Invariants", Comput. Vision, Graphics and Image Processing, Vol. 33, No. 3, pp: 318-326, Mar. 1989.

[213] C. Teh and R.T. Chin, "On Image Analysis by the Methods of Moments", IEEE Trans. Pattern Anal. Mach. Intell., Vol. 10, No. 4, Nov. 1988.

[214] A.H. Tewfik et al., An Efficient Maximum Entropy Technique for 2-D Isotropic Random Fields", IEEE Trans. Acoust. Speech Signal Processing, Vol. 36, No. 5, pp: 797-812, May 1988.

[215] D. Tjostheim, "Autoregressive Modelling and Spectral Analysis of Array Data in the Plane", IEEE Trans. Geosci. Remote Sensing, Vol. GE-19, pp: 15-24, Jan. 1981.

[216] D.W. Tufts and R. Kumaresan, "Singular Value Decomposition and Improved Frequency Estimation Using Linear Prediction", IEEE Trans. Acoust. Speech Signal Processing, Vol. ASSP-30, No. 4, pp: 671-675, Aug. 1982.

[217] D.W. Tufts and R. Kumaresan, "Estimation of Frequencies of Multiple Sinusoids: Making Linear Prediction Perform Like Maximum Likelihood", Proc. IEEE Vol. 70, No. 9, pp: 975-989, Sept. 1982.

[218] T.J. Ulrych and C.J. Walker, "High Resolution Two-Dimensional Power Spectral Estimation", Applied Time Series Analysis II, Ed. D.F. Findlay, NY: Academic Press, 1981.

[219] T. Usubuchi et al., "Adaptive Predictive Coding for Newspaper Facsimile", Proc. IEEE, Vol. 68, No. 7, July 1980.

[220] E. Vanmarcke, *Random Fields: Analysis and Synthesis*, The MIT Press, 1983.

[221] A. Van den Bos, "Alternative Interpretation of Maximum Entropy Spectral Analysis", IEEE Trans. Inform. Theory, Vol. 17, No. 4, pp: 493-494, July 1971.

[222] G.N. Vishnyakov et. al., "Optical Radon Procesor for analyzing images by the method of moment invariants", Opt. Spectrosk. (USSR) 67, pp: 860-865, Oct. 1989.

[223] W.G. Wee and T. Hsieh, "An Application of the Projection Transform Technique in Image Transmission", IEEE Trans. Syst. Man Cybern., Vol. SMC-6, No. 7, pp: 286-298, July 1976.

[224] S.J. Wernecke, "Two-Dimensional Maximum Entropy Reconstruction of Radio Brightness", Radio Sci., Vol. 12, pp: 831-844, Sept.-Oct. 1977.

[225] S.J. Wernecke and L.R. D'Addario, "Maximum entropy image reconstruction", IEEE Trans. Comput., Vol. C-26, pp: 351-354, Apr. 1977.

[226] P. Whittle, "On Stationary Processes in the Plane", Biometrika, Vol. 41, pp: 434-449, Dec. 1954.

[227] S. Wong et al., "Radiologic Image Compression - A Review", Proc. IEEE, Vol. 83, No. 2, pp: 194-219, Feb. 1995.

[228] S.L. Wood et al., Stochastic methods applied to medical image reconstruct ion", Proc. IEEE Conf. Decision and Control, New Orleans, LA, Dec. 1977, pp: 35-41.

[229] J.W. Woods, "Two-Dimensional Markov Spectral Estimation", IEEE Trans. Inform. Theory, Vol. IT-22, No. 5, pp: 552-559, Sept. 1976.

[230] S. Woolven et al., "Hybrid Implementation of a real time Radon-space image-processing system", Applied Opt., Vol. 32, No. 32, pp: 6556-6561, Nov. 1993.

[231] Z.Q. Wu and A. Rosenfeld, "Filtered Projections as an Aid in Corner Detection", Pattern Recognition, Vol. 16 No. 1, pp: 31-38, 1983.

[232] X.-D. Zhang and J. Cheng, "High Resolution Two-Dimensional ARMA Spectral Estimation", IEEE Trans. Signal Processing, Vol. 39, No. 3, pp: 765-770, Mar. 1991.

[233] L. Zou and B. Liu, "On Resolving Two-Dimensional Sinusoids in White Noise Using Different Spectral Estimates", IEEE Trans. Acoust. Speech Signal Processing, Vol. 36, No. 8, pp: 1338-1350, Aug. 1988.